TOPOLOGY DESIGN OF VEHICLE STRUCTURES FOR CRASHWORTHINESS USING VARIABLE DESIGN TIME

A Thesis

Submitted to the Faculty

of

Purdue University

by

Prasad Tapkir

In Partial Fulfillment of the

Requirements for the Degree

of

Master of Science in Mechanical Engineering

December 2017

Purdue University

Indianapolis, Indiana

THE PURDUE UNIVERSITY GRADUATE SCHOOL
STATEMENT OF COMMITTEE APPROVAL

Dr. Andres Tovar, Chair

Department of Mechanical Engineering

Dr. Jie Chen

Department of Mechanical Engineering

Dr. Khosrow Nematollahi

Department of Mechanical Engineering

Approved by:

Dr. Sohel Anwar

Chair of the Graduate Program

I dedicate this work to my family, which is the strongest pillar of my life. This work is also dedicated to my cousin Shashank and to all of his distant memories.

ACKNOWLEDGMENTS

I would like to express my most sincere gratitude to Dr. Andres Tovar for his guidance throughout the research work. Working under his direction in the Engineering Design Research Laboratory has helped me to grow professionally and personally. I am grateful to professionally interact with Dr. Chandan Mozumder, Dr. Punit Bandi, and Dr. Simon Xu, who provided me an opportunity to contribute in the research project of General Motors. I also want to thank the members of my committee, Dr. Jie Chen and Dr. Khosrow Nematollahi for their invaluable suggestions to improve this research project.

Finally, I want to thank my laboratory fellows, Sajjad Raeisi, Kai Liu, Homero Guerra, Joel Najmon, Prathmesh Chaudhari, and Tong Wu for their help during this project.

TABLE OF CONTENTS

Page

LIST OF TABLES vii

LIST OF FIGURES ix

ABBREVIATIONS xii

ABSTRACT xiii

1 INTRODUCTION 1

1.1 Passenger safety and crashworthiness 2

1.2 Nonlinear solvers for crash simulations 4

1.3 Structural optimization 5

1.4 Response surface methods 11

1.5 Objectives of the proposed work 13

1.5.1 Introduction of a new design control parameter 13

1.5.2 Targeting the desired crash responses 13

1.5.3 Crash response improvement of lightweight structures 14

2 HYBRID CELLULAR AUTOMATA (HCA) 15

2.1 Material parameterization 16

2.2 Problem formulation with traditional HCA 17

2.3 Local variable update 17

2.4 Convergence criteria 18

2.5 Issues associated with traditional HCA 18

3 THE IMPROVED HYBRID CELLULAR AUTOMATA 20

3.1 Design time 20

3.2 Problem formulation with the improved HCA 21

3.3 Targeting the crash responses 23

3.3.1 Step 1: Sampling 24

Page

3.3.2 Step 2: Topology synthesis . . . 24
3.3.3 Step 3: Evaluation of crash responses . . . 25
3.3.4 Step 4: Metamodelling . . . 25
3.3.5 Step 5: Cross-validation . . . 28
3.3.6 Step 6: Prediction . . . 29
3.3.7 Step 7: Error evaluation . . . 31
3.4 Advanced applications of design time . . . 32
3.4.1 Multi-design time . . . 32
3.4.2 Merged design . . . 33
4 NUMERICAL EXAMPLES . . . 35
4.1 Bumper . . . 35
4.1.1 Finite element model . . . 35
4.1.2 Time dependent field variable . . . 37
4.2 Front frame . . . 39
4.2.1 Finite element model . . . 39
4.2.2 Design of experiments (DOE) . . . 44
4.2.3 Topology synthesis and performance evaluation . . . 45
4.2.4 Targeting with full DOE . . . 50
4.2.5 Targeting with four experiments . . . 57
4.2.6 Results of the multi-design time . . . 81
4.2.7 Results of the merged design . . . 84
5 SUMMARY AND RECOMMENDATIONS . . . 89
5.1 Summary . . . 89
5.2 Future work . . . 94
5.2.1 Exploration of the design space . . . 94
5.2.2 Implementation of design time on a full scale model . . . 95
5.2.3 Multi-material topology synthesis . . . 98
REFERENCES . . . 99

LIST OF TABLES

Table Page

3.1 Database for metamodels 25
3.2 Regression and correlation functions 30
4.1 Properties of aluminum 36
4.2 Keywords related to bumper model 37
4.3 Details of the element model 41
4.4 Material properties 42
4.5 Control model 43
4.6 Design of experiments for topology synthesis 44
4.7 Crash responses of topology designs (a) 47
4.8 Crash responses of topology designs (b) 48
4.9 PRESS values for the kriging metamodel of volume fraction 52
4.10 PRESS values for the kriging metamodel of design time 52
4.11 Target and actual crash responses 56
4.12 Four experiments 57
4.13 Data set for iteration 1 60
4.14 Target and closest crash responses 63
4.15 Iteration 1: prediction for the closest crash responses 64
4.16 Summary of iteration 1 66
4.17 Data set for iteration 2 67
4.18 Iteration 2: target and closest crash responses 69
4.19 Iteration 2: prediction for the closest crash responses 71
4.20 Summary of iteration 2 73
4.21 Data set for iteration 3 73
4.22 Iteration 3: target and closest crash responses 76

Table Page

4.23 Iteration 3: prediction for the closest crash responses 77
4.24 Summary of iteration 3 80
4.25 Best possible results 80
4.26 Comparison of two proposed targeting approaches 80

LIST OF FIGURES

Figure Page

1.1 Size optimization 6
1.2 Shape optimization 7
1.3 Topology optimization 7
2.1 Neighborhood of the element 15
3.1 Trade-off between acceleration and displacement 22
3.2 Target crash responses 30
4.1 Boundary conditions of the design domain 36
4.2 IED at 1 millisecond 37
4.3 IED at 3 milliseconds 38
4.4 IED at 5 milliseconds 38
4.5 Modified design domain of the front frame 40
4.6 Dimensions of the modified design domain 40
4.7 Boundary conditions 41
4.8 Design space 45
4.9 Topology designs for volume fraction 10, 12.5, and 15 percent 46
4.10 Topology designs for volume fraction 17.5, 20, and 22.5 percent 46
4.11 Effect of the design time 48
4.12 Crash response space 49
4.13 Target crash responses 51
4.14 Contour plot of the volume fraction kriging metamodel 53
4.15 Contour plot of the design time kriging metamodel 53
4.16 The predicted volume fraction and design time 54
4.17 Topology design with the predicted volume fraction and design time 54
4.18 Behavior of the topology design under the dynamic load 55

Figure Page

4.19 Actual and target crash responses 55
4.20 Search of the closest point 59
4.21 Design space for iteration 1 61
4.22 Crash response space for iteration 1 61
4.23 Closest point for iteration 1 62
4.24 Volume fraction metamodel for iteration 1 63
4.25 Design time metamodel for iteration 1 64
4.26 Prediction of iteration 1 65
4.27 Topology design of iteration 1 65
4.28 Actual crash responses of iteration 1 66
4.29 Design space for iteration 2 67
4.30 Crash response space for iteration 2 68
4.31 Closest point for iteration 2 68
4.32 Volume fraction metamodel for iteration 2 70
4.33 Design time metamodel for iteration 2 70
4.34 Prediction of iteration 2 71
4.35 Topology design of iteration 2 72
4.36 Actual crash responses of iteration 2 72
4.37 Design space for iteration 3 74
4.38 Crash response space for iteration 3 74
4.39 Closest point for iteration 3 75
4.40 Volume fraction metamodel for iteration 3 76
4.41 Design time metamodel for iteration 3 77
4.42 Prediction of iteration 3 78
4.43 Topology design of iteration 3 79
4.44 Actual crash responses of iteration 3 79
4.45 Topology design generated with multiple loads 82
4.46 Accelration-displacement profiles of designs with VF of 20 percent 83

Figure Page

4.47 Performance of topology design generated with multiple loads 83

4.48 Topology designs with volume fraction of 10 percent 85

4.49 Crash responses of topology designs with volume fraction of 10 percent . . 85

4.50 Merged design 86

4.51 Acceleration-displacement profiles of merged design and other designs with VF of 20 percent 87

4.52 Crash responses of the merged design 88

5.1 Design space with latin hypercube sampling 95

5.2 Design domain of the front frame with engine bay 96

5.3 Topology deign with the design time of 2.5 milliseconds 97

5.4 Topology deign with the design time of 5 milliseconds 97

5.5 Topology deign with the design time of 10 milliseconds 97

ABBREVIATIONS

HCA	Hybrid Cellular Automata
IED	Internal Energy Desnity
BIW	Body In White
UDS	User Defined Sampling
LHS	Latin Hypercube Sampling
SQP	Sequential Quadratic Programming
RSM	Response Surface Methodology
FEA	Finite Element Analysis
FEM	Finite Element Model
FE	Finite Element
DOE	Design Of Experiments
MLE	Maximum Likelihood Estimation
correxp	Exponential Correlation Function
corrmatern52	Matern Gaussian Correlation Function
corrgauss	Gaussian Correlation Function
regpoly0	Zero Order Regression Function
regpoly1	First Order Regression Function
regpoly2	Second Order Regression Function
LOOCV	Leave One Out Cross-Validation
PRESS	Predicted Residual Error Sum of Squares

ABSTRACT

Tapkir, Prasad M.S.M.E., Purdue University, December 2017. Topology Design of Vehicle Structures for Crashworthiness Using Variable Design Time. Major Professor: Andres Tovar.

The passenger safety is one of the most important factors in the automotive industries. At the same time, in order to improve the overall efficiency of passenger cars, lightweight structures are preferred while designing the vehicle structures. Among various structural optimization techniques, topology optimization techniques are usually preferred to address the issue of crashworthiness. The hybrid cellular automaton (HCA) is a truly nonlinear explicit topology design method developed for obtaining conceptual designs of crashworthy vehicle components. In comparison to linear implicit methods, such as equivalent static loads, and partially nonlinear implicit methods, the HCA method fully captures all the relevant aspect of a fully nonlinear, transient dynamic crash simulation. Traditionally, the focus of the HCA method has been on designing load paths in the crash component that increase the uniform internal energy absorption ability; thus far, other relevant crashworthiness indicators such as peak crushing force and displacement have been less studied. The objective of this research is to extend the HCA method to synthesize load paths to obtain the different acceleration-displacement profiles, which allow reduced peak crushing force as well as reduced penetration during a crash event. To achieve this goal, this work introduces the concept of achieving uniform energy distribution at variable design simulation times. In the proposed work, the design time is used as a new design parameter in topology optimization. The desired volume fraction of the final design and the design time provided two dimensional design space for topology optimization, which is followed by the formulation of design of experiments (DOEs).

The nonlinear analyses of the corresponding DOEs are performed using nonlinear explicit code LS-DYNA, which is followed by topology synthesis in HCA. The performance of the resulting structures showed that the short design times lead to design obtained by linear optimizers, while long simulation times lead to designs obtained by the traditional HCA method. To achieve the target crucial crash responses such as maximum acceleration and maximum displacement of the structure under the dynamic load, the geological predictor has been implemented. The concept of design time is further developed to improve structural performance of a vehicle component under the multiple loads using the method of multi-design time. Finally, the design time is implemented to generated merged designs by performing binary operations on topology-optimized designs. Numerical example of the simplified front frame is utilized to demonstrate the capabilities of the proposed approach.

1. INTRODUCTION

In recent years, the crashworthiness of the passenger cars has become the intense research field as the integrity of the crashworthy structures directly determines the likelihood of the passenger injuries. In most of the passenger injury criteria, the acceleration pulse experienced by the passenger and the intrusion of the impacting body into vehicle structures are the most vital and effective factors, which define the severity index of the passenger injuries. Therefore, it becomes important to study these crash responses and the corresponding dependency on the design parameters. Besides the passenger safety, automotive industries are always concerned about the cost associated with the design and the manufacturing of the vehicle structures, which are subjected to external dynamic loading in the crash event. In other words, it is expected to design the crashworthy structures with the proper material utilization.

The purpose of the proposed research work is to address all these issues by developing a nonlinear topology synthesis tool, so the vehicle structures can be synthesized to achieve the desired structural integrity with appropriate material distribution. The prime goal of this thesis is to identify and utilize the meta-parameters, which can control and tune the structural performance of the final topology design. The analysis of the relationship between these meta-parameters and the crash responses of the topology designs can serve as a great guideline to accurately control the structural performance of the vehicle structures.

To review the fundamentals of the crashworthiness and the corresponding recent research contributions, the first section of this chapter briefly discusses issues associated with the passenger safety and the corresponding relationship with structural performance of the vehicle structures. Second section of the chapter presents nonlinear finite element method used for crash simulations. A brief introduction of the topology optimization techniques and the contribution of the researchers in the cor-

responding field are discussed in the subsequent section of the chapter. The third section of the chapter explains the importance of developing an implicit relation between the crash responses and meta-parameters or the design control parameters in order to predict the design parameters for the desired crash responses. Finally, the last section of the chapter presents the detailed discussion about the prime objectives of the proposed work.

1.1 Passenger safety and crashworthiness

In the crash event of commercial vehicles, passenger safety is of utmost importance. In the corresponding crash event, the merit of passenger safety is determined based on crashworthiness, which is a function of structural performance of the vehicle structure under the dynamic loads. In most of the vehicle structures, the ability of the structure to manage the impact energy by dissipating the kinetic energy of the impacting body into plastic deformation or internal energy is referred as a merit of the structural performance [1]. The subtypes of the structural performance depend on the type of dynamic load. For instance, because of the high inertia in case of frontal impact and highly stiff structure, the acceleration or the reaction forces experienced by the passenger cabin are enormous. Such factors can make a strong impact on the occupant head and chest, which are the prominent factors in the passenger injury criteria [2]. Whereas in case of side impact on the structure with poor stiffness, the excessive intrusion of the impacting body may slit the passenger compartment leading to sever injuries to occupant [3]. Thus, it is desired to have vehicle structures with high structural integrity, which depends on the overall design of the structure. Besides passenger safety, there are couple of other factors are considered while designing the vehicle structures, which indirectly affect the overall vehicle performance over the span of corresponding life cycle.

Firstly, as the performance of vehicle structures should comply with the high passenger safety requirements, additional components can be added to the vehicle

structure. However, these additional components add more weight to the vehicle, which can affect the fuel economy of the vehicle [4]. In some other cases, structure with high durability, which are made up of heavy material, are preferred to enhance the overall stiffness of the vehicle. However, these structures also worsen the issue of lightweight structures and in turn worsen the running efficiency of the vehicle.

Thus, design of vehicle structures with lightweight material has also become a research domain of a great interest. Indeed, such areas of research indicate that weigh reduction of vehicle structure is one of the affective way to increase fuel efficiency and to save the raw material [5]. Secondly, some of the research group also considered the maintenance cost of the vehicle while designing the crashworthy structures. The factor of repair cost is mostly very specific to the deformable structure at the front end of the vehicle. The maintenance cost mainly consist of the repairing cost of the damaged structure. Especially, in the research based on low speed collisions, efforts are made to design a structure, which could be damageable but must be cost effective to repair after the crash even happens [6].

In sum, while addressing the issue of heavyweight structures and the higher repair cost, the safety of the car occupants should not be compromised [5]. In other words, for optimal design of vehicle components, the structural performance must have more importance than other cost related factors. Therefore, with various analyses and optimization techniques, it is possible to obtain conceptual design of the vehicle structure with desired structural performance with the reduced design cycle time [7]. Some of these techniques are focused on enhancing the ability of the structure to dissipate the kinetic energy of the impacting body into internal energy [8]. Whereas some of the structural optimization techniques are specifically focused on the crash responses such as acceleration of the vehicle structure and intrusion of the impacting body into vehicle structure, which have direct effect on the passenger injury criteria. For obtaining the optimized structure for a particular loading condition, it is very important to simulate the crash event with appropriate loading and boundary factors. Therefore,

prior to structural optimization, nonlinear finite element solvers are used, which are briefly discussed in the subsequent section.

1.2 Nonlinear solvers for crash simulations

Crash simulations and the corresponding finite element outputs are time-dependent entities. These time dependent finite element outputs can be evaluated using solving the equilibrium equation by implicit method as well as by explicit method.

$$M\ddot{d}(t) + C\dot{d}(t) + Kd(t) = F(t) - R(d,t) \tag{1.1}$$

where entities M, C, and K represents the mass, damping, and stiffness matrix, respectively. (1.1) On the other side of the equation, F is the external force and R is the residual [9]. However, in case of implicit solvers, the global information about the displacement d is evaluated at each time-step. This makes implicit solver more accurate but also makes it computationally very expensive. On the other hand, in case of explicit solvers, the information of displacement is gathered using direct numerical integration of the equation of motion. This makes explicit solver quicker than the implicit solver. Therefore, the explicit method is usually implemented to solve and evaluate the finite element parameter in case of crash simulations.

Therefore, to implement explicit method to solve nonlinear problem, in the proposed work LS-DYNA package has been used to simulate the crash event. Apart from LS-DYNA, there are several commercial packages such as PAM-CRASH, ANSA, and ANSYS-EXPLICIT are available with the implementation of an explicit solver. Among these packages, LS-DYNA is widely used in the application of crash simulation. To define and create the finite element model of the crash scenario, LS-Pre/Post is usually used as pre-processor as well post-processor for LS-DYNA. However, LS-DYNA solver can also receive finite element model from other pre-processor such as MSC-Patran and Hypermesh [10], [11].

Moreover, with LS-DYNA capabilities, the finite element outputs or responses are usually show a very good agreement with the results of physical test or physical crash event [12]. The prime reason behind this accuracy in finite element outputs are the key features of the corresponding pre-processor. Some of these key features comprises of various controls over the energy balance, user defined time-step, and the control over the element section (shell and solids). Besides these features, default pre and post processor (LS-Pre/Post) of LS-DYNA also provides large number of contact models, material models, and element section models, which altogether flexibility for users to select desired or appropriate options [13], [14].

Furthermore, LS-Pre/Post also provides flexibility to evaluate finite element responses with respect to different number of center of gravity. Thus, with this advantage, the user can separately evaluate finite element responses of any particular node, part, set of the parts and whole system. The details of these key features are further explained in the chapter of numerical examples. The outputs of such an accurate finite element solver can be coupled with structural optimization techniques to solve the optimization problem of vehicle structure. The detailed discussion regarding the structural optimization techniques are provided in the subsequent section.

1.3 Structural optimization

For mechanical structures, it is very important to carry the externally applied loads with desired structural performance. In the case, where a particular structure fails to provide the desired structural performance, it creates the need of structural optimization. In most of the optimization problems, in order to find optimal design variable, the structural performance is treated as an objective function and it is subjected to one or more functional constraints as well as the box constraints. For instance, to find optimized cross-sectional dimensions of the simply loaded beam structure, maximization of the stiffness of the beam can be treated as an objective function. Whereas, the mass of the beam can be treated as a functional constraint

and upper as well as lower limits can be set on the cross-sectional dimensions as box constraints.

Thus, to address the issue of the structural performance for a particular loading condition, the corresponding structure can be optimized by three prime optimization techniques namely size optimization, shape optimization, and topology optimization [15]. In size optimization any geometric dimension of the structure can be treated as a design variable, which is further optimized based on the corresponding objective function and functional constraints.

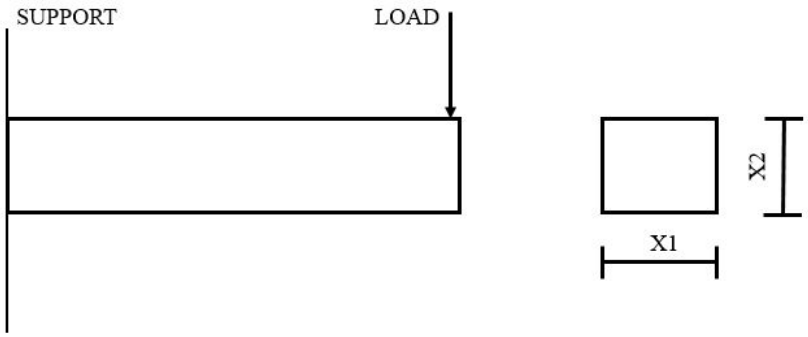

Figure 1.1. Size optimization

As shown in Figure 1.1, a cantilever beam is subjected to vertical load. With size optimization, X1 and X2 (cross sectional dimensions) can be treated as design variables, which are to be optimized by maximizing stiffness as an objective function. In this case, the upper and lower limit on X1 and X2 are box constraints, whereas mass of the beam can be treated as a functional constraint. In this technique of optimization, the focus is on finding the optimal values of X1 and X2, whereas the density distribution over the entire initial design is not altered.

In case of shape optimization, the same engineering problem can be solved by altering the form or contour of the specific areas of the initial design. In other words, instead of finding the optimal values of X1 and X2, shape optimization technique determines optimal outer shape or contour of the beam (Figure 1.2).

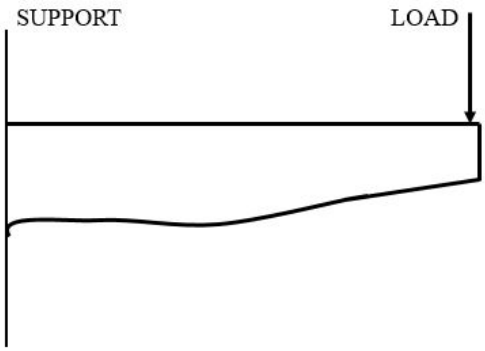

Figure 1.2. Shape optimization

In this technique, the connectivity between the nodes goes not get affected by the change in the contour. Also, the change in the contour is obtained without changing the boundaries of the initial design [15].

Finally, focusing on the structural optimization method implemented in the proposed work, the topology optimization is widely used structural optimization technique, in which the initial design is optimized by altering the density distribution within the corresponding design domain. To exemplify the capabilities of topology optimization, illustration of a cantilever beam problem is shown in Figure 1.3.

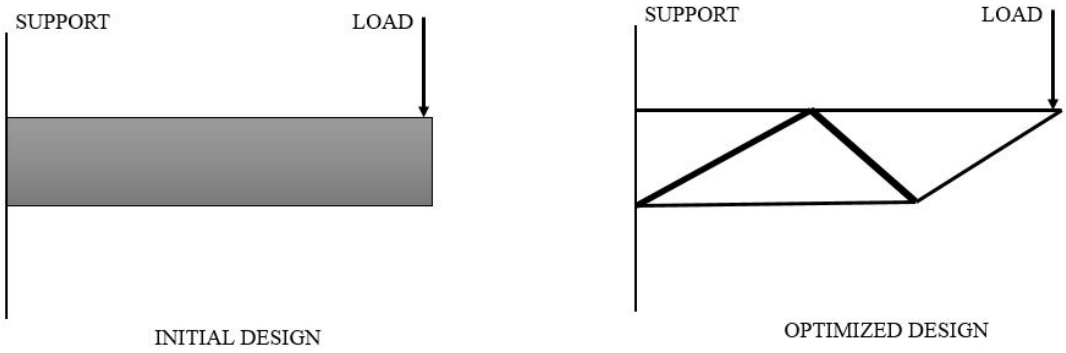

Figure 1.3. Topology optimization

In this problem formulation, the area with grey color is treated as a design domain, whereas the relative densities of discrete cells of the design domain are treated as design variables. The relative densities are determined by mapping the original density of the material between zero and one. In order to achieve the desired objec-

tive function, relative density distribution over the entire design domain is updated. Thus, the optimized structure usually consists of solid and void structure (Figure 1.3), where the solid area (black color) has relative density equal to one and void area has relative density equal to zero. The general problem formulation of the topology optimization is given as follows:

$$\begin{aligned} \text{To find} \quad & x \in \mathbb{R}^{\mathrm{N}} \\ \text{minimize} \quad & f(x) \\ \text{Subject to} \quad & xv - V = 0 \\ & 0 \leq x \leq 1 \end{aligned} \tag{1.2}$$

where $f(x)$ in an objective function, which is to be either maximized or minimized (problem dependent). The final design is always subjected to the volume fraction constraint V, where xv is the actual volume of the final design. As mentioned before, the relative density x is mapped between 0 and 1, which is then modified or updated based on the update rule of the optimization technique.

In recent years, there are various linear as well as nonlinear topology optimization techniques have been developed and implemented by number of research groups. To address the nonlinear dynamic problems such as obtaining the crashworthy designs for vehicle components, some of the research groups have introduced the nonlinear explicit topology optimization methods as nonlinear topology optimizers have ability to consider time-dependent crash parameters throughout the optimization process. Therefore, these solvers can be coupled with nonlinear finite element solvers to obtain the finite element outputs explicitly. However, some research groups have also simplified the nonlinear problem to perform the topology synthesis.

Focusing on the nonlinear topology optimization techniques, Tovar et al. introduced an implementation of a proper control strategy in cellular automaton (CA) [16], [17]. In their method, the control loops were distributed over the design domain, with which the local design variable (density) was updated based on the finite element response. In the control strategy, proportional, derivative, integral, and two position controllers had been used to make the method computationally

effective. Furthermore, Patel et al. [9] used the hybrid cellular automaton (HCA) for the continuum-based topology optimization at the component level. Their work demonstrated the ability of HCA to obtain crashworthy structures with maximum displacement constraints. The corresponding authors have also illustrated the advantages of the intermediate initial design, where initially relative density between 0 and 1 was assigned to each cell of the design domain. In the same point of time, Mullerschon et al. tested HCA to increase the uniform energy absorption for the given mass fraction, in which the HCA was developed into the software user interface LS-OPT/Topology [18]. In 2013, the HCA was further developed by Bandi et al. [19] for the compliant mechanism synthesis. The method showed promising ability to obtain different force-displacement profiles by tuning position of the output ports of compliant mechanism and the volume fraction of stiff and flexible design domains. This study also opened the scope of implementing the design of experiment to determine the effect of position of the output ports of the compliant mechanism on the force-displacement responses.

The HCA method was further extended from the continuum structures to the thin-walled structures in which, the HCA was successfully modified to distribute optimum thicknesses into sheet metal structures by Mozumder et al. [20], [21]. In their work, the optimal distribution of thickness in the thin-walled structure was obtained by incorporating the performance constraints such as displacement and reaction force as well as manufacturing constraints. Unlike the previously discussed HCA, this method treated the thickness of each meshed element as a design variable instead of the relative density. Furthermore, the advanced application of HCA for thin-walled structures was introduced by Shinde et al. [22]. Their work coupled the compliant mechanism and HCA in order to obtain the progressive buckling of the front rail of vehicle under the axial and oblique dynamic loading. With the progressive buckling, the method also maximized the internal energy absorption by limiting the peak reaction forces over the time of impact.

In the recent years, the HCA was further improved to HCATWS (hybrid cellular automata for thin-walled structures) by Duddeck et al. [23] with the work focused on the final mass of the topology design and the displacement constraints. Their method introduced an additional mass update rule based on the numerical discrepancy between current displacement response of the structure and the preset constraint. The corresponding author implemented a loop in which mass is added to the design if the design is infeasible to match the displacement constraints, whereas the mass was deducted if the design is feasible. With preliminary observation, it was concluded that this method works very well but only for small number of design variables. Therefore, Zeng and Duddeck [24] developed the same idea by proposing an idea of bi-section rule, which can converge the topology optimization problem with the exact target mass fraction but with no extra function evaluation. The bi-section rule provides the smaller change in the mass between infeasible and feasible designs, so algorithm can explore lighter design than the design with previously used HCATWS.

As it was mentioned earlier in this literature review, some of the research group have proposed methods of simplifying a nonlinear loading problem into the static loading problem to solve the problem of topology optimization. These methods are mainly developed to evaluate less number of function evaluation and to save the computational time. To achieve these objectives, a method of equivalent static load (ESL), which can transform the dynamic load into equivalent static loads based on the displacements information [25]. Kaushik and Ramani proposed the use of equivalent linear systems from the nonlinear dynamic simulation on two dimensional problems [26]. Their work consisted a discrete material topology optimizer to minimize the mass of the two-dimensional domain with displacement and acceleration constraints. The advanced applications of the ESL were introduced by Ahmad et al. for case studies consisting the material, geometry, and contact nonlinearities [27]. Further, the ESL was implemented on a larger scale by Tian and Gao to optimize the body in white (BIW) under the crash loads including frontal impact, side barrier impact, roof crush and rear impact [11]. With equivalent static or linear loads, their proposed

work considered single as well as multiple load cases with constraints on the maximum intrusion in the front, rear, and passenger cabin.

Beside the nonlinear optimizers and the method of equivalent static load, there are other unique topology optimization approaches to increase structural performance. The optimal material distribution with the approach of multi-domain and multi-step topology optimization was proposed by Wang in 2004 [28]. In their work, the propose method of homogenization showed a great promise in case of controlling the crash forces to the some extent. In 2010, Xu et al. proposed an idea of adding reinforcement supporters and triggers (weaknesses) into rail structure of the vehicle to form plastic hinges so structure can absorb maximum internal energy [1].

However, despite the efficiency of methods other than nonlinear optimization techniques, it was observed that the nonlinearities involved in the crash simulations can be handled by nonlinear optimizers in more sophisticated way. Therefore, the proposed work further developed the hybrid cellular automata (HCA) to obtain the lightweight designs with controlled crash responses. This extended version of HCA is then coupled with the response surface technique to predict and tailor the crash responses. The brief introduction of response surfaces techniques is given in the next section.

1.4 Response surface methods

In the design optimization problem, the optimal design parameters are determined by minimizing or maximizing the objective function. In such a case, it becomes very important to determine how objective changes with respect to the change in the design parameter. This change in the behavior of the objective function with respect to change in the design parameters is also called sensitivity.

For instance, if $f(x)$ is a specific response and x is the design parameter, then it is very important to determine the relationship between $f(x)$ and x. Because based on this relation, for any random design parameter x_{new}, the response $f(x_{new})$ can be

predicted. In some case, if the explicit relation or an explicit formula of the objective function with respect to design parameter is available, then it becomes very easy to predict $f(x_{new})$ for any x_{new}.

Focusing on the field of crashworthiness, in the physical crash event, the prediction of the crash responses is achievable with pre-crash system which is based on parameters such as time to collision and velocity of the vehicle [29]. However, while dealing with the computer simulations, most of the vehicle design optimization problems face two challenges in while predicting the crash responses with input design parameters: firstly, under the dynamic loading, ,these crash responses have a very high sensitivity with respect to the design parameters. In other words, small change in the design parameter such as volume fraction of the topology design can make drastic change in the acceleration of the vehicle structure. Secondly, it is very difficult to obtain the exact explicit relationship between the crash responses and the design parameters.

Therefore, to address such issues, it is very important to build an implicit relationship between crash responses and the corresponding design parameters. Response surface methods are proved to be very useful to build such an implicit relation between crash responses and design parameters [30]. This relationship further can be utilize to predict the value of the crash response with respect to the given design parameters or vice versa. Most of the response surfaces are based on the second or higher order polynomial regression. However, as previously mentioned, the crash responses are highly nonlinear and sensitive with respect to the design parameters, high fidelity meta-models such as Kriging, inverse distance weighing, and artificial neural network can be implemented to build an implicit relation between crash responses and the design parameters.

In the proposed work, Kriging meta-model has been utilized to predict the crash responses. The fidelity of the meta-model is determined using the techniques of cross validation. The detailed discussion of the prediction technique is provided in the corresponding chapter of methods.

1.5 Objectives of the proposed work

The literature review depicted the importance of the passenger safety and the crashworthiness of the vehicle structures. The practical requirements of the crashworthy designs are need to be defined and addressed in terms of technical design requirements. For this purpose, the issues regarding the practical requirements of the crashworthy designs are addressed in the proposed work by setting up the following objectives.

1.5.1 Introduction of a new design control parameter

In practical topology optimization problem, the volume fraction constraint is usually imposed on the design domain to be synthesized. Therefore, the performance of the final design (for example, stiffness) prominently vary according to the provided volume fraction. This implies, in order to obtain the particular performance, the designer has to compromise with the final volume or mass of the design. Therefore, it is important to find new control parameter, which can have significant effects on the performance of the final structure. Therefore, to improve the hybrid cellular automata (HCA) method, the proposed work introduces design simulation time as a new control parameter, which can affect the final structure, load paths, and the corresponding performance. It would also enable designer to obtain the number of topology designs for the same volume fraction. This would provide flexibility to designer to choose the structure with a better performance for the same mass.

1.5.2 Targeting the desired crash responses

The design time along with the volume fraction provides the bi-dimensional design space for the topology synthesis. In other words, there would be two design parameters that can control the performance of the final structure. Therefore, the second milestone of the proposed work is to implement a metamodelling technique to

set up the implicit relationship between the performance of the topology design and the input control parameters (deign time t_d and volume fraction VF). The proposed work utilizes the crash responses such as maximum acceleration and maximum displacement of the topology design as the performance measures. This implicit relation between crash responses and the design control parameters further can be utilize to predict the design control parameters to obtain the target crash responses. These predictions of t_d and VF can be supplied to the improved HCA to obtain the actual crash responses and the corresponding error relative to the desired crash responses.

1.5.3 Crash response improvement of lightweight structures

In the engineering problem of crashworthiness, it is important to improve the crash responses of the vehicle structures by minimizing the corresponding peak acceleration and the peak displacement. At the same time, it is preferred to have a lightweight design of the vehicle structure to minimize the overall mass of the car body. Therefore, in the final milestone, the proposed work implements the approach of the multi-design time and merged design to lower down both peak acceleration and peak displacement of the topology design with low volume fraction constraint. The approach of multi-design time converts the problem formulation of single dynamic loading into multiple dynamic loading, whereas the merged design approach consists the post-processing of the different topology designs to obtain a new design with a better crash responses.

2. HYBRID CELLULAR AUTOMATA (HCA)

This section thoroughly discusses the methods which have been utilized in the proposed work to generate topology designs with controlled crash responses. The first subsection of this chapter explains working of the hybrid cellular automata (HCA) and the importance of the design time in the corresponding topology synthesis of design under the single dynamic load. The chapter is further extended to discuss the contribution of the Kriging predictor to predict optimal design parameter for the target crash responses. The final section of this chapter shows the implementation of design time to enhance structural performance of the structure throughout the time of crash event by using multi-design time and binary operations.

The hybrid cellular automata method is based on the fundamental principles of cellular automaton (CA). Cellular automaton has grid of elements in which, each element has its corresponding neighborhood (Figure 2.1). As shown in Figure 2.1,

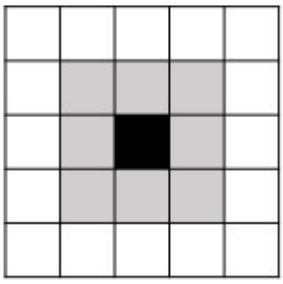

Figure 2.1. Neighborhood of the element

in the grid of elements, the black element is the element whose information is to be calculated and grey elements of the grid comprise the corresponding neighborhood of the element. The information of each element is stored in the vector form based on the information of the corresponding elements neighborhood. The HCA algorithm uses the finite element model of the structure under the dynamic load to obtain the local

information of each element, thus HCA is called as a hybrid form of CA [9]. In the proposed work, nonlinear explicit code LS-DYNA is used to obtain the information of each element. This information mainly consists a field variable and the design variable in the corresponding vector. This vector is continuously updated based on the finite element analysis of the updated design. The vector of each element is expressed by

$$\beta_i^k = \begin{Bmatrix} U_i^k \\ x_i^k \end{Bmatrix} \tag{2.1}$$

where, for kth iteration of topology synthesis, β_i is the information vector of ith element. The field variable U_i is the internal energy density (IED) and the design variable x_i is the relative density of the corresponding element.

2.1 Material parameterization

The relative densities x are obtained by mapping the actual density of the material between 0 and 1. These relative densities are also used to assign the intermediate material properties to every element throughout the topology optimization process [31]. The intermediate material properties are generated using the power law approach of solid isotropic material penalization (SIMP) [32], [9]. Therefore according to SIMP, the intermediate material properties are defined as

$$E(x) = x^p E_o \tag{2.2}$$

$$\sigma(x) = x^p \sigma_o \tag{2.3}$$

where, p is the penalization factor of SIMP. This penalization factor and relative density x interpolate the base material properties such as modulus of elasticity E_o and base yield stress σ_o. This interpolation results in $E(x)$ and $\sigma(x)$,which are the intermediate modulus of elasticity and yield stress respectively. To maintain numerical stability in the computation, this power law is also used to drive away the intermediate densities toward either 0 or 1.

2.2 Problem formulation with traditional HCA

For ith element, the internal energy density (IED) of each element of the neighborhood is then averaged to obtain $\bar{U}_i$, which is the an averaged IED. This averaged field variable $\bar{U}_i$ can be expressed as

$$\bar{U}_i = \frac{U_i + \sum_{n \in N} U_n}{N + 1} \tag{2.4}$$

where, N is the total number elements in the neighborhood of the ith element and U_n is the internal energy density of nth number of element in the neighborhood.
The set point for IED U_i^* of every element is also calculated when the corresponding relative density x_i is 1. Based on these terms, the topology optimization problem using traditional HCA can be formulated as

$$\begin{aligned} \text{find} \quad & x \in \mathbb{R}^N \\ \text{minimize} \quad & f(x) = \sum_{i=1}^{N} \left| \bar{U}_i(x) - U_i^* \right| \\ \text{subject to} \quad & g(x) = \sum_{i=1}^{N} x_i v_i - VF = 0 \\ \text{where} \quad & x_{min} \leq x \leq 0 \qquad\qquad i = 1.....N \end{aligned} \tag{2.5}$$

where, volume fraction VF is the ratio of mass of the final structure and mass of the design domain. The volume fraction is the global constraint set by the designer.

2.3 Local variable update

In every iteration of the topology optimization, the HCA reads the averaged IED or field variable $\bar{U}_i$. The numerical discrepancy between set point U_i^* and the averaged IED $\bar{U}_i$ is calculate to change the relative density x. The calculation of change in the relative density Δx is given as

$$\Delta x_i = K(\bar{U}_i - U_i^*)/U_i^* \tag{2.6}$$

where, K is the scaling factor. This change in the relative density Δx is then added to the current relative density x_i of the ith element [33]. Based on this update rule,

relative density of every element is updated and the new design is sent back to LS-DYNA for the finite element analysis of the next iteration. The minimum value of the relative density x_{min} is kept as a non-zero number to avoid the singularity in the calculations as well as to keep the structural stability throughout the topology synthesis.

2.4 Convergence criteria

The topology synthesis can converge because of two possible reasons. Firstly, the synthesis is terminated if it reaches the maximum number of iteration. In such case the design of the final iteration is considered as the optimized design. Second reason for synthesis termination is the overall change in the topology. As expressed in (2.7), if the overall change in the topology is less than or equal to preset value ϵ [31]. In the proposed work the value of ϵ is set as 0.001 as a termination criteria.

$$\sum_{i=1}^{N} \Delta x_i \leq \epsilon \tag{2.7}$$

2.5 Issues associated with traditional HCA

In the field of crashworthiness, topology synthesis is performed in order to obtain either stiff or deformable structures. In traditional HCA method, stiffness of the structures depends only on the volume fraction V set by the designer. It implies, the structure with higher volume fraction has more stiffness than the structure with the lower volume fraction. Therefore, the desired volume fraction and the corresponding stiffness directly affect the crash responses of the structure under the dynamic impact. For instance, if two structures with different stiffness are subjected to the same dynamic loading condition, then the structure with high stiffness will have less displacement than the structure with the low stiffness. Therefore, if designer is supposed to obtain structure with high structural integrity (high stiffness) then the final volume fraction will be compromised, which in turn result in the heavyweight struc-

ture. In sum, it is very important to relate the structural performance with other design parameter than volume fraction, so one can control and obtain a very good structural performance even with a lightweight design.

3. THE IMPROVED HYBRID CELLULAR AUTOMATA

As mentioned in the previous section, the stiffness of a vehicle structure drives the crash responses such as an intrusion of the impacting body and the acceleration of the passenger compartment. To control these crash responses even with a lightweight structure, the proposed method emphasizes on the importance of the simulation time of the dynamic crash event. The discrepancies between the proposed method and the traditional HCA are explained in this section.

3.1 Design time

In the HCA method, after every iteration of the topology synthesis, the finite vector of each element is updated with a new internal energy density (IED). The state of neighborhood of an element plays an important role, as the IED of each element is calculated based on IED of elements in the neighborhood. For dynamic loading cases, the IED of every element mainly depends on the propagation of the strain waves through the design domain. Based on the boundary conditions, the strain waves travel through the different load paths over the time span of the dynamic loading. Thus, at every point in time, each element has varying IED throughout the time span of the dynamic loading. However, with traditional HCA, the IED at the end of the dynamic loading is taken under the consideration for topology synthesis. Thus, it is important to utilize the whole time span of the dynamic loading to store the IED at specific times. A finite element model (FEM) in LS-DYNA can record and store IED at different times throughout the dynamic loading, which can be supplied to the HCA for topology synthesis.

In the proposed method, the specific time at which internal energy density (IED) is recorded is defined as a design time t_d. The role of design time affects all important

entities related to each element of the structure. Firstly, the IED of whole neighborhood of each element becomes the function of the design time. As the calculation of field variable U_i of each element is based on the IED of the corresponding neighborhood, field variable $\bar{U}_i$ and set point U_i^* become the time dependent entities. Finally, as the updates on design variable x_i are made based on the numerical discrepancy between the averaged field variable $\bar{U}_i$ and set point U_i^*, the design variable x_i also becomes the function of design time. Therefore, the information vector of each element is now expressed as

$$\beta_i^k(t_d) = \begin{Bmatrix} U_i^k(t_d) \\ x_i^k(t_d) \end{Bmatrix} \tag{3.1}$$

where, t_d is the design time at which a new field variable $U_i^k(t_d)$ is supplied to HCA for topology synthesis.

3.2 Problem formulation with the improved HCA

Based on these time-dependent entities, the topology synthesis problem, now can be formulated as

$$\begin{array}{ccc} \text{find} & x \in \mathbb{R}^N & t_d \in \mathbb{R}^N \\ \text{minimize} & f(x,t_d) = \sum_{i=1}^{N} \left| \bar{U}_i(x,t_d) - U_i^*(t_d) \right| & \\ \text{subject to} & g(x,t_d) = \sum_{i=1}^{N} x_i(t_d) v_i - V = 0 & \\ \text{where} & x_{min} \leq x \leq 0 & i = 1.....N \end{array} \tag{3.2}$$

The problem formulation given in (3.2) implies that the update in the local design variable (relative density) x_i has totally become a time-dependent process. Therefore, at the convergence of topology synthesis, the overall stiffness of the structure and the corresponding performance under the dynamic load will vary according to the chosen design time. Now, with this approach, the final volume fraction V and design time t_d will be having combined effect on the structural performance. The preliminary observations showed that the load paths of the final structure and corresponding structural integrity greatly depend on the design time.The crash responses shown in

Figure 3.1 represents the behavior of any structure under the dynamic loading. The acceleration-displacement profiles are evaluated at minimum and maximum possible design time. Here, the maximum t_d is equal to the termination time of the dynamic impact. Interestingly, with the minimum design time (t_d), the HCA functions similar

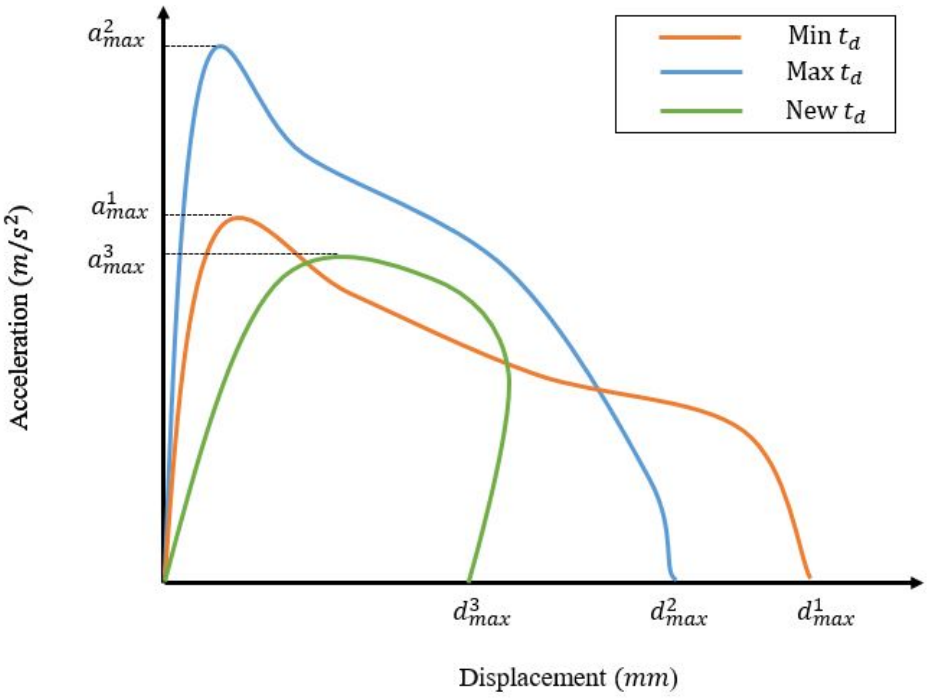

Figure 3.1. Trade-off between acceleration and displacement

to the linear optimizer. Whereas, when t_d is set to maximum, the HCA performs as nonlinear optimizer and generates the optimized structure. Thus, it can be observed with minimum t_d, the peak acceleration of the final structure is less than the corresponding acceleration of structure with maximum t_d. On the other hand, the displacement of the structure with minimum t_d is more than the displacement of the structure with maximum t_d (Figure 3.1).

It is very clear that there is a trade-off between acceleration-displacement profiles and the design time. However, there is no proof about the monotonic relationship between acceleration-displacement profiles and the design time t_d, it becomes very interesting to evaluate the effect of the intermediate design time (t_d between minimum

and maximum) on the acceleration-displacement profiles. Therefore, the proposed work makes use of this advantage and tries to obtain the structure with the low acceleration and low displacement, which is shown by green profile in Figure 3.1

Also, as one can vary design time for the same value of volume fraction, it is now possible to obtain number of topology designs without changing the mass of the final design. This in turn opens up the scope of obtaining desired crash responses even with a lightweight structure (with low volume fraction). The strategy to reach close to the target crash response is explained in the subsequent section.

3.3 Targeting the crash responses

The proposed work deals with the computer models and the corresponding simulations of crash events. As mentioned in the previous section, the improved HCA can be utilized to generate structure with the desired or the target crash responses. To achieve this goal, it is very important to understand behavior of the crash responses of the structure with respect to the corresponding design parameters. Studies show that building an approximation model of crash responses with respect to design parameters is a very effective technique to deal with non-smooth behavior of crash response [34].

As the proposed work introduced the design time as an effective parameter in order to generate topology designs with varying structural performance, along with volume fraction of the final design, the design time can play the role of second design parameter. On the other hand, the acceleration of the topology design and intrusion or displacement of the impacting body into topology design are used as outputs responses. While dealing with the number of computer models, Kriging can be used as an effective technique in order to generate the approximation of output responses with respect to input design parameters [35].

3.3.1 Step 1: Sampling

The first step to build an approximation model of outputs with respect to input is to select the samples of design variables to build design of experiments (DOE). There are several sampling techniques, which are widely used such as Latin hypercube sampling, full-factorial sampling, and composite sampling [36].

However, in the proposed work, the user defined sampling is used to build the design of experiments t_d of design time and the volume fraction VF. While sampling the design time, computational cost is considered. Whereas, in case of the samples of volume fraction, the upper limit of the volume fraction is kept as low as possible to generate lightweight structures. Therefore, the total number of design of experiments Z can be given as

$$Z = n \times m \tag{3.3}$$

where, n and m are the sample sizes of the design time and volume fraction respectively. The finite element models (FEM) of all experiment are prepared using LS-Pre/Post under the specific and same boundary conditions, so the information about the design time t_d can be provided to HCA.

3.3.2 Step 2: Topology synthesis

Once the design of experiments (DOE) is ready, topology synthesis can be performed using the improved HCA. For every experiment, the improved HCA updates the relative density x_i of each element based on the field variable U_i at the given design time t_d. The volume fraction constraint is also satisfied based on the value of VF for the corresponding experiment. after every iteration of topology synthesis, the updated design is sent back to solver of LS-DYNA to perform finite element analysis. After the convergence of topology synthesis, the final design is sent back to LS-DYNA to evaluate the corresponding structural performance.

3.3.3 Step 3: Evaluation of crash responses

Topology design of every experiment is imported to LS-DYNA to perform finite element analysis of the corresponding structure under the specific boundary conditions. The simulation time for these all analyses is kept constant. The proposed work considers the acceleration and displacement as crucial crash responses under the dynamic loading. Therefore, for every topology design, maximum acceleration a_{max} and maximum displacement d_{max}, throughout the analysis, are evaluated. These values are then supplied to metamodeling technique to build the approximation model of crash responses with respect to design parameters (t_d and VF) or vice versa.

3.3.4 Step 4: Metamodelling

Once LS-DYNA evaluates the crash responses (a_{max} and d_{max}) for Z number of topology designs, the available set of data is used to build the metamodels (Table 3.1).

Table 3.1.
Database for metamodels

DOE	Design time	Volume fraction	Max dis	Max acc
1	t_d^1	VF_1	d_{max}^1	a_{max}^1
.	.	.	.	.
.	.	.	.	.
Z	t_d^Z	VF_Z	d_{max}^Z	a_{max}^Z

In this case, Kriging metalmodel is implemented to build relations between input design parameters and output crash responses. With the proposed approach, designer has total control over the design time and volume fraction, which are used to generate a topology design with a specific structural performance. Therefore, it is better to build an approximation models or metamodels of design time t_d and volume

fraction VF in terms of available set of maximum acceleration a_{max} and maximum displacement d_{max}. These reversed metamodels can be expressed as

$$\hat{t_d} = y(a_{max}, d_{max}) \tag{3.4}$$

$$\hat{VF} = y(a_{max}, d_{max}) \tag{3.5}$$

where, $\hat{t_d}$ and $\hat{VF}$ are the metamodels of design time and volume fraction respectively. In this case, these metamodels representing design time and volume fraction as implicit functions of maximum acceleration and displacement.

To understand the fundamentals of metamodeling technique, it is very important to understand the stochastic process model of any function. Supposing that the function $y(s_i)$ depends on the variable s_i, whose sample size is Z $(i = 1, .., Z)$. This would result in Z number of function evaluation. If the linear regression technique is applied to relate the function $y(s)$ and variable s, then the regression model is expressed as

$$y(s) = \sum_{i=1}^{Z} \beta f(s_i) + \epsilon^i \tag{3.6}$$

where, $f(s_i)$ is the linear approximation of the function with respect to s_i and β is the coefficient of regression. ϵ^i is the normally distributed error of the approximation [37]. The issue with this model is, the individual error ϵ associated with each sample of s is ignored and it is normally distributed.

Thus, Kriging technique emphasizes on individual error $\epsilon(x_i)$. If the function $y(s)$ is continuous then the corresponding error $\epsilon(x)$ is also continuous. In such case, if two samples $s_i and s_j$ are close then the corresponding errors $\epsilon(x_i)$ and $\epsilon(x_j)$ are also close. Therefore, it is not appropriate to normally distribute the regression error ϵ^i.

It implies that the correlation between the errors associated with individual samples of the variable x. This correlation between errors ($\epsilon(x_i)$ and $\epsilon(x_j)$) highly depends on the distance between x_i and x_j. This distance can be expressed as

$$d(x_i, x_j) = \Theta \left| x_i - x_j \right|^p \tag{3.7}$$

$$\Theta \geq 0 \quad \text{and } p \in [1, 2]$$

where, p denotes the smoothness of the function and θ represents the sensitivity of function with respect to the corresponding variables. In other words, higher the value of θ, higher the change in the function even with a small change in $|x_i - x_j|$. This implies, if a small change in two values of acceleration or displacement is making the considerable change in the prediction of design time t_d or volume fraction VF, then value of θ is high. This distance formula is utilize to determine the correlation between the errors associated with x_i and x_j, which is given by

$$\text{Corr}[x_i, x_j] = \exp[-d(x_i, x_j)] \tag{3.8}$$

It can be observed that, more the distance between the two sample points of the variable ($x_i and x_j$), lower will be the value of correlation between the corresponding errors (3.7) and (3.8). The correlation between errors has all relevant and important properties of metamodel of the function such as smoothness of the function p and sensitivity of the function with respect to variables θ. Therefore, it becomes a very powerful technique to build a metamodel based on the correlation between errors so that one can afford to convert regression term a constant term. Thus, Equation (3.6) now can be expressed as

$$y(s_i) = \mu + \epsilon(x_i) \tag{3.9}$$

where, μ is the mean of the stochastic process and $\epsilon(x_i)$ is the error associated with the corresponding mean [37] the value of $\epsilon(x_i)$ is either 0 or σ^2 (variance). The equation of correlation of errors suggests that value of $\epsilon(x_i)$ can never be zero, thus the Equation (3.9) can be re-written as

$$y(s_i) = \mu + \sigma^2 \tag{3.10}$$

Now, the variance has the characteristics of both smoothness p and the sensitivity of the function θ. Therefore, for any new input s_new, the prediction of the output is obtained by internally optimizing the values of μ, σ, θ, and p using the likelihood function. The likelihood function represents how likely the prediction will fit into the metamodel. The explanation of the likelihood function and the estimates of optimal μ and σ can be found in the article of efficient global optimization [37].

Thus, with metamodel $y(s)$, for any new input s_{new}, the mean μ represents the predicted output, which comes with the corresponding variance σ. As the quality of the metamodel $y(s)$ has become the combination of regression constant μ and the correlation factor σ, the type of approximation and correlation function used greatly affect the prediction. Therefore, it is very important to evaluate quality of the metamodel $y(s)$ by some sort of cross-validation technique. The validation technique implemented in the proposed work is explained in the subsequent section.

3.3.5 Step 5: Cross-validation

The cross-validation techniques are implemented to evaluate the quality of the metamodel prediction (μ) and the corresponding variance (σ). Usually, the metamodel is validated three simple steps. First step is to delete some of already available inputs and the corresponding actual outputs. Second step is to obtain the predicted outputs for the deleted inputs. Final step is to evaluate the error between the actual and the predicted output to evaluate the quality of the metamodel [38].

The proposed work uses leave one out cross-validation (LOOCV) technique to evaluate Kriging metamodels of design time $\hat{t_d}$ and volume fraction $\hat{VF}$ (3.4) and (3.5). In LOOCV three steps of validation (mentioned above) are followed by deleting only one input at a time. For instance, if there are z number of samples of variable s then there will be equal number of actual function evaluation. Thus, LOOCV deletes a sample point s_i and the corresponding actual function evaluation $y(s_i)^*$. Now, the database has $z-1$ number of samples and the corresponding actual functions. The Kriging metamodel is then build based on the $z-1$ samples. The deleted sample point s_i is fed to this new metamodel to evaluate the corresponding predicted function value $y(s_i)$. The numerical discrepancy between the actual function $y(s_i)^*$ and the predicted function $y(s_i)$ is evaluated. This discrepancy is normalized by the standard

deviation of metamodel with $z-1$ points to evaluate the error of the corresponding sample point. The error evaluation is expressed as

$$e_i = \left|(y(s_i)^{z-1} - y(s_i)^*)/\sigma_i^{z-1}\right| \tag{3.11}$$

This error e_i is evaluated for every sample point of the available database. Therefore, for z number of samples, the final error vector is given by

$$e = \begin{bmatrix} e_1 \\ . \\ . \\ . \\ e_z \end{bmatrix} \tag{3.12}$$

This error vector e is further characterized to evaluate the predicted residual error sum of squares (PRESS) to conclude the cross-validation [39]. The PRESS evaluation is given by

$$\text{PRESS} = \sqrt{\frac{1}{z} \quad e^T e} \tag{3.13}$$

where, z is the total number of samples in the database.

As mentioned in the previous section , the quality of the Kriging metamodel has the combined effects of regression functions and the correlation functions. Therefore, this procedure of PRESS evaluation is conducted using all possible combinations of available regression functions and the correlation function. The following table provides some of the regression and correlation function found in the literature [35]. Finally, the combination of regression and correlation function with the lowest PRESS value is selected for the prediction of the design time t_d and volume fraction VF for the target crash responses (a_{max} and d_{max})

3.3.6 Step 6: Prediction

The target crash responses (a_{max} and d_{max}) are selected to minimize both acceleration and the displacement of the resulting topology design. To test the efficiency

Table 3.2.
Regression and correlation functions

Regression functions	**Correlation functions**
Zero order (regpoly0)	Exponential (correxp)
First order (regpoly1)	Gaussian (corrgauss)
Second order (regpoly2)	Matern (corrmatern52)

of the metamodel, the selected target responses are usually away from the highly populated areas of available z number of acceleration-displacement profiles. Figure 4.13 represents the randomly generated data for the explanation of the target crash responses and the highly populated areas. The target responses (a_{max} and d_{max}) are

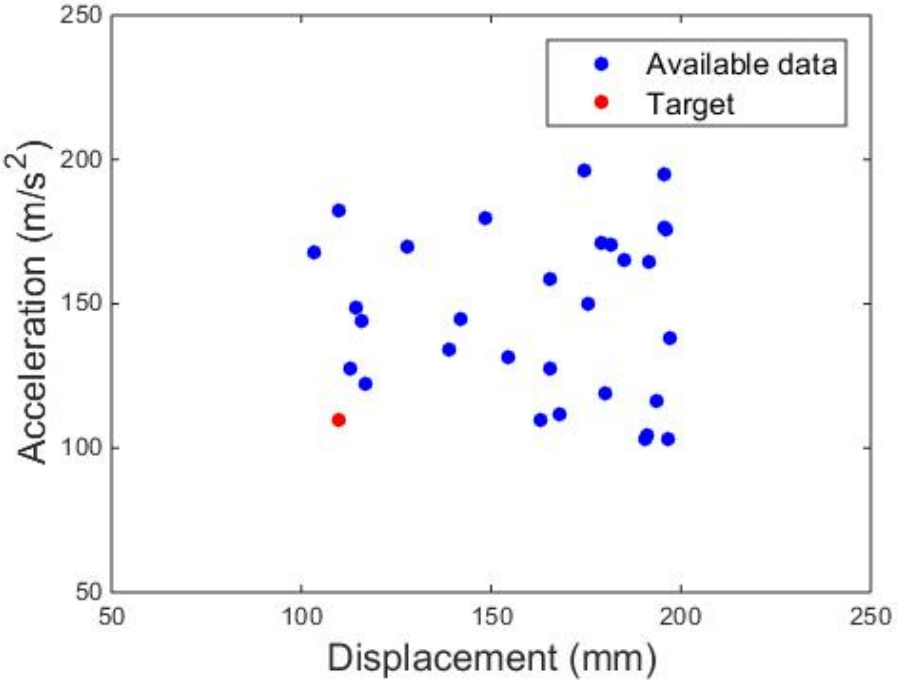

Figure 3.2. Target crash responses

fed to the metamodels of design time t_d and volume fraction VF with the lowest PRESS values to obtain the predicted values of the design time and volume fraction. Therefore, based on the Equation (3.4) and (3.5), the predictions can be expressed as

$$t_d{}^* = y(a_{max}^{Target}, d_{max}^{Target}) \tag{3.14}$$

$$VF^* = y(a_{max}^{Target}, d_{max}^{Target}) \tag{3.15}$$

where, $t_d{}^*$ and VF^* are the predicted values of design time and volume fraction respectively. These predicted values are now can be supplied to the improved HCA to generate corresponding topology design.

3.3.7 Step 7: Error evaluation

To generate the topology design with predicted design time and volume fraction, the improved HCA uses the problem formulation given in (3.2). A nonlinear finite element solver LS-DYNA communicates with the HCA to provide the field variable information at the predicted design time $t_d{}^*$. At the same time, the topology synthesis tries to satisfy the volume fraction constraint VF^* and sends back the updated design to LS-DYNA in each iteration. As the topology synthesis converges, using LS-DYNA, the final design is subjected to the same boundary condition to evaluate the actual crash responses of the structure (a_{max}^{act} and d_{max}^{act}). The errors between the actual and the target crash responses are then evaluated, which are given by

$$\text{Error}_{acc} = \frac{\left|a_{max}^{act} - a_{max}^{Target}\right|}{a_{max}^{act}} \times 100 \tag{3.16}$$

$$\text{Error}_{dis} = \frac{\left|d_{max}^{act} - d_{max}^{Target}\right|}{d_{max}^{act}} \times 100 \tag{3.17}$$

These error can further be reduced with search direction approach and less number of design of experiment (DOE). The corresponding approach is shortly explained in the chapter of numerical example. There are couple of other approaches to minimize both acceleration and displacement with less computational efforts, These advanced approaches are explained in the subsequent section.

3.4 Advanced applications of design time

The improved HCA provides flexibility to utilize the variable design time to generate number of topology designs. This approach so far provided the advantage of sampling the intermediate design time t_d (between 0 and max) to reach minimum acceleration and displacement using metamodeling technique. However, multiple combinations of design times can also be utilized to generate topology designs with lower acceleration and displacement. Moreover, this technique requires less number of function evaluation, which would significantly reduce the computational efforts. The proposed work uses couple of these advanced applications of design time, which are explained in the following subsections.

3.4.1 Multi-design time

The improved HCA enhances the internal energy absorbing ability of the structure based on the field variable (internal energy density) at the specific design time t_d over the span of dynamic loading. Therefore, combination of the multiple design times can be used to enhance the internal energy absorption ability of the structure over the span of dynamic loading. This approach converts the problem formulation of single loading case (3.2) into the multi-loading case.

In case of multi-loading, for the given multiple design times, the internal energy absorption abilities of the structure are simultaneously enhanced. In other words, the final structure would be capable of absorbing more internal energy at different times over the span of dynamic loading. For instance, for the given j number of design times, based on Equation (3.2), the averaged field variable of every element $\bar{U}_i$ now becomes $\bar{U}_i^m$ and it is given by,

$$\begin{aligned} & \bar{U}_i^m = \textstyle\sum_{j=1}^{M} w_j \bar{U}_i(t_d)_j \\ \text{Subject to} \quad & \textstyle\sum_{j=1}^{M} w_j = 1 \\ & 0 \leq w_j \leq 1 \qquad j = 1, ..., M \end{aligned} \tag{3.18}$$

where, w_j is the weighing factor of the each loading case. The range of the weighing factor is from 0 to 1. Based on the importance of individual design time, the weighing factors are assigned in such a way that it sums up to 1. Now, the Equation (3.18) can be substituted back into Equation. (3.2) to formulate the multi-loading problem.

As this problem is solved with the formulation of the improved HCA, this technique also has total control on the final volume fraction of the resulting topology design. To substantiate this application of design time, the numerical example of multi-loading is explained in the chapter of numerical examples.

3.4.2 Merged design

As mentioned in the sampling sections, the sampling of design time t_d and volume fraction VF provided Z number design of experiments (3.3). These experiments are used to generate Z number topology designs with the different structural performance. The post-processing can be performed on these designs to further improve the structural performance by using the binary operations. In the proposed work, LS-Pre/Post is used to merge the two or more topology designs to generate a new design. For instance, If the designer is supposed to generate the merged design using given number of topology designs then the logic of the binary operations can be expressed as

$$S_{Mer} = S_{k1} \cup S_{k2} \cup S_{k3} \tag{3.19}$$

where, S_{k1}, S_{k2}, and S_{k3} are the structures to be merged. Parameters $k1$, $k2$, and $k3$ contain the information about the design time t_d and the volume fraction VF with which, the corresponding topology design (S) is obtained. During this process of union or merging, the common elements and the corresponding nodes are automatically duplicated. Thus, it is necessary to delete those duplicated elements and nodes to complete the process of merging. This new design is then subject to the same boundary conditions to evaluate the corresponding crash responses using LS-DYNA.

Unlike the multi-design time approach,this approach does not have the control on the final volume fraction of the merged design. However, the corresponding crash responses (a_{max} and d_{max}) can be compared with the crash responses of other topology designs with the same volume fractions. The efficiency of the merged design approach is illustrated in the chapter of numerical examples.

4. NUMERICAL EXAMPLES

The capabilities of the improved HCA method are illustrated in this chapter using two examples. In the first example, a simple case of the moving pole and the fixed design domain of bumper is explained to demonstrate the dependency of the field variable (internal energy density) on the design time. The second example demonstrates topology synthesis of the simplified front frame of the passenger car. The crucial crash responses of the front frame (maximum acceleration and displacement) are targeted with the Kriging metamodeling technique. Finally, the advanced application of the design time such as multi-design time and the merged design are demonstrated using the front frame model.

4.1 Bumper

In the previous chapter, it is mentioned that the field variable of each element is a time-dependent variable. To demonstrate this segment of the proposed work, this example utilizes a nonlinear dynamic analysis of a simple design domain. The corresponding finite element model and the contours of the field variable or internal energy density (IED) at different design times are explained the following subsections.

4.1.1 Finite element model

For the finite element modeling in LS-Pre/Post, the design domain with a square cross-section is used resemble the design domain for the car bumper. Both ends of the design domain are constrained in all directions. As shown in Figure 4.1, the pole with the mass of 300 kg is crashing at the center of the design domain with a velocity of 5 m/s.

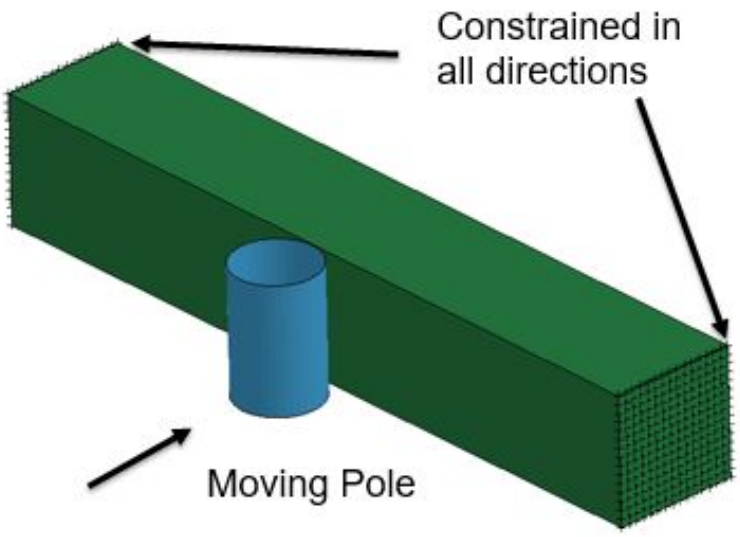

Figure 4.1. Boundary conditions of the design domain

The material model of PIECEWISE LINEAR PLASTICITY is used for the design domain with material properties of Aluminum(Table 4.1). Whereas, the RIGID material model is assigned to the moving pole. Some of the other keywords related to the design domain are given in the Table 4.2.

Table 4.1.
Properties of aluminum

Property	**Value**
Density	2.7×10^{-6} kg/mm^3
Young's modulus	70 GPa
Poisson's ratio	0.3
Yield stress	180 MPa

The finite element model was solved using LS-DYNA with the termination time of 5 millisecond, so the changes in the field variable can be observed over the span of dynamic loading.

Table 4.2.
Keywords related to bumper model

Parameter/ Keyword	**Value/ Type**
Element type	Hexahedral
Element size	$4 \times 4 \times 4$
Section type	Solid
Between the bumper and pole	AUTOMATIC SURFACE TO SURFACE
Between elements of bumper	AUTOMATIC SINGLE SURFACE
Coefficient of friction	0.6

4.1.2 Time dependent field variable

The internal energy density (IED) contours are recorded at different design times (1, 3, 5 milliseconds), so one can clearly observe the discrepancy among the contours. At a design time of one millisecond, the impacting pole is barely in contact with a bumper. Thus, the corresponding IED has the lowest numerical value (Figure 4.2). As the design time increases, the value IED also increases until the end of the dynamic loading (Figure 4.3 and 4.4).

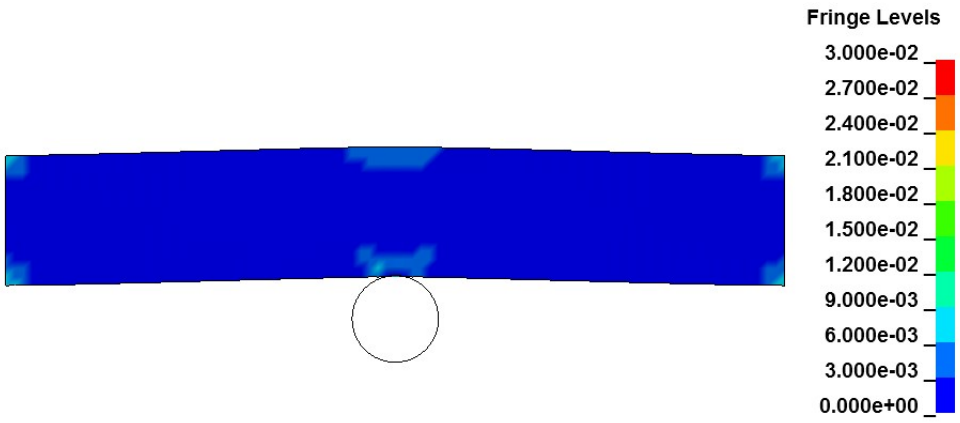

Figure 4.2. IED at 1 millisecond

This demonstration shows the internal energy density (IED) of each element varies according to the corresponding design time. With this illustration, it is clear

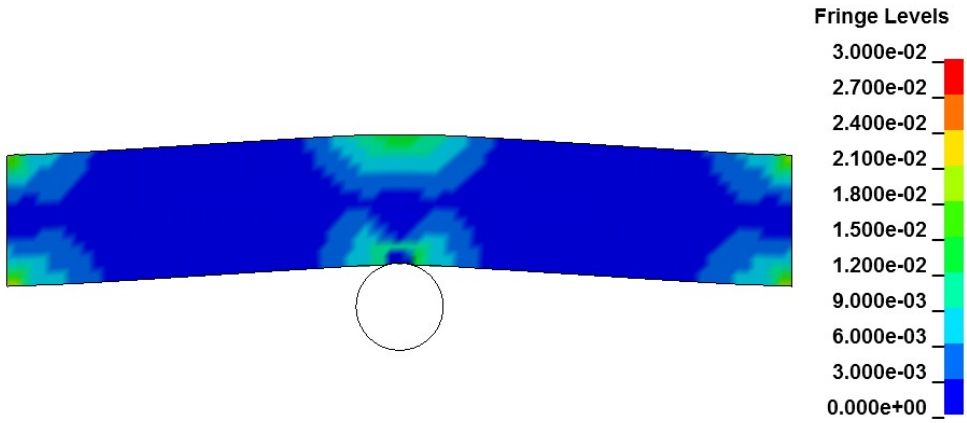

Figure 4.3. IED at 3 milliseconds

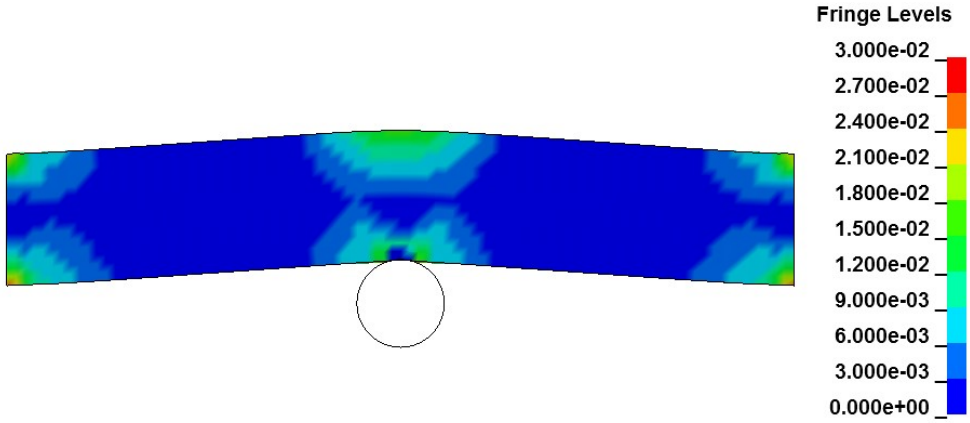

Figure 4.4. IED at 5 milliseconds

that in the case of dynamic loading, finite element analysis enables designer to record the IED at the different design times. As the IED of every element changes, the averaged field variable, which is the average of IED of neighborhood, also changes with respect to design time. Now, this time dependent field variable $\bar{U}_i$ can be supplied to improved HCA in order to synthesize the topology of the design domain for the same volume fraction constraint, so different topology designs can be obtained with the same mass. The effects of design time on the final topology design and its performance are explained in the subsequent sections with the numerical examples of the simplified front frame.

4.2 Front frame

In this example, the frontal car crash is simulated by using the simplified design domain of the front frame of the passenger car. The approach of obtaining the crash responses, which are very close to the target crash responses using the Kriging metamodel is explained in this example. Furthermore, in order to reduce the computational time of reaching close to the target crash responses, Kriging metamodel with minimum design of experiments is also demonstrated. In the final section, the front frame model is also used to demonstrate the advantages of the multi-design time and the merged design.

4.2.1 Finite element model

In order to reduce the computational time of nonlinear dynamic analyses and the topology synthesis, the design domain of the front frame was simplified by reducing the corresponding lateral thickness to 15 mm (Figure 4.5). However, the reduced thickness introduces risk of lateral bending of the design domain under the dynamic loading.Thus, in this example, the main challenge for the proposed methodology is to overcome the uncertainty of lateral bending and enhance the structural performance to minimize both acceleration and the displacement of the topology design. The basic dimensions of the modified front frame are shown in Figure 4.6

a) Boundary conditions:

To define the boundary conditions, PLANAR FINITE fixed rigid wall of dimensions 1000 $\times$ 1000 mm is used in LS-Pre/Post [40]. A small box at the lower back end of the design domain is modelled, which represents the mass of the passenger compartment (Figure 4.7). As the design domain was modified, the mass of the passenger compartment was also reduced to 70 kg to keep the stability in the dynamic analysis. The nodes of the box and the design domain are merged to avoid the corresponding

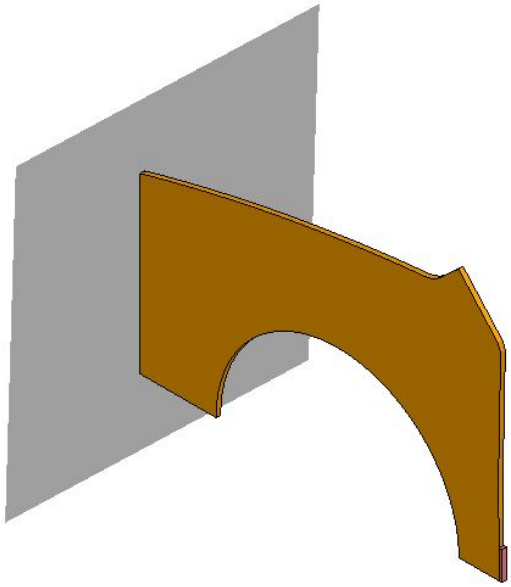

Figure 4.5. Modified design domain of the front frame

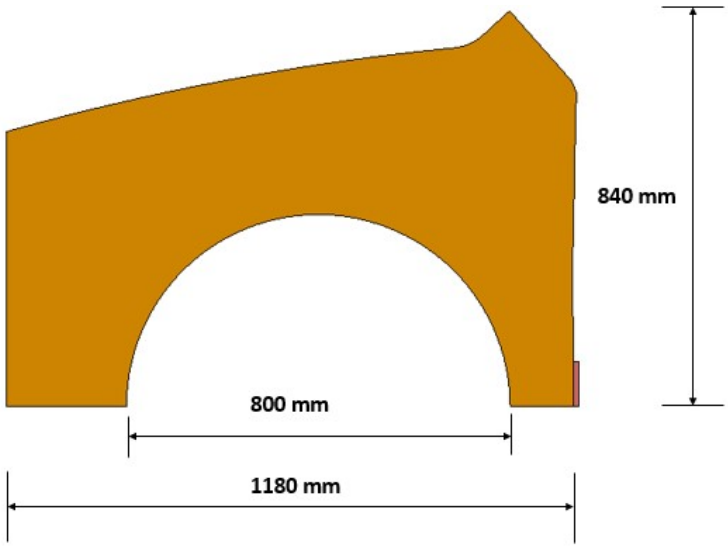

Figure 4.6. Dimensions of the modified design domain

contact definitions. The crash responses of the model are measured with respect to the center of gravity of the box. The design domain and the rigid box were give the initial velocity of 15.65 m/s (33 mph) in the direction of the rigid wall.

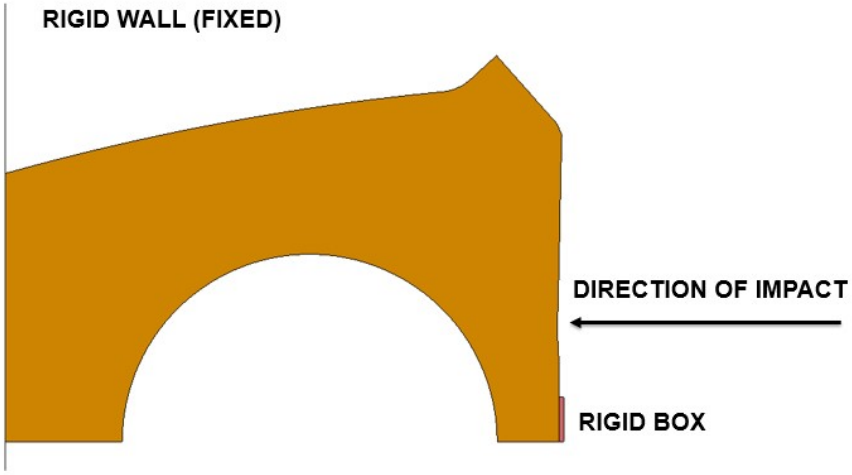

Figure 4.7. Boundary conditions

b) Element model:

The efficiency of the proposed approach of topology synthesis highly depends on the element size. Some of the preliminary observations showed that with fine mesh size, the load paths of the final topology design are more detailed and complex but with a higher cost of the computational time. However, as the design domain is already simplified, a very fine mesh size is used in the proposed work (Table 4.3).

Table 4.3.
Details of the element model

Parameter/ Keyword	**Value/ Type**
Element type	Hexahedral
Element size	$5 \times 5 \times 5$
Total elements	71820
Section type	Solid

As the thickness of the simplified design domain is 15 mm, the element size of 5 × 5 × 5 also keeps three elements in the lateral direction and increases the integrity of the load paths of the final topology design.

c) Material model:

As the crash responses such as maximum acceleration and the displacement (a_{max} and d_{max}) are measure with respect to the box (Figure), the involvement of field variables of the box is blocked, so that none of the elements of the rigid box gets deleted in topology synthesis. To ensure this RIGID material type is assigned to the box. Whereas, for the design domain, the material type PIECEWISE LINEAR PLASTICITY is selected with the material properties of steel (Table 4.4).

Table 4.4.
Material properties

Property	**Value**
Density	7.83 $\times 10^{-6}$ kg/mm^3
Young's modulus	207 GPa
Poisson's ratio	0.29
Yield stress	200 MPa

d) Contact model:

As the type rigid wall is set as PLANAR FINITE, there is no need to define the separate contact information for the interface between the rigid wall and the design domain. In the definition of rigid wall, the dynamic coefficient of friction is set as 0.6. In dynamic analysis, as the design domain goes under the plastic deformation, there would be interface between the elements of the design domain. Therefore,

an AUTOMATIC SINGLE SURFACE CONTACT is selected for the corresponding interface.

e) Control model:

In order to improve the accuracy of the dynamic analysis, the control parameters can be defined in LS-Pre/Post. The control parameters which are added to the model of front frame are enlisted in the following table with a brief description of their functions.

Table 4.5.
Control model

Control parameter	**Description**
Contact control	This option is added to the model to check and track the penetration at the interface.
Hourglass control	Hourglass modes are zero energy deformation modes, which are caused by highly distorted elements.One way to avoid these modes are to refine the mesh and another way is to add hourglass coefficient to the model. As per the guidelines of LS-DYNA explicit code, hourglass coefficient of 0.1 is added to the frame model.
Maximum time step	The upper limit of the time step of a nonlinear analysis is a vital parameter as it can accelerate the analysis at the cost of the additional mass. This factor can affect the outputs of the analysis. Therefore, to improve the accuracy of the dynamic analysis, the time step is constrained to the default value.
Termination	This control is used to assign the termination time of 50 milliseconds to the dynamic loading.

4.2.2 Design of experiments (DOE)

As mentioned in the chapter of the improved hybrid cellular automata, the volume fraction (VF) and design time (t_d) are considered as the design variables. These variables were sampled based on their corresponding rationale. For lightweight structures, the minimum feasible volume fraction was selected as 10% of the whole design domain of the front frame, and then it was increased by the step of 2.5% up to 22.5%. The design time was sampled to keep the computational cost as low as possible. After some preliminary crash simulations, it was observed that with the provided boundary conditions, one millisecond was enough for the strain wave to propagate to the rigid box. In other words, the design time of one millisecond is enough to obtain load paths using the proposed approach. Thus, the design time of 1, 5, 10, and 50 milliseconds were selected. As there are six volume fractions and four design times, this ended up with total 24 experiments (Table 4.6). The design space of the corresponding DOE is shown in the Figure 4.8.

Table 4.6.
Design of experiments for topology synthesis

Volume Fraction, VF (%)	Design time, t_d (ms)			
10	1	5	10	50
12.5	1	5	10	50
15	1	5	10	50
17.5	1	5	10	50
20	1	5	10	50
22.5	1	5	10	50

Thus, these all-possible combinations of the volume fraction VF and design time t_d were supplied to HCA to generate topology-optimized structures to analyze the

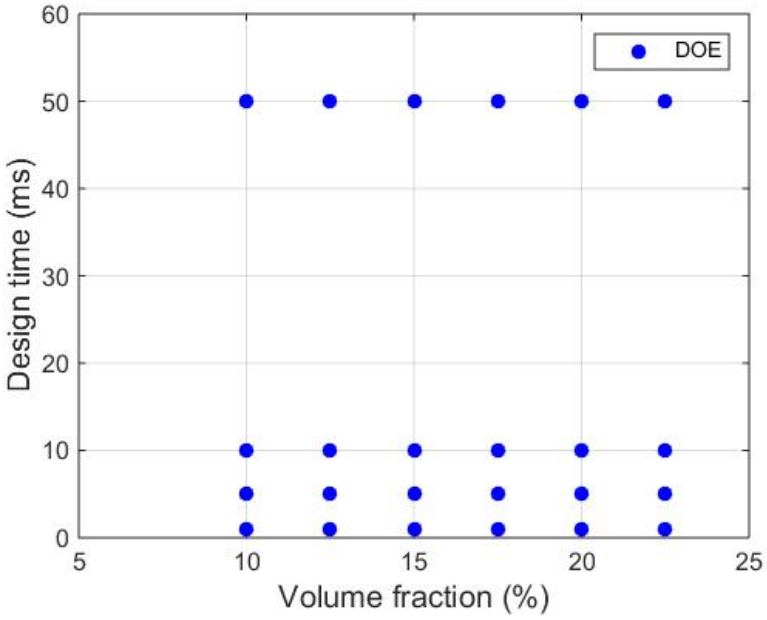

Figure 4.8. Design space

effect of design time on the crash responses such as the maximum acceleration (a_{max}) and maximum displacement (d_{max}) of the rigid box.

4.2.3 Topology synthesis and performance evaluation

The topology designs show the consistent trend of material distribution for each volume fraction with respect to change in the design time. As shown in Figure 4.9 and Figure 4.10, the topology designs with design time of one millisecond have most of the material distributed at the front end of the design domain. This is because of the internal energy density absorbing capacity of the front end at 1 millisecond is more than rest of the design domain. Therefore, the load paths are denser at the front end than rest of the design domain. As the design time increases, the material is more uniformly distributed throughout the design domain, which in turn makes the load paths more complex.

The topology designs obtained with available design of experiments are then imported back to LS-Pre/Post to perform dynamic analysis under the same boundary

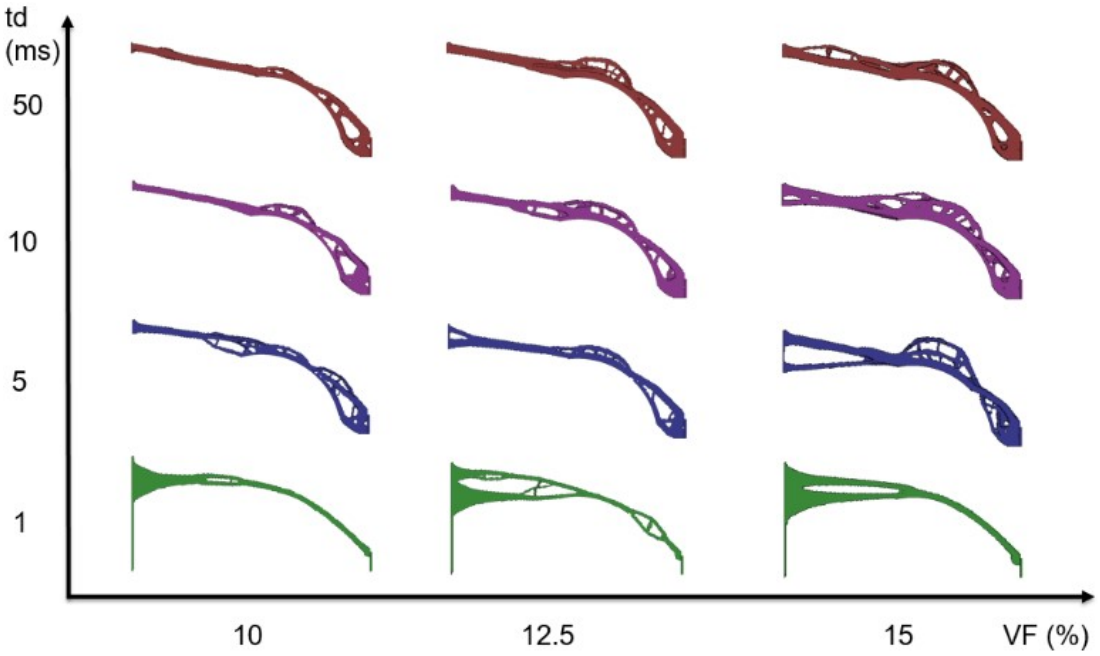

Figure 4.9. Topology designs for volume fraction 10, 12.5, and 15 percent

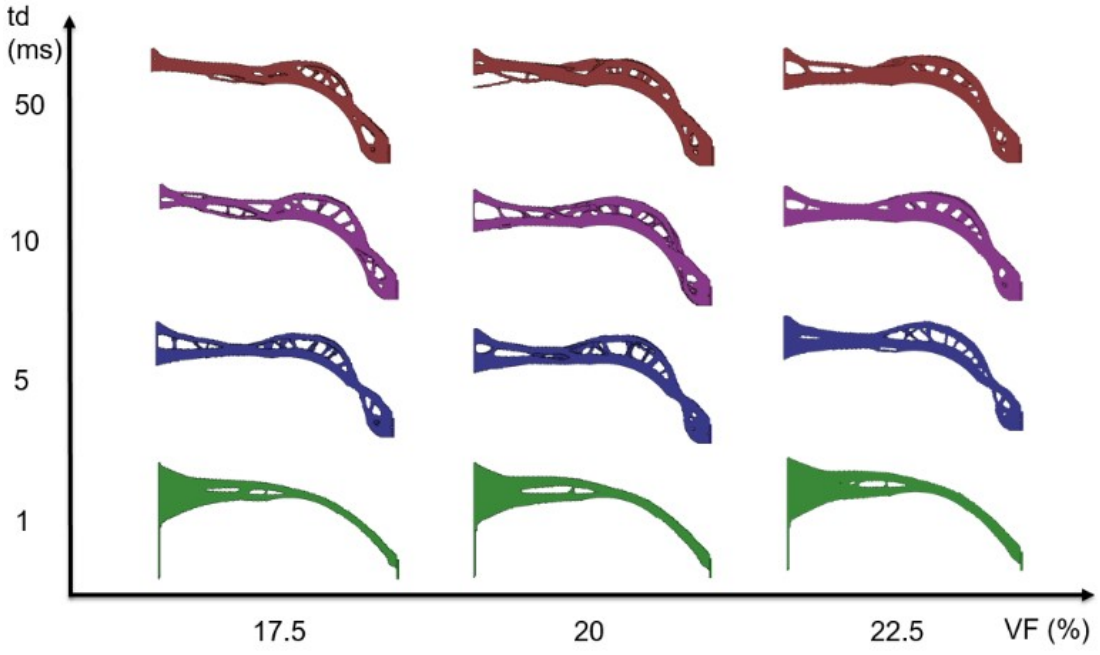

Figure 4.10. Topology designs for volume fraction 17.5, 20, and 22.5 percent

conditions. The simulation time for these analyses was set as 50 milliseconds. The output option RBDOUT is used to get the crash responses. This option considers the center of gravity of the rigid box in order to calculate the maximum acceleration and maximum displacement (a_{max} and d_{max}). The crash responses of the corresponding designs are provided in the following tables.

Table 4.7.
Crash responses of topology designs (a)

VF (%)	t_d (ms)	d_{max} (mm)	a_{max} (m/s^2)
10	1	707	704
10	5	537	749
10	10	496	775
10	50	484	818
12.5	1	700	588
12.5	5	431	907
12.5	10	388	901
12.5	50	451	946
15	1	659	808
15	5	403	1026
15	10	334	1095
15	50	266	1064

With the improved HCA, for the same volume fraction with different design times, it is now possible to obtain structures with different acceleration-displacement profiles. Figure 4.11 demonstrates the effect of design time on the load paths obtained for the structures with same volume fraction. The maximum acceleration and maximum displacement (a_{max} and d_{max}) of the structures with the volume fraction of 15% are plotted with the corresponding color code.

Table 4.8.
Crash responses of topology designs (b)

VF (%)	t_d (ms)	d_{max} (mm)	a_{max} (m/s^2)
17.5	1	626	982
17.5	5	348	1064
17.5	10	305	1237
17.5	50	304	1225
20	1	551	1255
20	5	284	1434
20	10	228	1312
20	50	155	1315
22.5	1	515	1383
22.5	5	201	1308
22.5	10	184	1463
22.5	50	155	1391

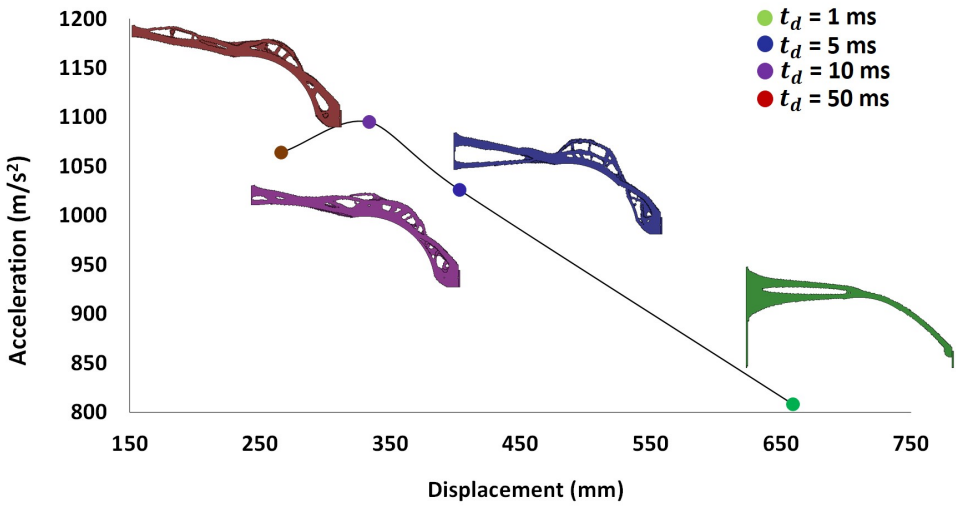

Figure 4.11. Effect of the design time

Similarly, the crash responses obtained from 24 topology designs are plotted with scatter plot with lines (Figure 4.12). Each line represents the different volume fraction

(VF), whereas, different colors are allotted to each design time (t_d). To enhance the clarity of plot of the crash responses, the marker size has been assigned based on the numerical value of the volume fraction (As VF increases, the corresponding marker size also increases).

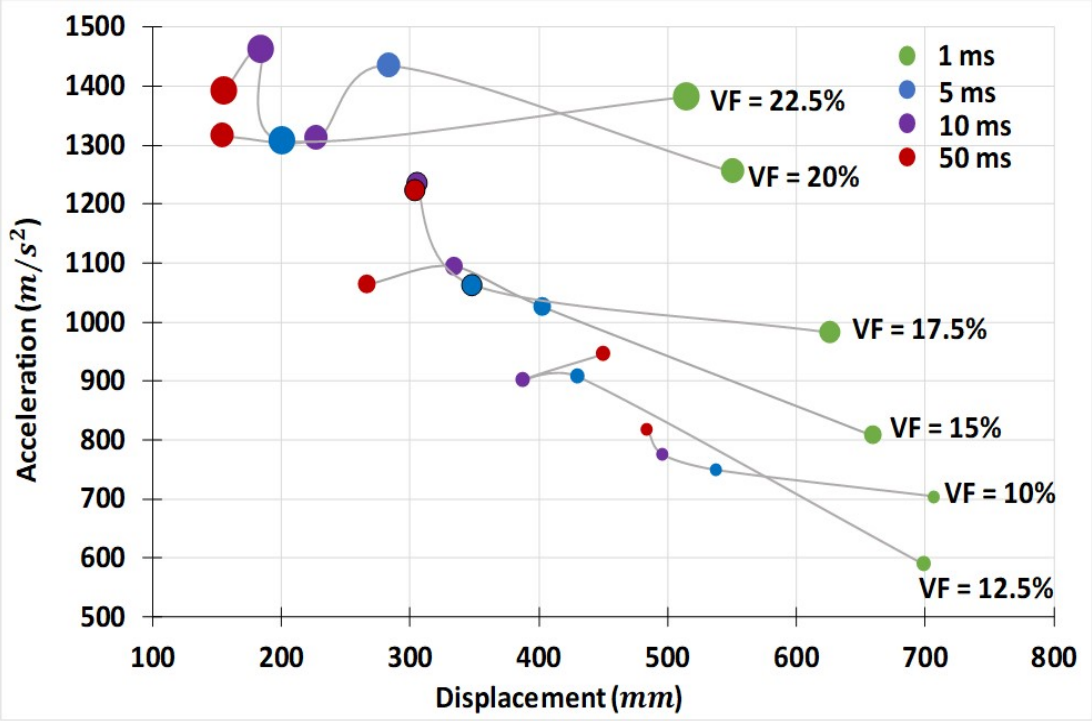

Figure 4.12. Crash response space

As the structures with low design time have most of the material at the front end of the design domain, this allows the rigid box to move in the direction of the impact without considerable resistance. Thus, for each volume fraction, structures with low design time result in high displacement and low acceleration (Figure 4.12). As the design time increases, the displacement of the rigid box is likely to be reduced, but at the cost of increasing acceleration.

However, this monotonic relationship between maximum displacement and maximum acceleration with respect to design time is not true in every case. For instance,

in case of volume fraction 12.5%, 20%, and 20.5% the acceleration of the rigid box does not always increase with respect to increasing design time (Figure 4.12). This behavior introduces nonlinearity in the trend of crash responses. Therefore, it is a challenging task to select an appropriate design time t_d and volume fraction VF to obtain the desired acceleration-displacement profile. A metamodeling techniques can set a guideline to obtain the desired crash responses by predicting the design time t_d and volume fraction VF. In the proposed work, the Kriging metamodel is used to predict t_d and VF by using available data set of 24 experiments and the corresponding crash responses, which is demonstrated in the next section.

4.2.4 Targeting with full DOE

The implicit relation between input variables and the output responses is developed using the database given in Table 4.7 and 4.8. At this point, for topology synthesis, design time t_d and volume fraction VF are performing the role of inputs, whereas, maximum acceleration and displacement of the rigid box (a_{max} and d_{max}) are the outputs. However, as mentioned in the previous chapter, designer now has total control on the design time and volume fraction. Therefore, the proposed work has used the reverse metamodeling. In other words, using the implicit relation between crash responses (a_{max} and d_{max}) and control variables (t_d and VF), reverse metamodel would predict the control variables by using the desired crash responses as an input to the Kriging metamodel. This approach can be expressed as

$$\hat{t_d}^* = y(a_{max}^T, d_{max}^T) \tag{4.1}$$

$$\hat{VF}^* = y(a_{max}^T, d_{max}^T) \tag{4.2}$$

where, $\hat{t_d}^*$ and $\hat{VF}^*$ are the prediction of the Kriging metamodel for the desired or the target crash responses a_{max}^T and d_{max}^T.

To evaluate the ability of the metamodel, the target crash responses are selected away from the highly populated area of the crash response space (Figure 4.12). The

selected target crash responses are given in the following table and corresponding location in the crash response space is illustrated in Figure

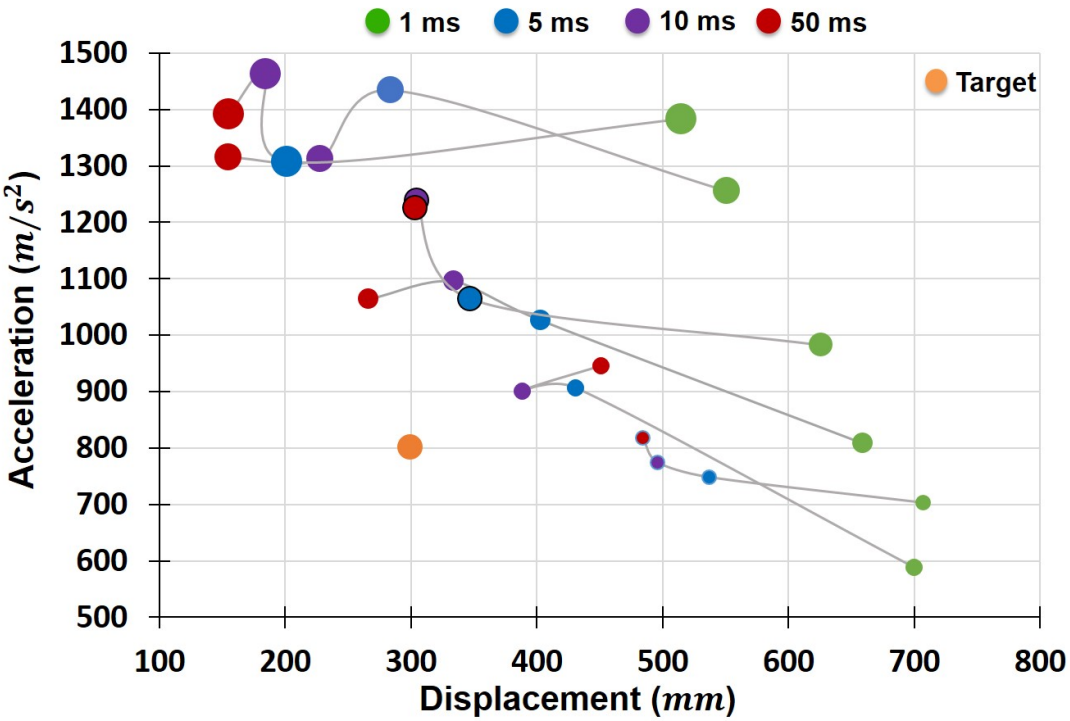

Figure 4.13. Target crash responses

The prediction of the selected target is made by using the Kriging metamodel with appropriate combination of regression function and correlation function. The appropriate combination is chosen by performing cross-validation, which is followed by the PRESS value evaluation of the each combination. The PRESS values of the Kriging metamodels of volume fraction and the design time are given the following tables.

The combination of exponential correlation function (correxp) and first order regression function (regpoly1) has the lowest PRESS values for the metamodels of both design time and volume fraction (Table 4.9 and 4.10). Therefore, the corresponding

Table 4.9.
PRESS values for the kriging metamodel of volume fraction

		Correlation function		
		correxp	corrgauss	corrmatern
Regression Function	regpoly1	**0.37**	0.53	0.39
	regpoly2	0.5	0.51	0.53

Table 4.10.
PRESS values for the kriging metamodel of design time

		Correlation function		
		correxp	corrgauss	corrmatern
Regression Function	regpoly1	**0.27**	0.47	0.37
	regpoly2	0.29	0.42	0.59

combination is selected to predict the design time t_d and volume fraction VF for the target crash responses.

The contours of the volume fraction VF and design time t_d are obtained with the corresponding Kriging metamodels (Figure**??** and **??**). The trends of the maximum acceleration-displacement profiles with respect to the volume fraction and design time are shown using the isolines (black colored). Whereas, the approximated values of the volume fraction and design time are characterized using the color code, which is shown in the color bar of the corresponding contour plots (Figure 4.14 and 4.15).

The predicted volume fraction $\hat{VF}^*$ and design time $\hat{t_d}^*$ for the target crash responses are shown in the design space (Figure 4.16). These control parameters are then supplied to the problem formulation of the improved HCA to generate the corresponding topology design (Figure 4.17).

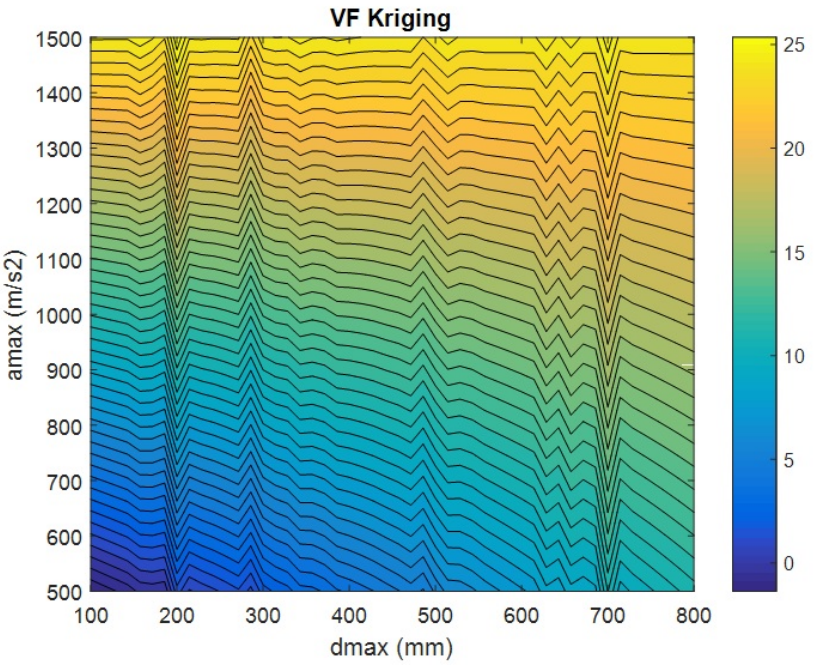

Figure 4.14. Contour plot of the volume fraction kriging metamodel

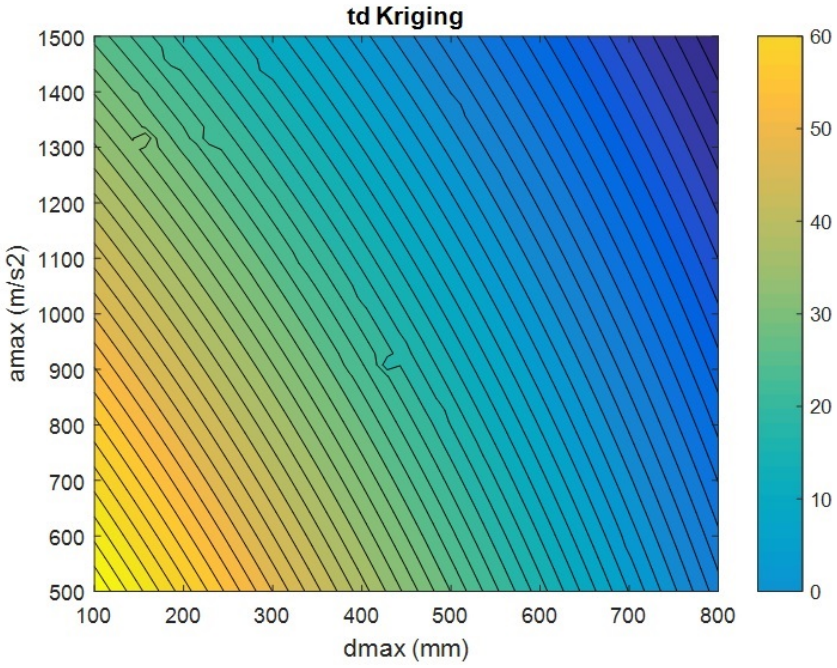

Figure 4.15. Contour plot of the design time kriging metamodel

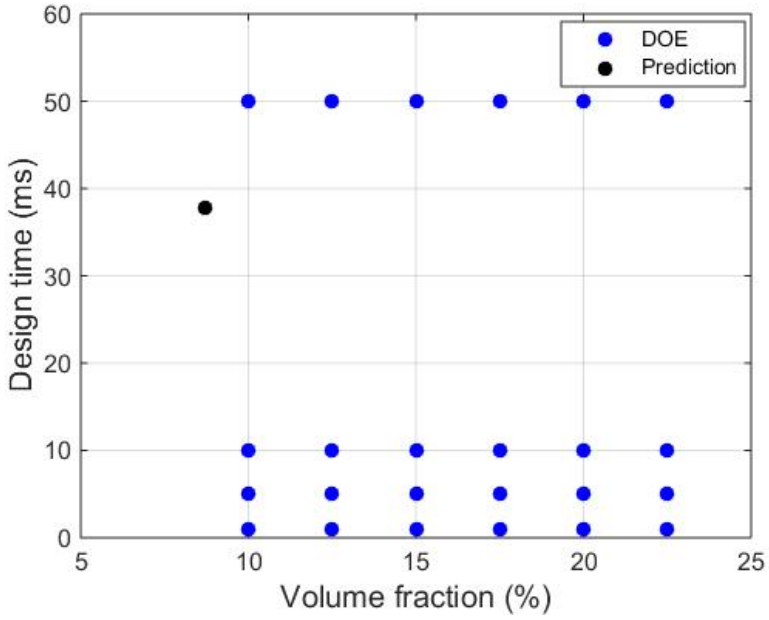

Figure 4.16. The predicted volume fraction and design time

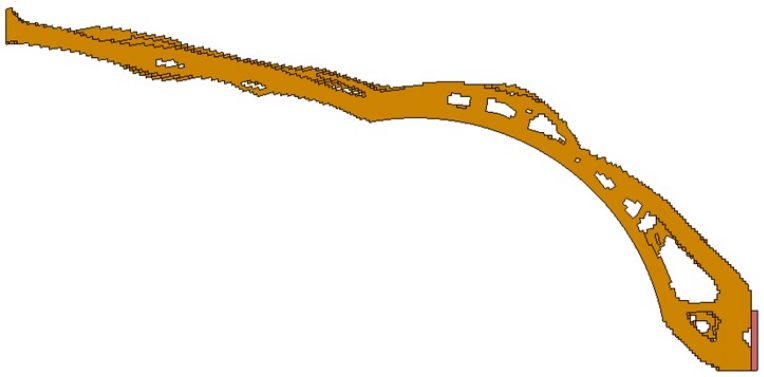

Figure 4.17. Topology design with the predicted volume fraction and design time

The generated topology design is then imported to LS-Pre/Post to evaluate the actual crash responses by performing dynamic analysis under the same loading and the boundary conditions.

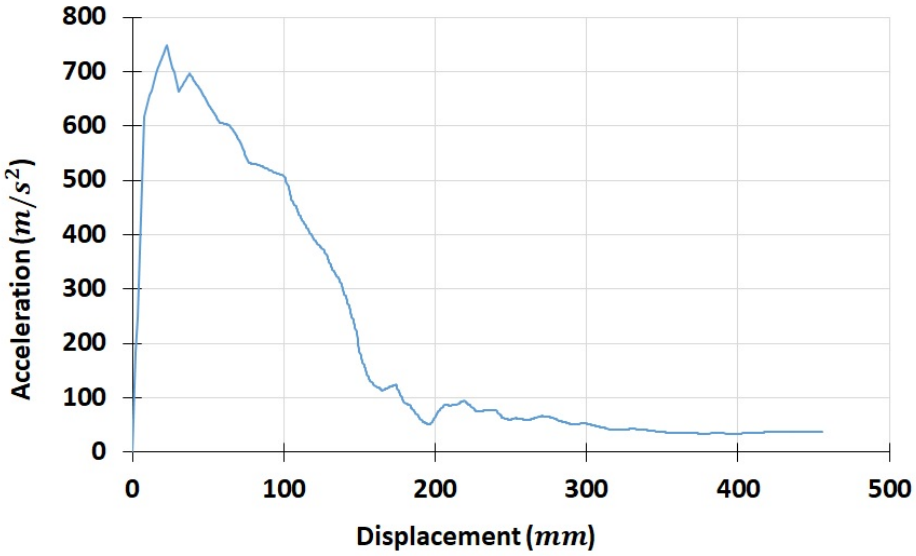

Figure 4.18. Behavior of the topology design under the dynamic load

The acceleration-displacement plot of the topology design under the loading condition is shown in Figure ??, whereas the discrepancy between the target crash responses and the actual crash responses is graphically shown in Figure 4.19.

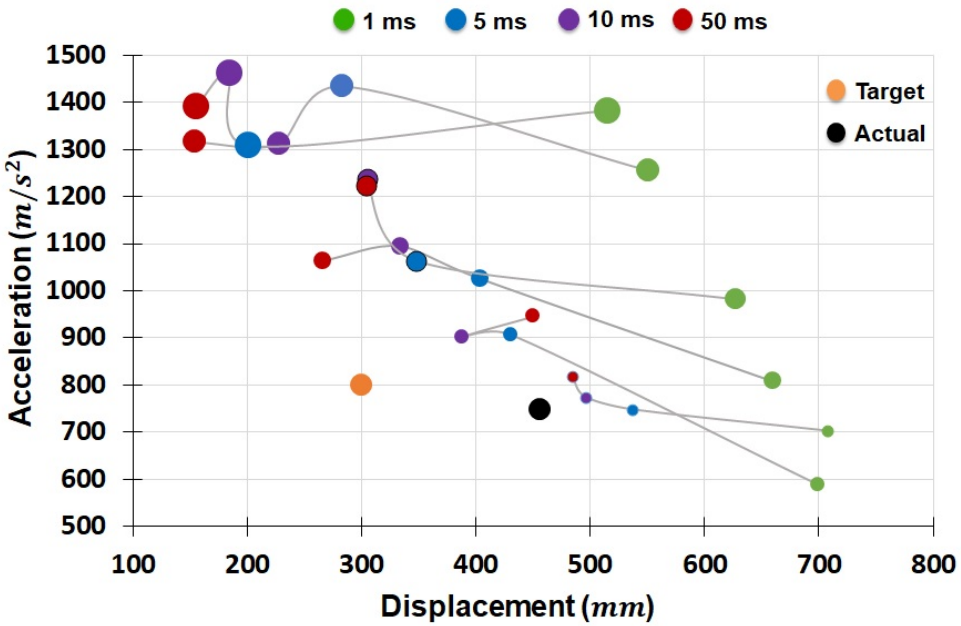

Figure 4.19. Actual and target crash responses

As shown in Figure 4.19, the actual maximum acceleration is close to the target acceleration. Whereas, the discrepancy between the actual displacement and the target displacement is considerable. However, considering the quality of the metamodel, the error between the actual and the target crash responses are in the acceptable range. The numerical values of actual and the target crash responses are given the Table 4.11.

Table 4.11.
Target and actual crash responses

Target Crash Responses		**Actual Crash Responses**	
a_{max} (m/s^2)	d_{max} (mm)	a_{max} (m/s^2)	d_{max} (mm)
800	300	748	456

These values of the crash responses are then used to calculate the corresponding error. According to the error formula given in the previous chapter, the errors are obtained by dividing the discrepancy between the target and the actual crash responses by the actual crash responses. Therefore, the errors in maximum acceleration and displacement are calculated as

$$Error_{acc} = \frac{|748 - 800|}{748} \times 100 = 6.95\%$$

$$Error_{dis} = \frac{|456 - 300|}{456} \times 100 = 34.21\%$$

These errors can further be reduced by improving the quality of the metamodel, which is based on the type of sampling and the number experiments. However, this approach would increase the number of function evaluation, which in turn increases the computation time. Therefore, the proposed work introduces a novel approach to get better solution with the less number of function evaluation, which is explained in the next section.

4.2.5 Targeting with four experiments

The computation time is a great concern especially when the topology synthesis is to be performed on the high fidelity computer model (with fine mesh). To reduce this time, less number of experiments are used to cover the design parameter space and the crash response space. Similar to the previous approach, this method also uses the Kriging predictor. Additional features of this technique are the implementation of the line equations and search for the crash response closest to the target crash response. The steps involved in this method are briefly explained in the following subsections.

a) Step 1:

In the design parameter space, four extreme combinations of the volume fraction VF and design time t_d are selected (Table 4.12).

Table 4.12.
Four experiments

	VF^{min}	VF^{max}
t_d^{min}	E_1	E_2
t_d^{max}	E_3	E_4

b) Step 2:

The topology designs for using these four experiments are generated with the formulation of the improved HCA. In this case, these topology designs and the corresponding crash responses are already evaluated in the previous method. This completes the initial data set $D_{initial}$ of experiments E_1, E_2, E_3, E_4 with the corresponding acceleration-displacement profiles or crash responses C1, C2, C3, and C4.

c) Step 3:

In the crash response space, the crash responses are connected with line plot. Similar to the previous method the target crash responses (a^T_{max} and d^T_{max}) are selected.

d) Step 4:

It is clear that the range of the maximum acceleration and displacement are not compatible (Figure 4.19). Therefore, the maximum acceleration and displacement values are scaled down and normalized between 0 and 1. For instance, if C1, C2, C3 and C4 are four values crash responses and C4 is the maximum among them, then these four values are individually divided by C4 to obtain the corresponding normalized values. This makes range of both acceleration and displacement compatible to each other.

e) Step 5:

The perpendicular line (orange colored) is drawn from the target crash responses towards the line connecting two crash responses of the experiments (Figure 4.20). Now, the next step is to find the closest distance between the point of target crash responses and the connecting line between two crash responses of the experiments. Therefore, the equation of the perpendicular line and the line connecting two crash responses are satisfied to find the co-ordinates of the closest point (Figure 4.20).

f) Step 6:

Once the normalized coordinates of the closest point is obtained, it is important to scale them up to get the original values of the acceleration and displacement ($a^{closest}_{max}$ and $d^{closest}_{max}$). Therefore, the x-coordinate and y-coordinate of the closest point is multiplied by the maximum values of displacement and acceleration in the

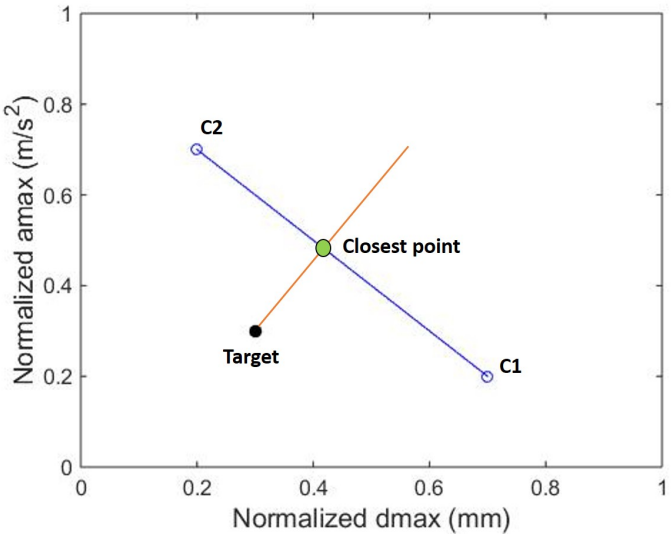

Figure 4.20. Search of the closest point

data set respectively (Refer step 4). This process transfers the crash responses from the normalized scale to the real scale (Figure 4.19).

g) Step 7:

The Kriging metamodel with cross-validation is implemented, to predict the control parameters (t_d^* and VF^*) for the crash responses obtained with the closest point approach ($a_{max}^{closest}$ and $d_{max}^{closest}$). Further, theses control parameters (t_d^* and VF^*) are supplied to the formulation the improved HCA to generate corresponding topology design.

h) Step 8:

The actual crash responses of the topology design generated with predicted control parameters t_d^* and VF^* are obtained by performing the dynamic analysis with same boundary conditions (Refer section 4.2.1 a). These actual crash responses and the corresponding control parameters (t_d^* and VF^*) are added to the original data set ($D_{initial}$) to form a new data set D_{new}.

i) Step 9:

Now, with this new data set D_{new}, the procedure from step 3 to step 8 is again conducted to evaluate a new closest point, to predict the corresponding control parameters, and to obtain the actual crash responses. This loop is continued unless and until the method obtains worse or dominated crash response than the previous iteration. These iterative process is demonstrated as follows

Iteration 1:

For the first iteration, four experiments are selected using the extreme values of the volume fraction VF and design time t_d (minimum-maximum values of the VF and t_d).The data set for the first iteration is given in the following table.

Table 4.13.
Data set for iteration 1

$d_{max}(mm)$	$a_{max}(m/s^2)$	$t_d(ms)$	$VF(\%)$
707	704	1	10
515	1383	1	22.5
155	1391	50	22.5
484	818	50	10

These experiments and the corresponding crash responses are illustrated in Figure 4.21 and 4.22 respectively. The crash responses of the four experiments are connected with linear line plot to cover the crash response space (Figure 4.22).

Now, in order to find the closest point to the target point, the values of the maximum acceleration and displacement are normalized. From Table, it is clear that maximum of acceleration data is 1383 m/s^2, whereas maximum of the displacement data is 707 mm. Therefore, acceleration and displacement values are normalized by dividing them by maximum values of respective data sets. To keep the consistency,

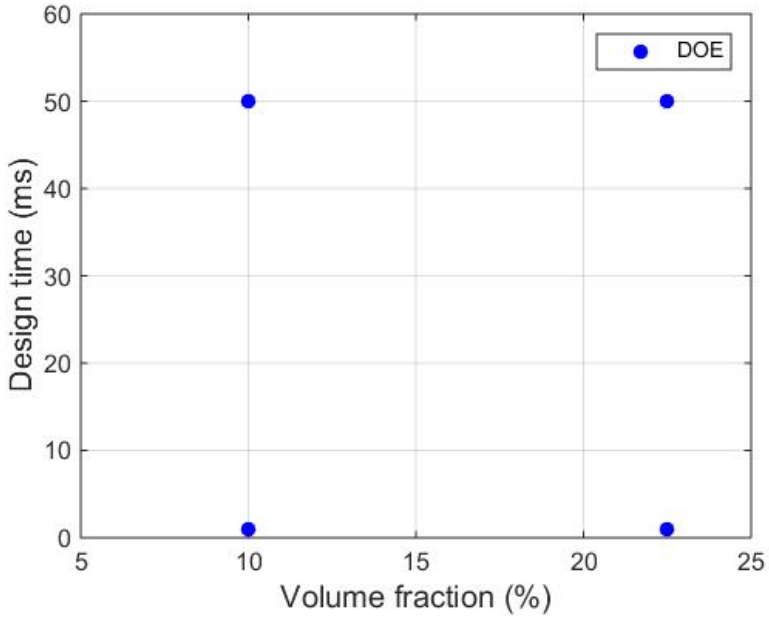

Figure 4.21. Design space for iteration 1

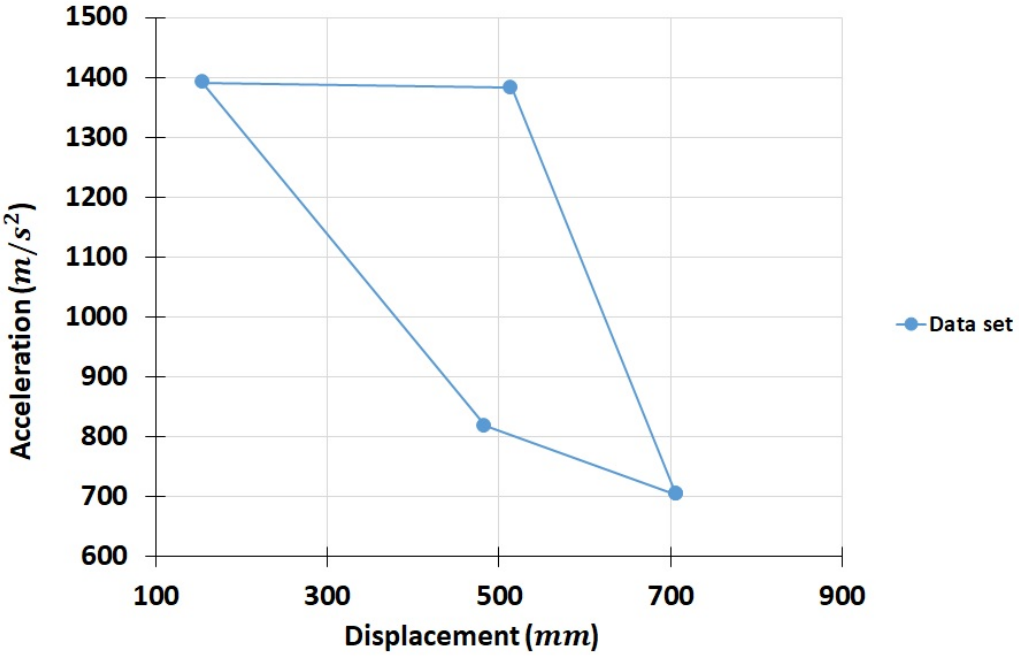

Figure 4.22. Crash response space for iteration 1

the target crash responses are kept same as the previous approach ($a^T_{max} = 800m/s^2$ and $d^T_{max} = 300mm$).

As shown in Figure 4.23, a perpendicular line is drawn from the target point towards the line connecting the crash responses. The coordinates of the closest point are evaluated by satisfying the equation of both perpendicular line and the line connecting the crash responses (Figure 4.23).

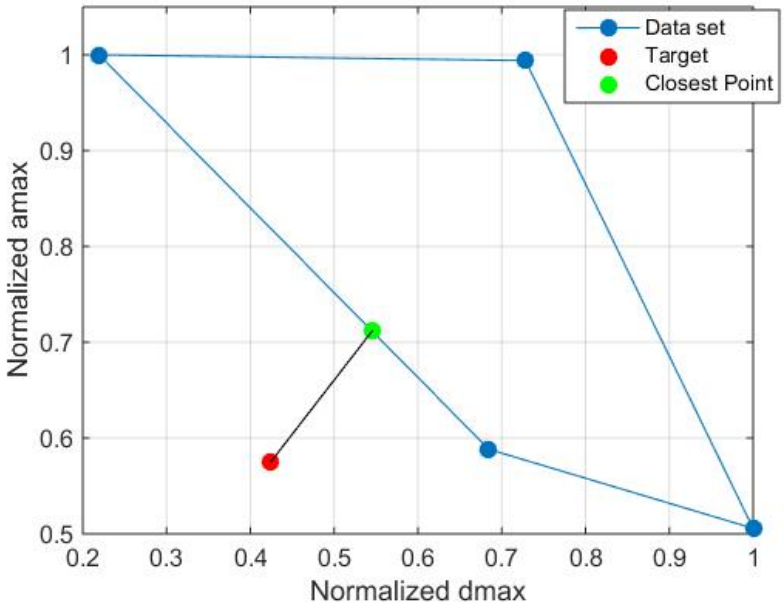

Figure 4.23. Closest point for iteration 1

The real scale values of the crash responses at the closest point are obtained by multiplying the X-coordinate and Y-coordinate of the closest point by maximum values of respective data sets. This process scales up the crash responses of the closest point which are shown in the following table.

The prediction of control parameters for the crash responses of the closest point (Table 4.14) is made with the Kriging metamodels of the volume fraction VF and design time t_d. The standard procedures of cross validation and PRESS value evaluation are performed to select best combination regression function and correlation function.

Table 4.14.
Target and closest crash responses

Target Crash Responses		**Closest Crash Responses**	
a_{max} (m/s^2)	d_{max} (mm)	a_{max} (m/s^2)	d_{max} (mm)
800	300	990	385

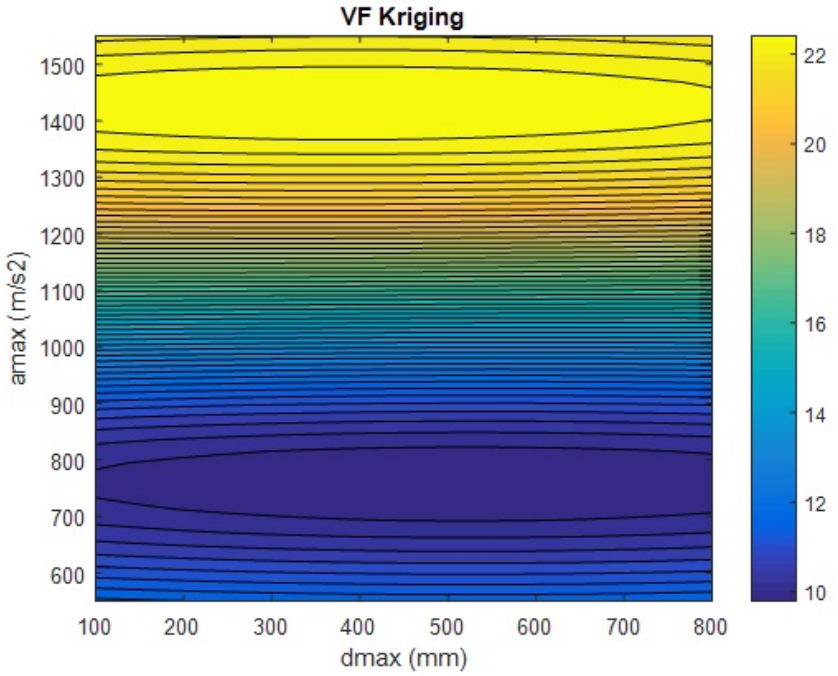

Figure 4.24. Volume fraction metamodel for iteration 1

As this approach only has four experiments in initial data set, only regpoly0 is suitable as a regression function, whereas, for the first iteration Gaussian correlation function (corrgauss) is suitable as its combination with zero order regression (regpoly0) has the lowest value of PRESS.

The contour plots of the volume fraction metamodel ($\hat{VF}$) and design time metamodel ($\hat{t_d}$) are shown in Figure 4.24 and 4.25.

The contour plots are not much informative, as the metamodel is built with a very number of computer experiments (four), which results in the poor and flat approximation (Figure 4.24 and 4.25).

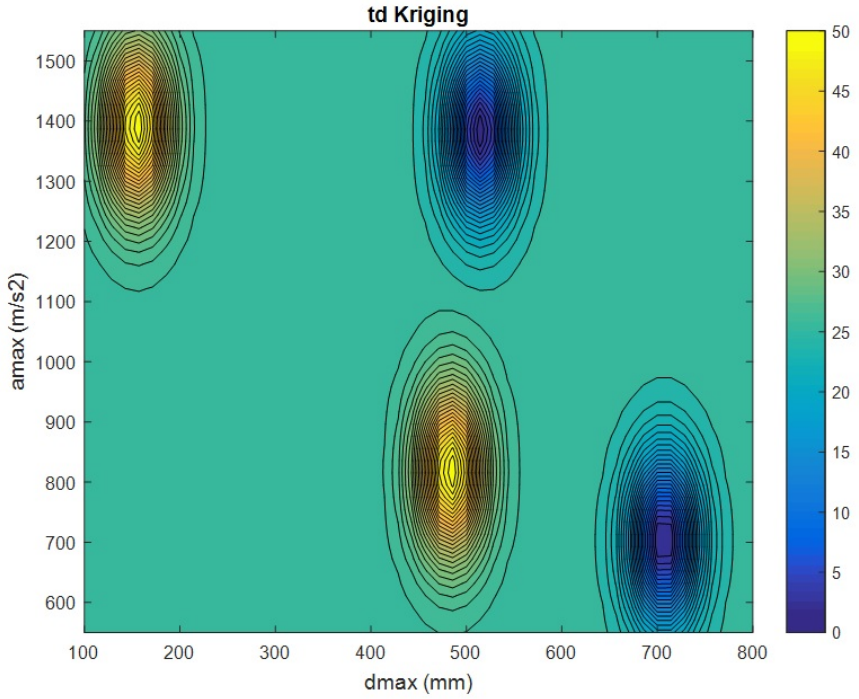

Figure 4.25. Design time metamodel for iteration 1

These metamodels predicted the values of volume fraction and the design time, which are given in the Table 4.15 and graphically shown in Figure 4.26.

Table 4.15.
Iteration 1: prediction for the closest crash responses

Closest Crash Responses		**Predictions**	
a_{max} (m/s^2)	d_{max} (mm)	$VF^*(\%)$	${t_d}^*(ms)$
990	385	16.12	25.5

The predicted volume fraction VF^* and design time ${t_d}^*$ are supplied to the problem formulation of the improved HCA to generate the corresponding topology design (Figure 4.27). This topology design is then subjected to the dynamic loading and

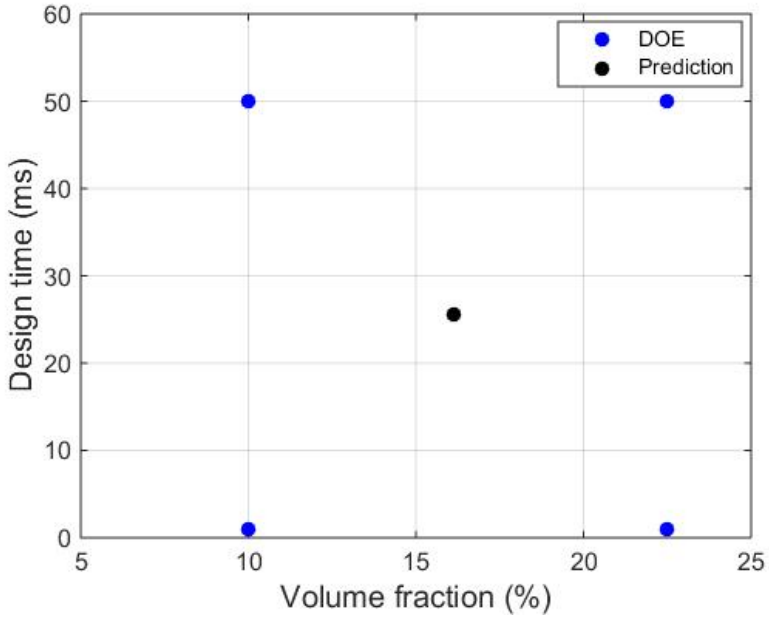

Figure 4.26. Prediction of iteration 1

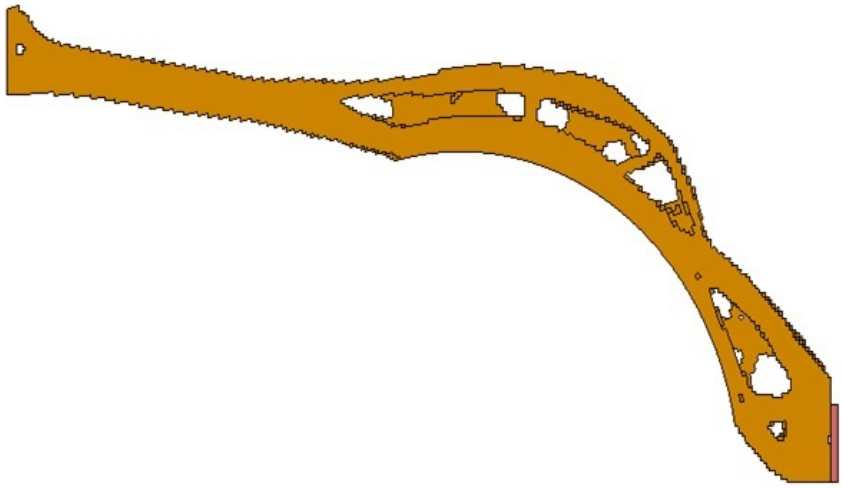

Figure 4.27. Topology design of iteration 1

boundary conditions (Refer 4.2.1 a) to evaluate actual values of maximum acceleration and maximum displacement. These actual crash responses are graphically shown in Figure 4.28, whereas iteration 1 is summarized in Table 4.16.

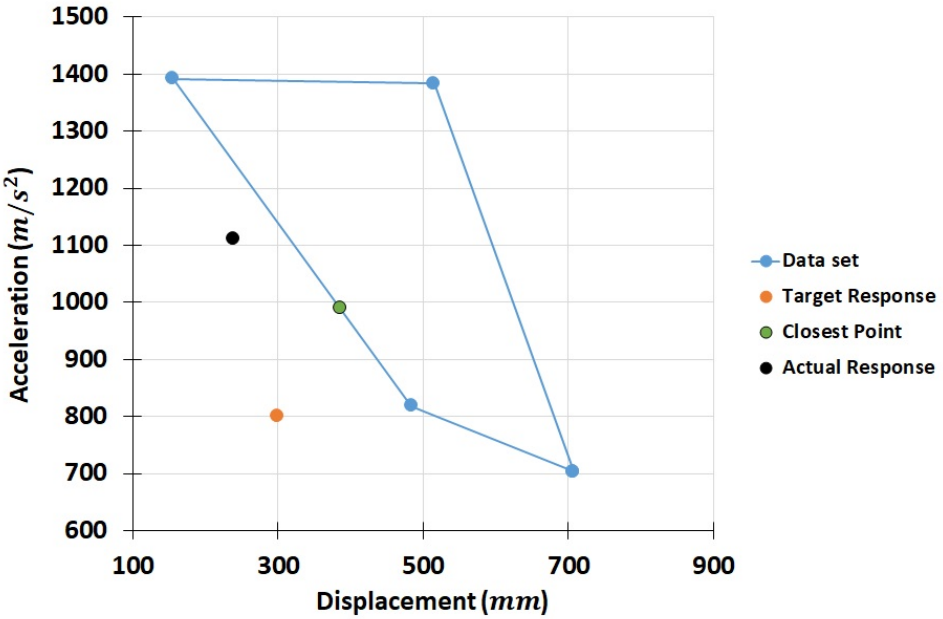

Figure 4.28. Actual crash responses of iteration 1

Table 4.16.
Summary of iteration 1

Closest Crash Responses		**Predictions**		**Actual Crash Responses**	
$d_{max}(mm)$	$a_{max}(m/s^2)$	$VF^*(\%)$	$t_d^*(ms)$	$d_{max}(mm)$	$a_{max}(m/s^2)$
385	990	16.12	25.5	239	1111

As shown in Figure 4.28, the actual crash response (black marker) is not dominated by any of the crash responses of the initial data set. Therefore, this response will be carried forward into next iteration as to form a new data set.

Iteration 2:

For the second iteration, the predictions of the control parameters (VF^* and $t_d{}^*$) and the corresponding actual response of the first iteration is added to the data set (Table 4.17).

Table 4.17.
Data set for iteration 2

$d_{max}(mm)$	$a_{max}(m/s^2)$	$t_d(ms)$	$VF(\%)$
707	704	1	10
515	1383	1	22.5
155	1391	50	22.5
484	818	50	10
239	1111	25.5	16.12

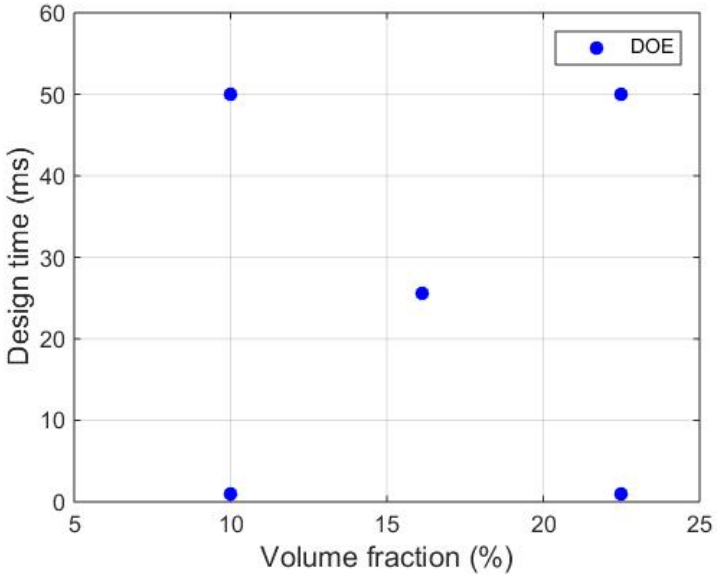

Figure 4.29. Design space for iteration 2

These experiments and the corresponding crash responses are illustrated in Figure 4.29 and 4.30 respectively. These crash responses are connected with linear line plot to cover the crash response space (Figure 4.30).

Similar to the first iteration, the values of the maximum acceleration and displacement are normalized. From Table 4.17, it is clear that maximum of acceleration data is 1383 m/s^2, whereas maximum of the displacement data is 707 mm. Therefore, acceleration and displacement values are normalized by dividing them by maximum values of respective data sets.

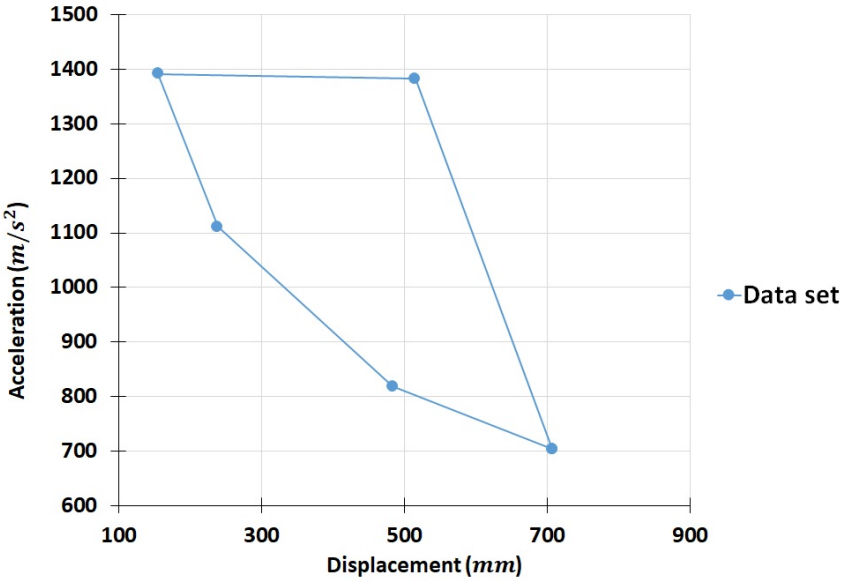

Figure 4.30. Crash response space for iteration 2

As shown in Figure 4.31, a perpendicular line is drawn from the target point towards the line connecting the crash responses.

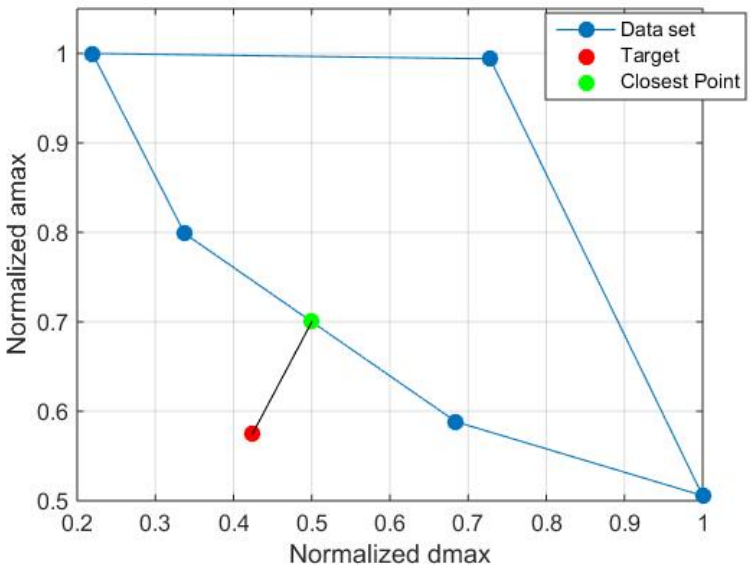

Figure 4.31. Closest point for iteration 2

The coordinates of the closest point are evaluated by satisfying the equation of both perpendicular line and the line connecting the crash responses (Figure 4.31).

The normalized crash responses of the closest point are scaled up by multiplying the X-coordinate and Y-coordinate of the closest point by maximum values of respective data sets. This process converts the normalized values of crash responses into real scale values (Table 4.18).

Table 4.18.
Iteration 2: target and closest crash responses

Target Crash Responses		**Closest Crash Responses**	
a_{max} (m/s^2)	d_{max} (mm)	a_{max} (m/s^2)	d_{max} (mm)
800	300	974	354

The crash responses of the closest point (Table **??**) are fed to the Kriging metamodels of the volume fraction VF and design time t_d to predict the corresponding control parameter. The standard procedures of cross validation and PRESS value evaluation are performed to select best combination regression function and correlation function.

This iteration also has only five experiments in initial data set. Therefore, only regpoly0 is suitable as a regression function. Unlike the previous iteration, the exponential correlation function (correxp) is suitable as its combination with zero order regression (regpoly0) has the lowest value of PRESS.

The contour plots of the volume fraction and design time metamodels ($\hat{VF}$ and $\hat{t_d}$) are shown in Figure 4.32 and 4.33. As metioned previously, beacuse of a very few number of experiments (five), the contour plots are not much informative. Therefore, this results in the poor and flat approximation (Figure 4.32 and 4.33).

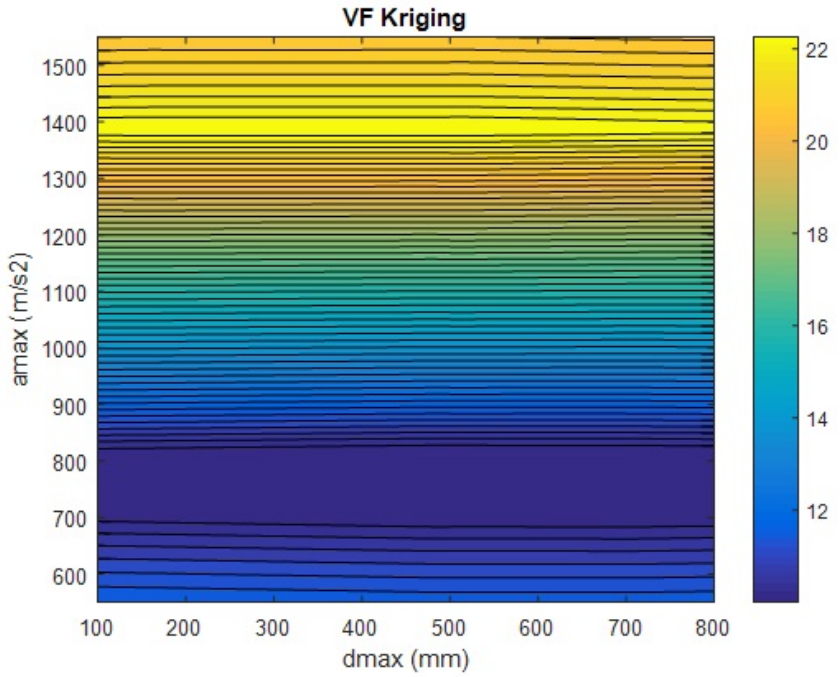

Figure 4.32. Volume fraction metamodel for iteration 2

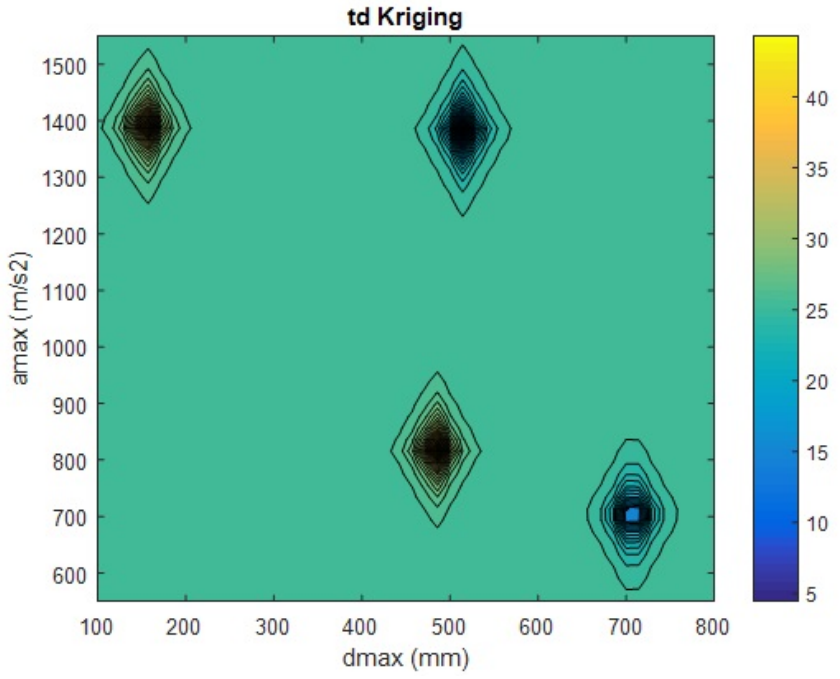

Figure 4.33. Design time metamodel for iteration 2

These metamodels predicted the values of volume fraction and the design time, which are given in the Table 4.19 and graphically shown in Figure 4.34.

Table 4.19.
Iteration 2: prediction for the closest crash responses

Closest Crash Responses		**Predictions**	
a_{max} (m/s^2)	d_{max} (mm)	$VF^*(\%)$	${t_d}^*(ms)$
974	354	14.55	25.5

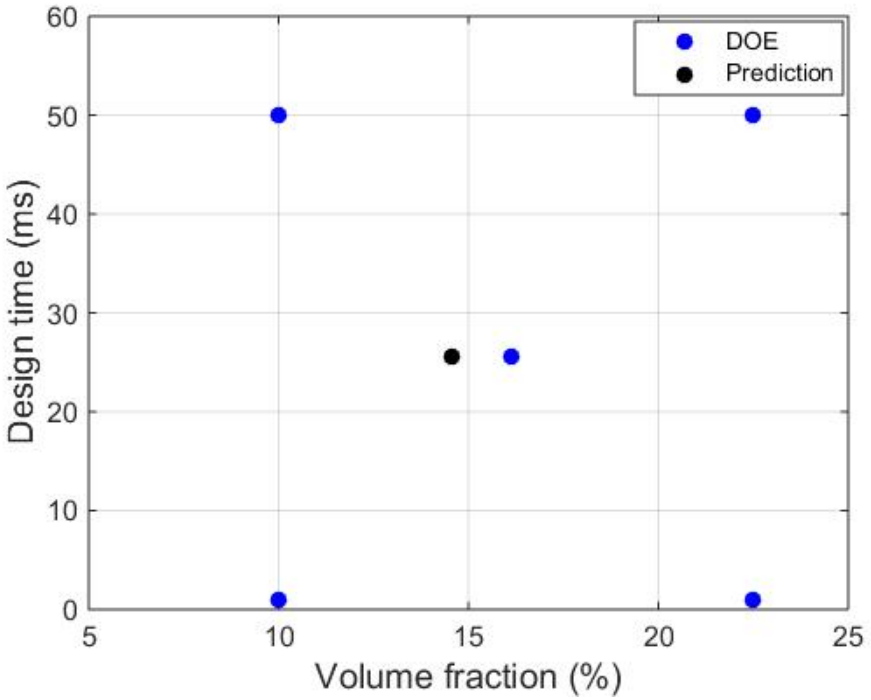

Figure 4.34. Prediction of iteration 2

Similar to the previous iteration, the predicted volume fraction VF^* and design time ${t_d}^*$ are supplied to the problem formulation of the improved HCA to generate the corresponding topology design, which is shown in the following figure.

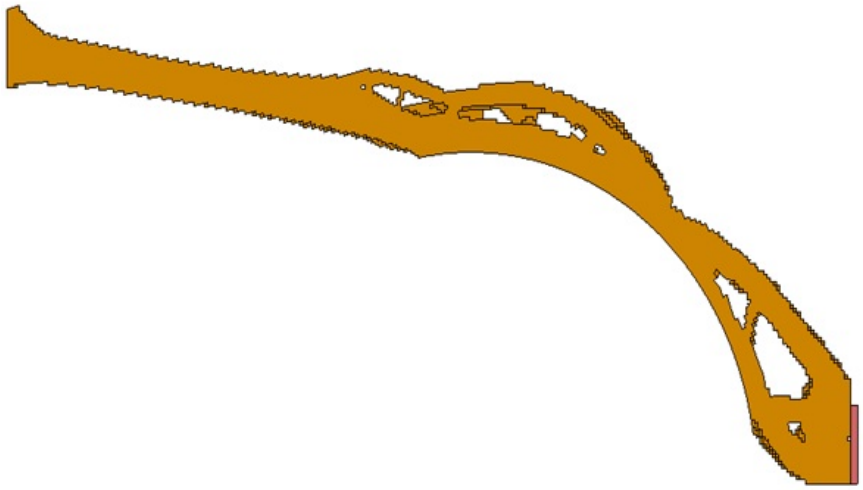

Figure 4.35. Topology design of iteration 2

Similar to the first iteration, the generated topology design (Figure 4.35) is then subjected to the dynamic loading and boundary conditions (Refer 4.2.1 a) to evaluate actual values of maximum acceleration and maximum displacement. These actual crash responses are graphically shown in Figure 4.36.

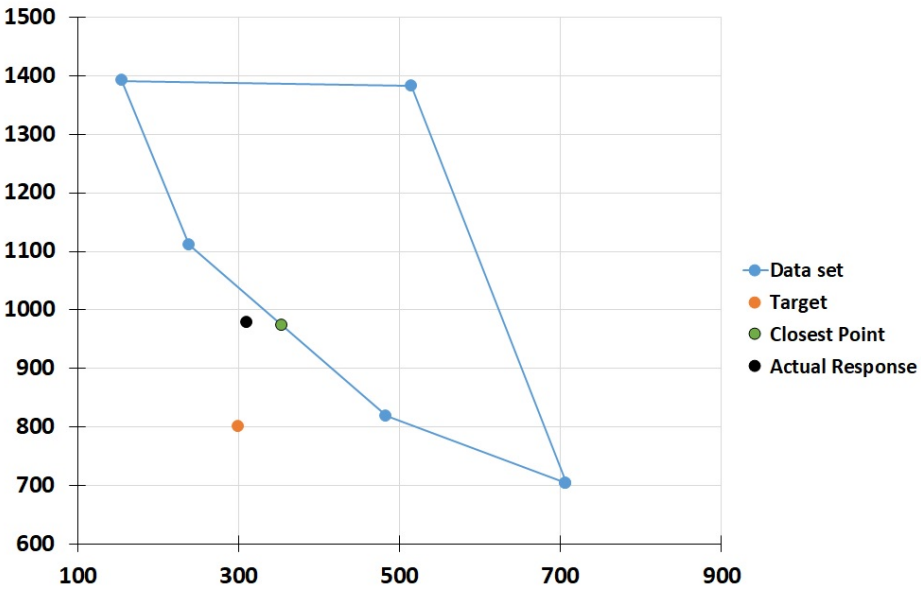

Figure 4.36. Actual crash responses of iteration 2

Table 4.20.
Summary of iteration 2

Closest Crash Responses		**Predictions**		**Actual Crash Responses**	
$d_{max}(mm)$	$a_{max}(m/s^2)$	$VF^*(\%)$	$t_d^*(ms)$	$d_{max}(mm)$	$a_{max}(m/s^2)$
354	974	14.55	25.5	310	978

The summary of the second iteration is given in the Table 4.20. The actual crash response (black marker) is not dominated by any of the crash responses of the initial data set. Therefore, the actual crash response (Table 4.20) can be added to the available data set to form a new data set, which will be used in the next iteration.

Iteration 3:

The predictions of the control parameters (VF^* and $t_d{}^*$) and the corresponding actual response of the second iteration are added to the data set of the third iteration (Table 4.17).

Table 4.21.
Data set for iteration 3

$d_{max}(mm)$	$a_{max}(m/s^2)$	$t_d(ms)$	$VF(\%)$
707	704	1	10
515	1383	1	22.5
155	1391	50	22.5
484	818	50	10
239	1111	25.5	16.12
310	978	25.5	14.55

These experiments and the corresponding crash responses are illustrated in Figure 4.37 and 4.38 respectively. Similar to the previous iterations, these crash responses of

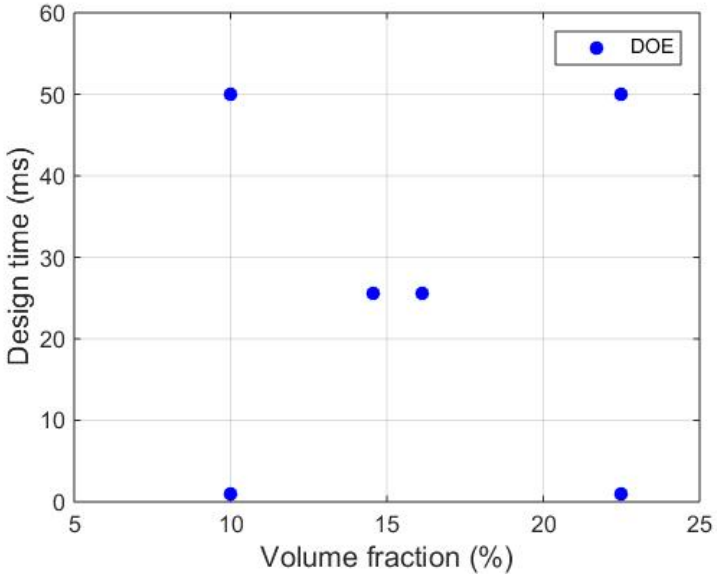

Figure 4.37. Design space for iteration 3

data set are connected with linear line plot to cover the crash response space (Figure 4.38).

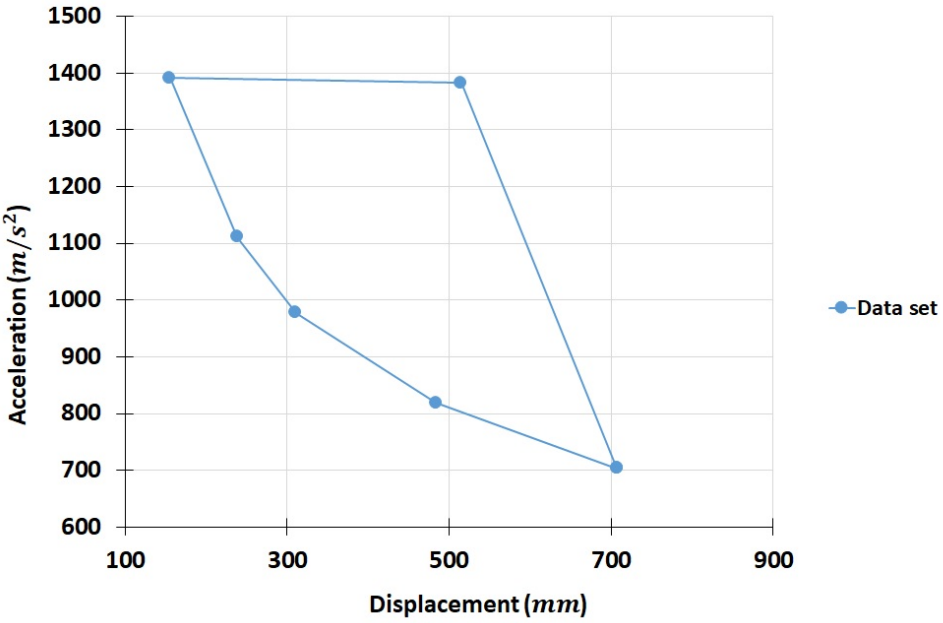

Figure 4.38. Crash response space for iteration 3

The values of the maximum acceleration and displacement of the available data set are normalized using the maximum of acceleration data (1383 m/s^2) and maximum of the displacement data (707 mm) respectively (Table 4.21).

Figure 4.39, to initialize the search of the closest point to the target, a perpendicular line is drawn from the target point towards the line connecting the crash responses. The coordinates of the closest point are evaluated by satisfying the equation of both perpendicular line and the line connecting the crash responses (Figure 4.39).

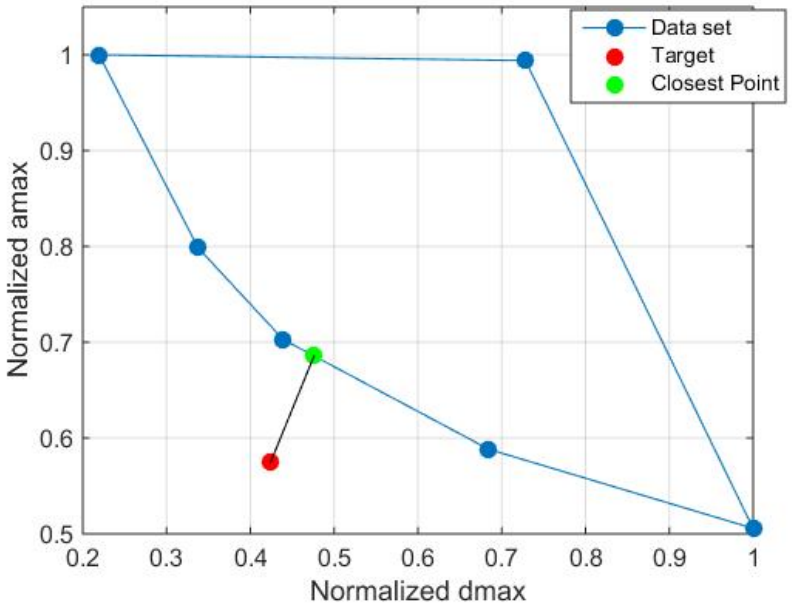

Figure 4.39. Closest point for iteration 3

The normalized crash responses of the closest point are scaled up by multiplying the X-coordinate and Y-coordinate of the closest point by maximum values of respective data sets. This process converts the normalized values of crash responses into real scale values (Table 4.22).

The crash responses of the closest point (Table 4.22) are fed to the Kriging metamodels of the volume fraction $\hat{VF}$ and design time $\hat{t_d}$ to predict the corresponding control parameters (VF^* and ${t_d}^*$). The standard procedures of cross validation and

Table 4.22.
Iteration 3: target and closest crash responses

Target Crash Responses		**Closest Crash Responses**	
a_{max} (m/s^2)	d_{max} (mm)	a_{max} (m/s^2)	d_{max} (mm)
800	300	954	337

PRESS value evaluation are performed to select best combination regression function and correlation function.

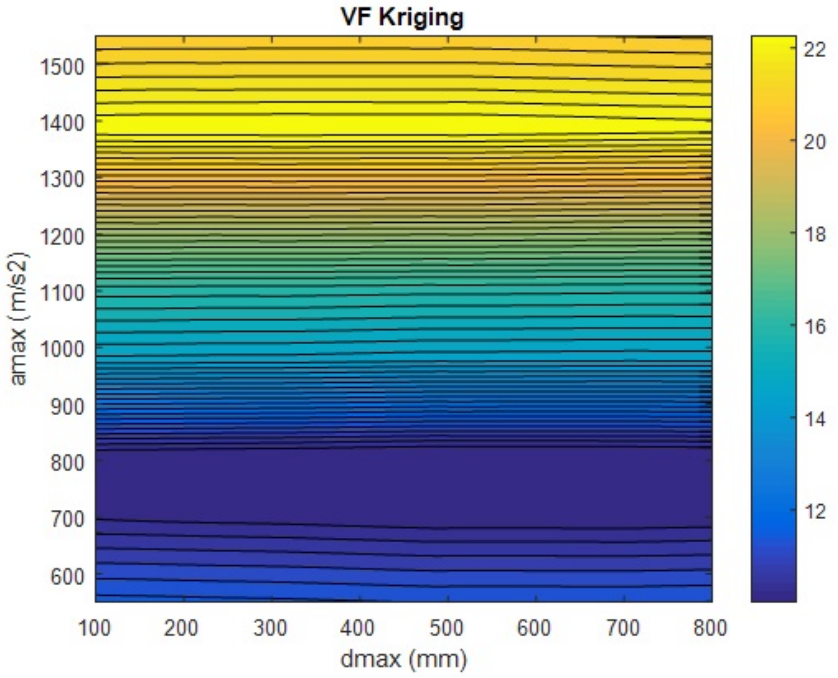

Figure 4.40. Volume fraction metamodel for iteration 3

While performing the cross-validation, it was observed that the combination of the the exponential correlation function (correxp) and the zero order regression (regpoly0) has the lowest value of PRESS. The contour plots of the volume fraction and design time metamodels ($\hat{VF}$ and $\hat{t_d}$) are shown in Figure 4.40 and 4.41. Similar to the previous iterations, the contour plots are not much informative as these metamodels

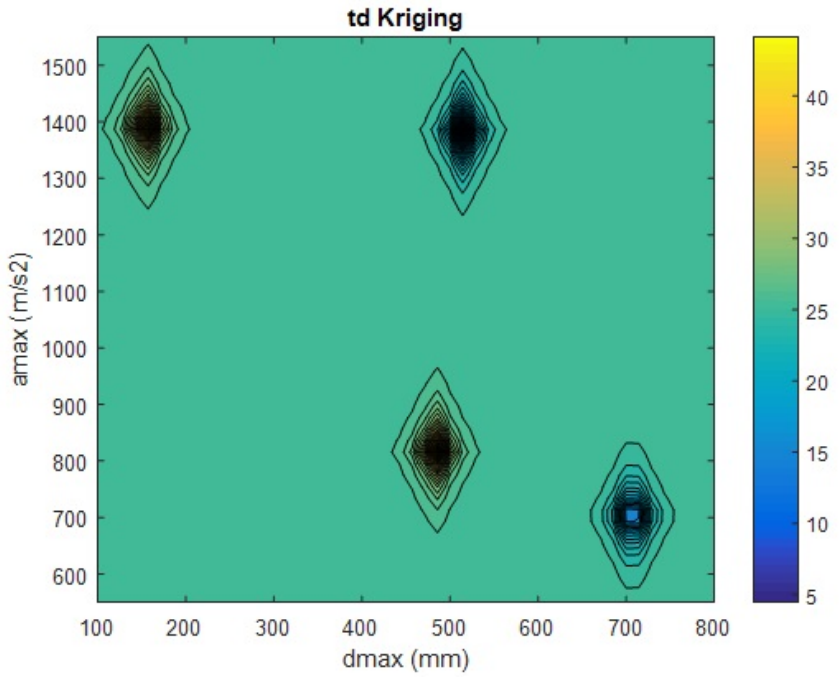

Figure 4.41. Design time metamodel for iteration 3

are built with a very few number of experiments (six). Therefore, this results in the poor and flat approximation (Figure 4.40 and 4.41).

The prediction of the volume fraction and design time is made with the corresponding metamodels. The predicted values of volume fraction and the design time, which are given in the Table 4.23 and graphically shown in Figure 4.42.

Table 4.23.
Iteration 3: prediction for the closest crash responses

Closest Crash Responses		**Predictions**	
a_{max} (m/s^2)	d_{max} (mm)	$VF^*(\%)$	$t_d{}^*(ms)$
954	337	14.35	25.5

The prediction of the volume fraction is very close to the previous iteration. However, because of the high sensitivity of the crash responses with respect to the

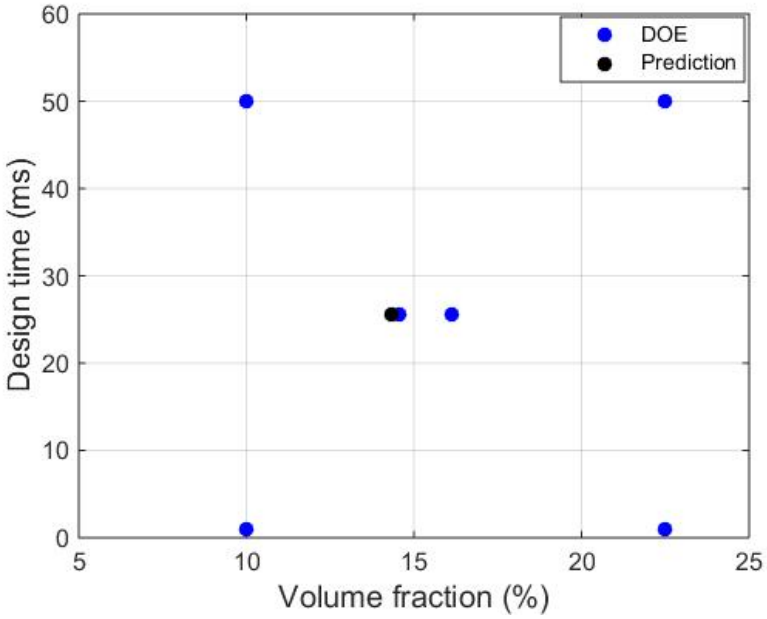

Figure 4.42. Prediction of iteration 3

control parameters (VF and t_d), it is very interesting to see the change in the actual crash responses of the iteration 3. The predicted volume fraction VF^* and design time $t_d{}^*$ are supplied to the problem formulation of the improved HCA to generate the corresponding topology design (Figure 4.43).

The actual values of maximum acceleration and maximum displacement are evaluated by performing the dynamic analysis on the generated topology design (Figure 4.43). These actual crash responses are graphically shown in Figure 4.44.

It is clear from Figure 4.44, the actual crash response (black marker) of this iteration is dominated by the one of the crash responses of the data set. Therefore, the actual crash responses of this iteration(Table 4.24) cannot be added to the available data set to form a new data set for the next iteration. This implies the iterative process has reached its convergence.

Therefore, it is concluded that the actual responses of the second iteration is best result obtained with this approach (Table 4.25).

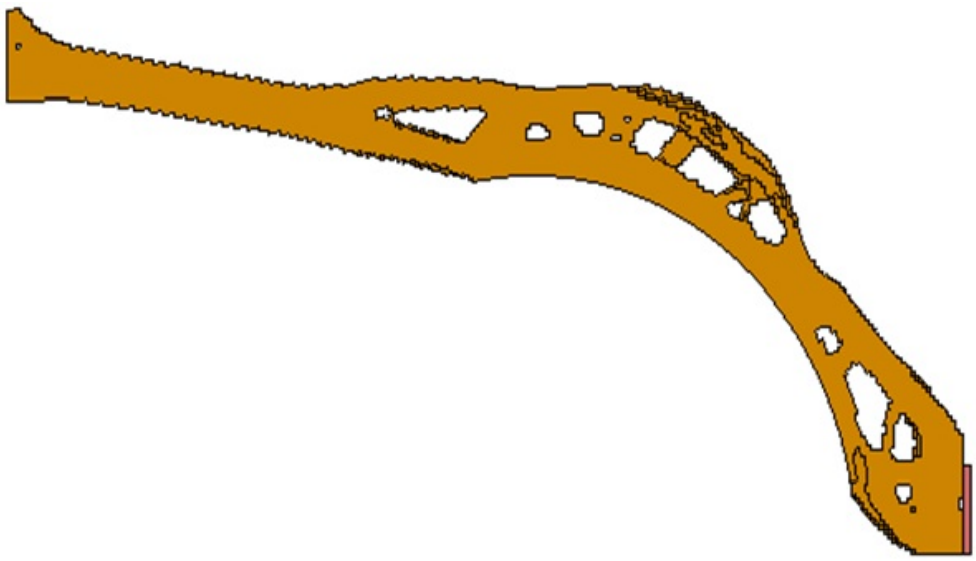

Figure 4.43. Topology design of iteration 3

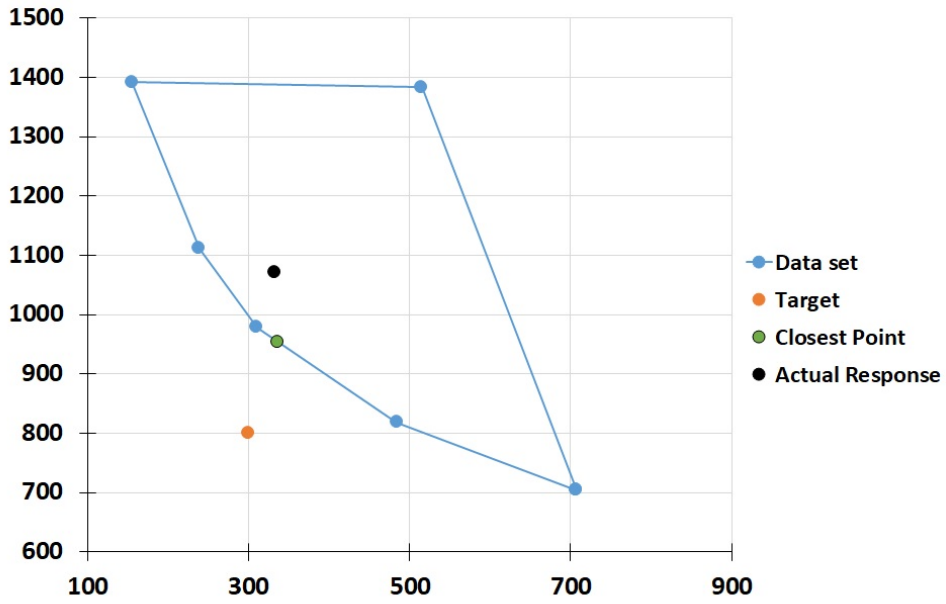

Figure 4.44. Actual crash responses of iteration 3

The error between the target crash responses and the actual crash responses are calculated dividing the numerical discrepancy between the actual and the target

Table 4.24.
Summary of iteration 3

Closest Crash Responses		**Predictions**		**Actual Crash Responses**	
$d_{max}(mm)$	$a_{max}(m/s^2)$	$VF^*(\%)$	$t_d^*(ms)$	$d_{max}(mm)$	$a_{max}(m/s^2)$
337	954	14.35	25.5	333	1071

Table 4.25.
Best possible results

Target Crash Responses		**Actual Crash Responses**	
$d_{max}(mm)$	$a_{max}(m/s^2)$	$d_{max}(mm)$	$a_{max}(m/s^2)$
300	800	310	978

response by the actual response. Therefore, the errors in the acceleration and the displacement are given as

$$Error_{acc} = \frac{|978 - 800|}{978} \times 100 = 18.2\%$$

$$Error_{dis} = \frac{|310 - 300|}{310} \times 100 = 3.2\%$$

As it is clear that, with this approach, the error in the acceleration is increased by some amount. However, the reduction in the displacement error is quite significant as compare to the previous approach (targeting with 24 DOE). The summary of both targeting approach is given in the following table

Table 4.26.
Comparison of two proposed targeting approaches

	With 24 DOE	**With 4 DOE**
Function evaluations	25	7
Error in acceleration	6.5%	18.2%
Error in displacement	52%	3.2%

The design of experiments (DOE) of the previous approach has 24 initial function evaluations. Furthermore, for target crash responses, the prediction of the volume fraction and the design time are made and the corresponding topology design is generated. Altogether, the previous approach has 25 function evaluations (Table 4.26). On the other hand, the approach with four experiments has four initial function evaluations and 3 additional iterations. Thus, as shown in Table 4.26, this approach ended up with only 7 function evaluations with significant reduction in the displacement error as compared to the previous approach. With these targeting approaches, the predictions of volume fraction is are made based on the quality of the metamodel and the desired or target crash responses. With the advanced applications of the design time, the crash responses can be further improved by keeping the volume fraction as low as possible. These applications are demonstrated in the subsequent sections

4.2.6 Results of the multi-design time

The crash responses (a_{max} and d_{max}) are further improved with the implementation of the multi-design time method on the model of front frame with multiple load cases. The boundary conditions and the loading conditions for the dynamic analysis with multiple loads are kept same as the case of a single load (Refer 4.2.1 a). Based on the samples of the design time t_d, time of 1, 10, and 50 milliseconds were selected for the corresponding three load cases. Therefore, with theses multiple design times, the averaged field variable of the each element $\bar{U}_i$ now becomes $\bar{U}_i^m$ under the multiple loads. This new averaged field variable can be expressed as

$$\bar{U}_i^m = \frac{1}{3}\bar{U}_i(t_d = 1) + \frac{1}{3}\bar{U}_i(t_d = 10) + \frac{1}{3}\bar{U}_i(t_d = 50) \tag{4.3}$$

Here, three design times are utilized for topology synthesis. Therefore, the numerical value of weight for each loading case is assigned as 1/3, so the summation of total weights will be equal to one (Refer section 3.4.1).

The topology synthesis is performed using a new averaged field variable $\bar{U}_i^m$, and the final volume fraction of 20% in the problem formulation of the improved

HCA (Refer section 3.2). Therefore, in order to generate the final topology design, the volume fraction constraint is satisfied while reducing the numerical discrepancy between $\bar{U}_i^m$ and the set point U_i^* for every element.

The final topology design clearly shows the load paths under the multiple loads (**??**). As observed previously, the material distribution in the final topology design varies according to the corresponding design time (Figure 4.9 and 4.10). However, in this case, the multiple design times were fed for the topology synthesis. Therefore, this problem formulation attempted to enhance the structural integrity at 1, 10, 50 milliseconds, which in turn distributes the material more uniformly distributed from the front end to the rear end of the design domain(Figure 4.45). Thus, it very important to evaluate the effect of multiple design times in the overall structural integrity and the corresponding crash responses.

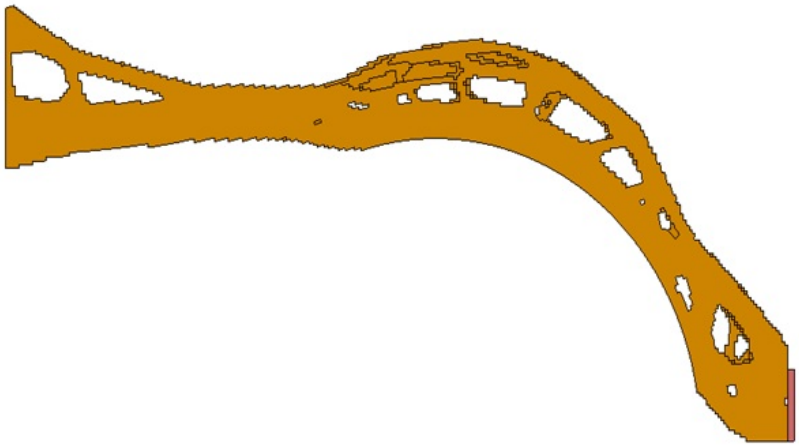

Figure 4.45. Topology design generated with multiple loads

To evaluate the crash responses of the topology design with multi-design time, it is subjected to the previously used boundary conditions and the loading conditions. The topology design generated using multiple load cases has the final volume fraction of 20%. Therefore, the corresponding crash responses are compared with the crash responses of the topology designs with the same volume fraction but obtained with single dynamic loading (Refer section 4.2.3). The corresponding acceleration-displacement profiles are shown in the following figure.

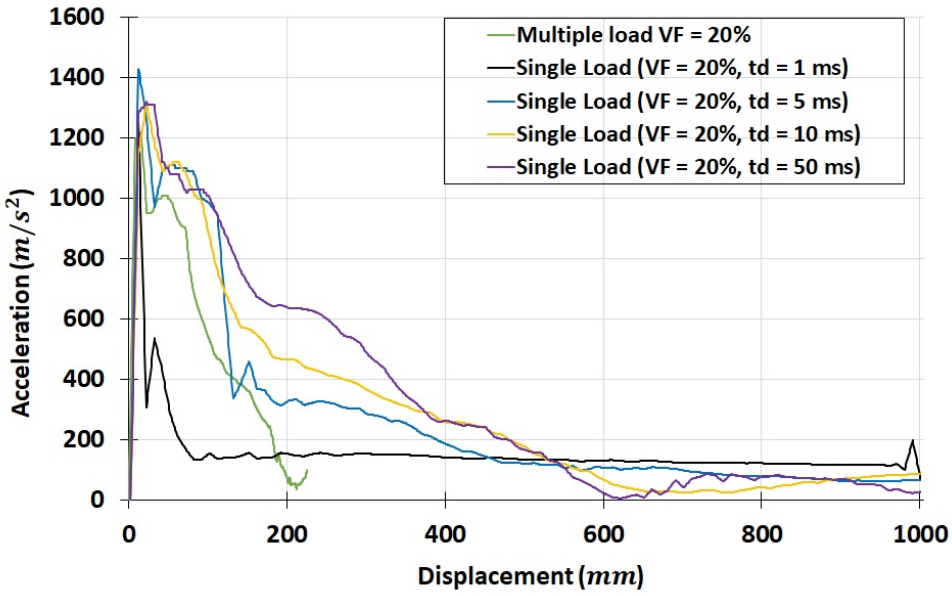

Figure 4.46. Accelration-displacement profiles of designs with VF of 20 percent

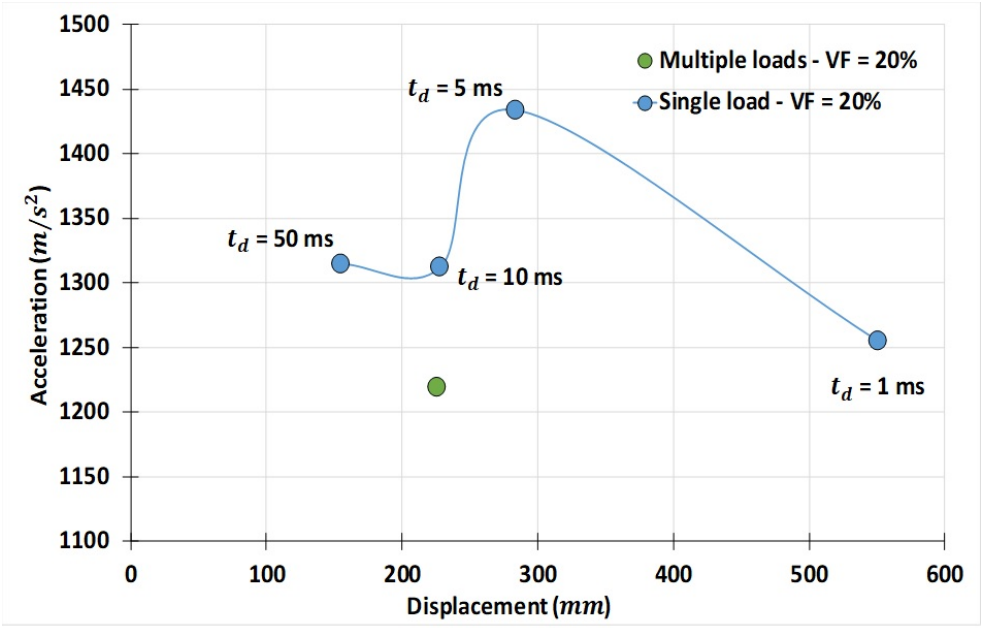

Figure 4.47. Performance of topology design generated with multiple loads

In Figure 4.47, blue markers are the crash responses of of the topology designs synthesized with single dynamic load case with the volume fraction of 20% and variable design time (1, 5, 10, and 50 milliseconds). Focusing on the crash responses of

the topology generated with multiple loads, the maximum acceleration of the rigid box is 1219 m/s^2, whereas the maximum displacement is 226 mm (green marker). These crash responses are non-dominated by any of the blue markers. In fact, this acceleration-displacement profile (green marker) dominates most of the acceleration-displacement profiles of the topology designs generated with single dynamic load (blue markers).

This demonstrates the ability of multi-design time method to control and improve the crash responses even with a lower volume fraction. Another application of design time to improve the crash responses with lower volume fractions is demonstrated in the next section.

4.2.7 Results of the merged design

The method is an explicit way to post-process the already synthesized topology designs to obtain a new design with better crash responses. With this method, the topology designs obtained with 24 combinations of the design time t_d and volume fraction VF (Refer section 4.2.3) are post-processed by performing the binary operations. Specifically, the union operation is performed on two or more topology designs (out of 24 topology designs) to generate the merged design.

Considering the issue of lightweight structures, the combination of the topology designs to be united is selected in such a way that the final volume fraction of the merged design will be as low as possible. For the model of front frame, the lowest volume fraction utilized for topology synthesis is 10% of the entire design domain. Therefore, topology design with 10% volume fraction and variable design time are selected for post-processing operations (Figure 4.48). The crash responses of the structures with 10% volume fraction are graphically shown in Figure 4.49

To generate the merged design, selection of the topology designs to be merged is a very important factor. The motive behind the selection of these topology designs is to reduce both maximum acceleration and displacement of the resulting merged

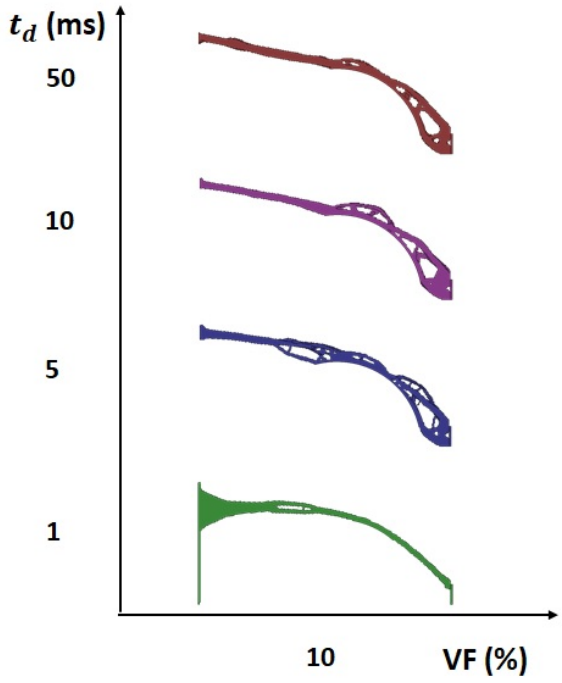

Figure 4.48. Topology designs with volume fraction of 10 percent

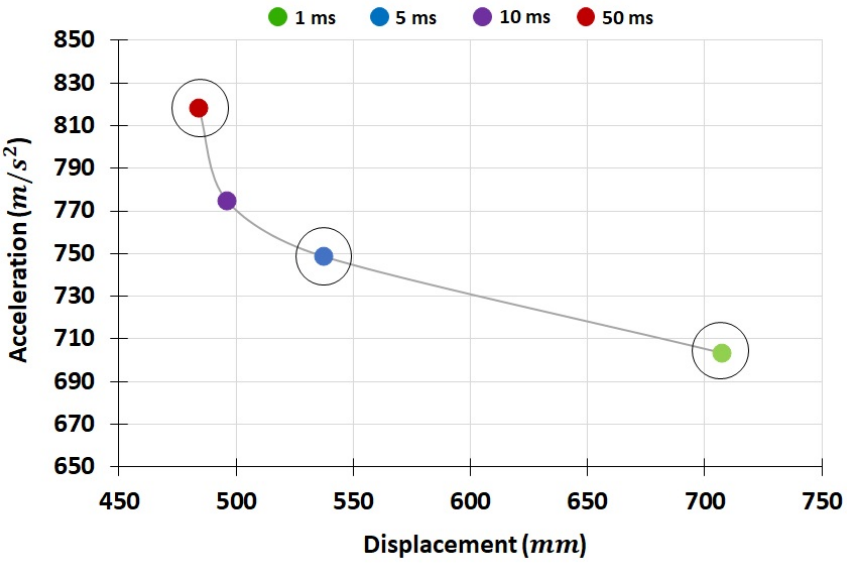

Figure 4.49. Crash responses of topology designs with volume fraction of 10 percent

design. As shown in Figure 4.49, the topology design with 1 ms design time has lowest acceleration, whereas, the design with 50 ms design time has lowest displacement. Finally, the design with 5 ms design time has intermediate values of maximum

acceleration and displacement. Therefore, these three topology designs are selected to generate the merged design. Therefore, rewriting the expression of merging (Refer section 3.4.2)

$$S_{Mer} = S_{k1} \cup S_{k2} \cup S_{k3} \tag{4.4}$$

$$k1 = [VF = 10, \quad t_d = 1]$$
$$k2 = [VF = 10, \quad t_d = 5]$$
$$k3 = [VF = 10, \quad t_d = 50]$$

where, k1, k2, and k3 are the structures to be merged with the corresponding volume fraction VF and design time t_d. The merged design formed by performing the union operation on the selected topology designs in LS-Pre/Post. The common nodes and the common elements of these three topology designs are automatically get duplicated. Therefore, these duplicated nodes and elements are deleted to keep the structural stability.

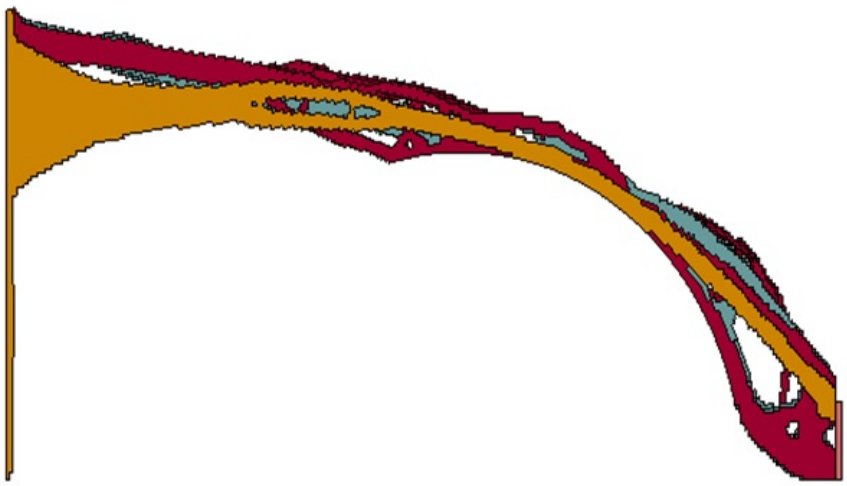

Figure 4.50. Merged design

The resulting merged design is shown in Figure 4.50. Topology designs are highlighted with distinct colors. To evaluate the crash responses of the merged design, the dynamic analysis is performed with the boundary and loading conditions which are consistently used in the proposed work. The final mass of the merged design is 13.2

kg, which is the 20% of the mass of the entire design domain of front frame (66 kg). Therefore, the crash responses of the merged design is compared with the crash responses of the topology designs with the 20% volume fraction but obtained with single dynamic loading (Refer section 4.2.3). The corresponding acceleration-displacement profiles are shown in the figure.

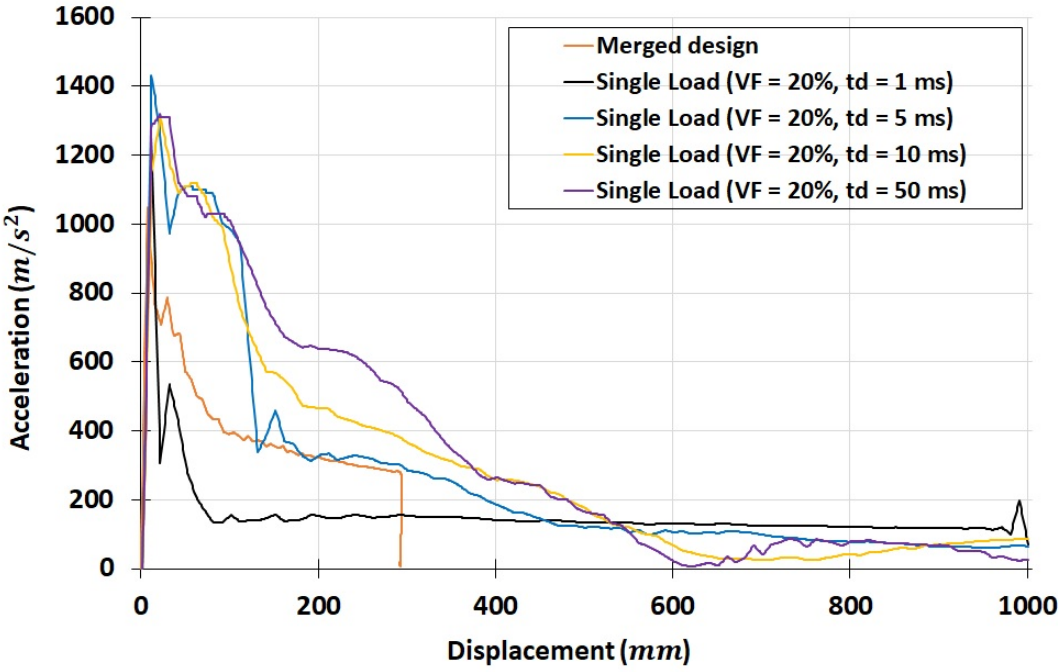

Figure 4.51. Acceleration-displacement profiles of merged design and other designs with VF of 20 percent

The maximum acceleration and displacement of the merged design are shown in Figure 4.52. The blue markers represents the crash responses of the topology design are synthesized using single dynamic load and have volume fraction of 20% with variable design time (1, 5, 10, 50 milliseconds). With the strategy of merging the design, the resulting structure shows great reduction in the maximum acceleration (orange marker), which dominates maximum acceleration of the every design with same volume fraction (blue markers). Furthermore, the performance of the merged design is not fully dominated by any of the other designs (Figure 4.52). one of the great advantages of this method is, while selecting the structures to be merged (k1, k2

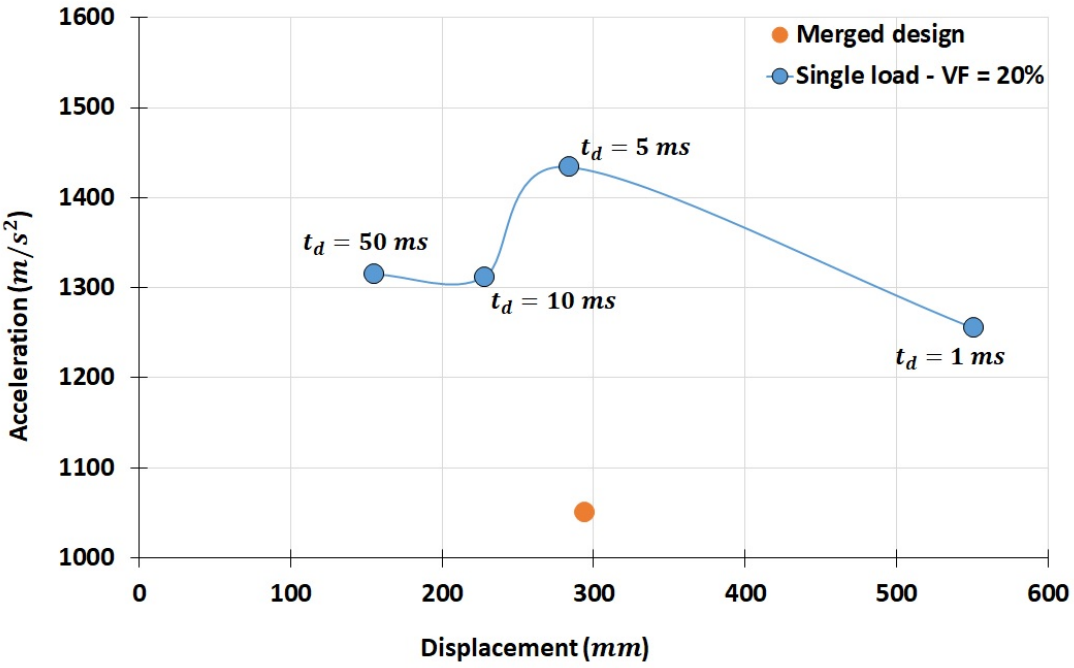

Figure 4.52. Crash responses of the merged design

...kn), one can choose topology designs with any volume fraction VF and any design time t_d. This flexibility can further be used to reduce both maximum acceleration and maximum displacement.

5. SUMMARY AND RECOMMENDATIONS

This chapter highlights the key aspects of the engineering problem addressed in this work, the corresponding implemented methods, and findings of the implemented methods in the numerical examples. The second half of this chapter enlists some of the plausible future recommendations for the proposed work.

5.1 Summary

The first chapter initialized the discussion of some of the important aspects of the passenger safety and effects of structural performance of vehicle components on passenger safety. It was clear from the literature review that heavy vehicle structures can make the passenger cabin safer but at the same time it increases overall weight of the vehicle, which in turn worsens the fuel efficiency of the vehicle. This aspect raised the issue of crashworthy lightweight structures. The chapter further discussed the nonlinear and linear structural optimization techniques that are previously used to address the issue of lightweight structures, which depicted that the crash responses such as internal energy absorption, reaction forces are well studied by the researchers. The chapter further highlighted the major development in hybrid cellular automata (HCA) method as a nonlinear structural optimization technique.

In the final section of the first chapter, the objectives of the proposed work were discussed, in which the minimization of the peak acceleration and displacement of the vehicle structures were set as the objectives to generate lightweight topology designs.

The second chapter explained the hybrid cellular automata (HCA) method as a heuristic method of topology synthesis. The HCA communicates with a nonlinear

finite element solver LS-DYNA to obtain the internal energy density, which is treated as a field variable in the topology synthesis process.

For topology synthesis, the density of of the material is mapped from 0 to 1. This relative density of the every element is updated between 0 and 1 based on the field variable of the corresponding element. The intermediate properties of the material is interpolated using solid isotropic material penalization (SIMP) method. In HCA, the objective was to reduce the numerical discrepancy between field variable og every element and the corresponding set point, where the set point is a field variable calculated when the relative density of the element is equal to 1.

For a specific dynamic loading, the HCA could generate topology designs, whose stiffness and the corresponding performance greatly depends in the volume fraction constraint which is imposed on the topology synthesis problem. Therefore, in some of the cases, in order to obtain specific performance of the resulting topology design, the designer had to compromise with the final volume fraction or mass of the topology design. This generates a need of generating lightweight structures without compromising with the structural performance.

The third chapter presented the contribution of the proposed work to improve the current HCA method. As the volume fraction tunes the stiffness of the final structure, it becomes quite difficult to obtain specific structural performance with lower volume fraction. Therefore, it was important to introduce a new control variable, which can affect the performance of the topology design. Therefore, the concept of the design time was introduced in the current version of HCA method. The design time is time at which the HCA communicates with LS-DYNA to obtain the information of the internal energy density (IED) of every element of the structure. As the dynamic loading progresses, usually the strain wave finds the different load paths at different time throughout the design domain to be synthesized.

Therefore, the internal energy distribution would be different at different time over the entire span of dynamic loading. This made IED or field variable a time-dependent entity. As the density of every element is updated based on the time-dependent field

variable, the density of the every element also becomes the time-dependent entity. Therefore, the final topology design and the corresponding structural performance can be tuned using the variable design time.

The introduction of the design time made the topology synthesis problem bi-dimensional, where the design time t_d and volume fraction VF were the two dimensions or the control variables. This created the scope for generating the design space by sampling both volume fraction and the design time, so one can build the design of experiments (DOE). Once the DOE is ready, each experiment (combination of design time and volume fraction) was fed to the problem formulation of the improved HCA, where the field variable (IED) and the design variable (density) are the time-dependent entities.The performance of the generated topology design were evaluated to create the crash response space, where the maximum acceleration and displacement of the topology design under the dynamic loads were the crucial crash responses.

The Kriging metamodeling technique was implemented to build the implicit relation between crash responses (maximum acceleration and maximum displacement) and design control variables (volume fraction and design time). The selection of the appropriate metamodel was made by conducting the cross validation, so the prediction of the control variables will be accurate. so one can set the target or desired crash responses and predict the corresponding design control variables. These predicted design control variables were sent to the problem formulation of the improved HCA to generate the topology design. The actual crash responses were obtained by performing the dynamic analysis on the generated design with the boundary and the loading conditions, which are previously used in the proposed work. The error between target crash responses and the actual crash responses.

The design time was further extended to the concept of multi-design, where the multiple design time and the same volume fraction were supplied to the formulation of the improved HCA to generate the topology design. This implies, in this case, the topology synthesis tried to reduce the numerical discrepancy between the actual field variable and the set point of the field variable each element at multiple design times.

This would enhance the performance of the structure not only at specific time bu the multiple design times.

Finally, the third chapter presented another implementation of the design time by performing the binary operations on the topology design generated at the different design time t_d and different volume fraction VF. The proposed idea was to merge different the topology designs of different crash responses to enhance the crash responses of the final merged design.

The capabilities of the improved HCA were demonstrated in the fourth chapter using the numerical example of simplified front frame model of a car. To simulate the crash event, the finite element model of the front frame was set up with corresponding boundary conditions and loading conditions. A nonlinear finite element explicit code LS-DYNA was used to solve the dynamic analysis problem and to obtain the information of each element of the design domain of the front frame for topology synthesis purposes.

To address the issue of lightweight structures, low range of volume fraction VF with six samples (10%, 12.5%, 15%, 17.5%, 20%, and 22.5%). Four samples of the design time t_d were selected considering the computational cost of the topology synthesis (1, 5, 10, and 50 milliseconds). Thus, with six volume fractions and four design time, design of experiment was built with 24 combinations of t_d and VF. These experiments were fed to the improved HCA to generate the corresponding topology designs. It was clearly observed that for the same volume fraction and variable design time, the load paths of the topology designs were greatly affected by the corresponding design time.

The performance of these 24 topology designs was obtained by performing the dynamic analysis on the topology designs using the previously used boundary and loading conditions. The maximum acceleration a_{max} and the maximum displacement d_{max} were evaluated as the measures of the structural performance. The maximum acceleration-displacement profiles showed a monotonic trend with respect to change in the design time in most of the volume fraction. However, for some of the vol-

ume fractions, the trend of the maximum acceleration-displacement profiles was very nonlinear with respect to change in the design time.

The implicit relation between these nonlinear crash responses (a_{max} and d_{max}) and design control variables (t_d and VF) was established using the Kriging metamodeling technique. The quality of the metamodel was determined by evaluating the predicted residual error sum of squares (PRESS) with number of combinations of the correlation functions and the regression functions. The maximum acceleration of 800 m/s^2 and the maximum displacement of 300 mm were set as the target crash responses. The volume fraction and the design time were predicted for the target crash responses using the validated Kriging metamodel. The predicted volume fraction VF^* and design time t_d^* were supplied to were supplied to the improved HCA to generate the topology design. The maximum displacement of the resulting topology design showed considerable discrepancy with respect to the target displacement. However, the error between the actual and the target maximum acceleration was within the acceptable limit.

This targeting approach was further extended with four experiments instead of full design of experiment. These four experiments were formed using the possible combinations of minimum and maximum values of volume fraction and design time. This approach used low fidelity metamodel (based on very few experiments) with search of the closest crash responses to the target crash responses. This approach was converged in only three iteration with a topology design whose actual crash responses were in the great agreement with the target crash responses. the error between the actual maximum displacement and targer maximum displacement was significantly reduced with relatively less computational time.

The advanced application of the design time such as multi-design time and merged design were also demonstrated using the example of the front frame. The approach of multi-design time provided flexibility in picking up the multiple design time, at which the performance of the final topology was enhanced. This resulted in the

improvement in the crash responses when compared to the other topology designs with same volume fraction.

The merged design were also showed promising performance by reducing both maximum acceleration and maximum displacement when compared to he other topology designs with same volume fraction. The limited control on the final mass of the merged design may limit the usage of this approach. However, this approach provides flexibility of merging the different topology designs with any volume fraction and any design time. Therefore, one can have more number of options to improve the performance of the resulting structure.

5.2 Future work

In the proposed work, the numerical example of the simplified front frame demonstrated that the implementation of the design time t_d has promising abilities to affect the performance of the topology designs. However, these abilities can further be enhanced by extending the proposed work with the following improvements.

5.2.1 Exploration of the design space

In the proposed work, the design space for the topology synthesis is a bi-dimensional space of design control variables (volume fraction and design time). The samples of the volume fraction VF and design time t_d were manually selected to build the corresponding design of experiment. This user defined sampling method did not explore total design space. For instance, the proposed worked picked 1, 5, 10, and 50 milliseconds as samples of the design time. In this case, the design time between 10 and 50 millisecond is not considered.

Therefore, this sampling technique can further be improved by implementing Latin hypercube sampling (LHS) technique. This sampling method has ability to explore whole design space with same or less number of samples. Ideally, 10 samples are recommended per design variable. As the proposed work has two design control

variables (VF and t_d), 20 samples would be the minimum requirement to explore the design space and to build the design of experiments.

As shown in Figure 5.1, every region of the design space is explored with 20 samples even if the upper and lower bounds of the volume fraction VF and design time t_d are kept same as the previously implemented user defined sampling. This can be helpful in determining the trend of the crash responses with respect well explored design time and volume fraction, which in turn would improve the quality of the metamodel and the corresponding prediction of the design control variables (VF and t_d).

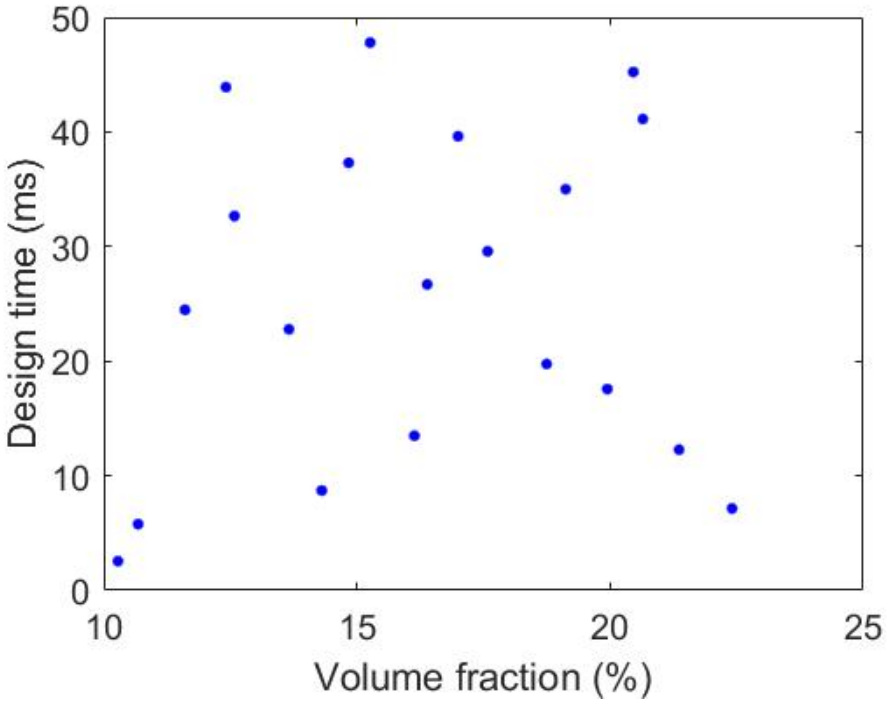

Figure 5.1. Design space with latin hypercube sampling

5.2.2 Implementation of design time on a full scale model

The proposed work used the simplified model of front frame to reduce the computational cost of the topology synthesis process. However, with a very powerful

processing units, the proposed method can be implemented on the body in white (BIW) components, which altogether weigh almost 40%of the total weigh of the passenger car. For the sample demonstration, the proposed method is implemented on the design domain of a full scale front frame of the car (Figure 5.2).

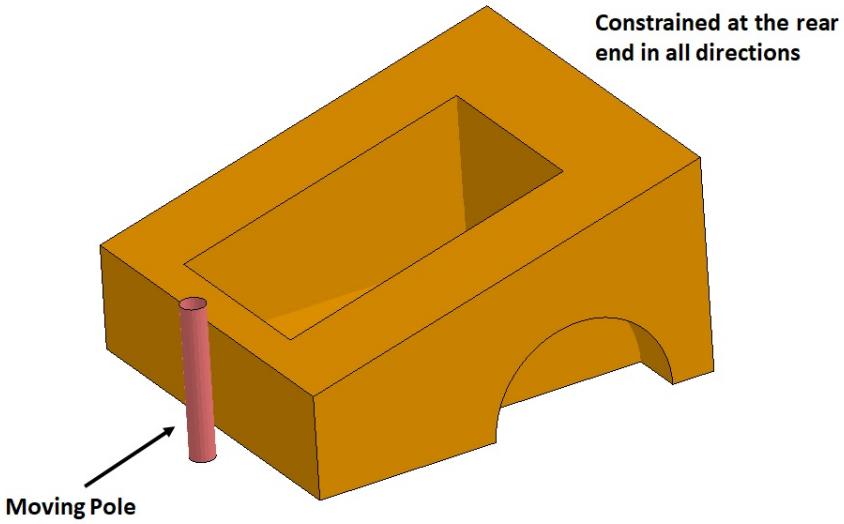

Figure 5.2. Design domain of the front frame with engine bay

The pole moving with 15.65 m/s is crashing against the design domain whose rear end is constrained in all directions. The computational time is greatly reduced by using a very coarse element size. With improved HCA, the topology synthesis was performed with volume fraction constraint of 20% and variable design time of 2.5, 5, 10 milliseconds. The generated topology designs are shown in the following figures.

The effects of the design time on the load paths of the topology designs shown above are interesting. However, these load paths are not detailed and complex as one would expect. The prominent reason for this kind of design is the fidelity of the finite element model. Here, the low fidelity model (coarse mesh) is used to reduce the computational time considering the processing unit of the local machine. Therefore, to obtain the topology designs with better crash performance, super-computing processing units can be utilized. This approach would serve as a guideline to implement the proposed work on the other components of the entire body in white (BIW).

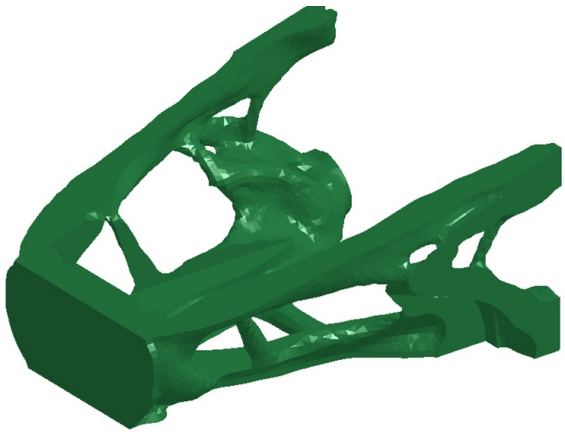

Figure 5.3. Topology deign with the design time of 2.5 milliseconds

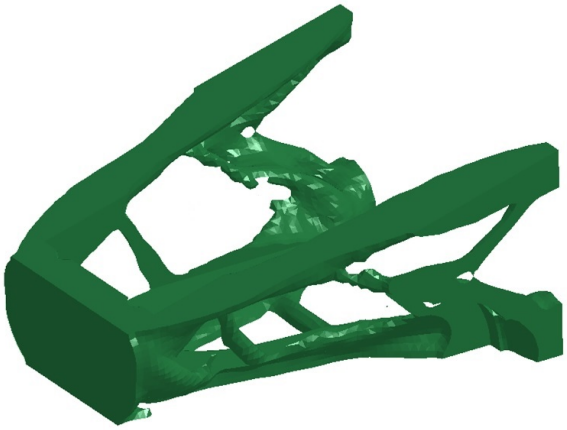

Figure 5.4. Topology deign with the design time of 5 milliseconds

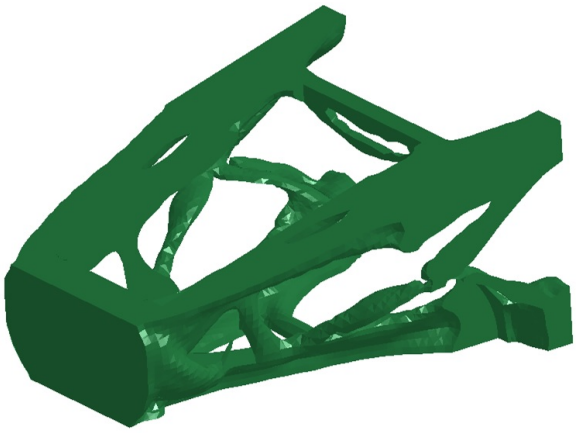

Figure 5.5. Topology deign with the design time of 10 milliseconds

5.2.3 Multi-material topology synthesis

The proposed work so far studied the effects of the design on single material type with single as well as multiple dynamic load. Therefore, it would be interesting to analyze the effects of the design time on the design domain with multiple materials. This can explicitly achieved by the assigning the distinct material cards to each element of the material based on the final relative density of the corresponding element. Some threshold values of the relative densities are need to be set, so appropriate material card can be assigned to each element. This approach can logically be expressed as

$$\begin{aligned} \text{if} \quad x_i < x_{t1} \quad \text{assign} \quad M_0 \\ \text{if} \quad x_{t1} < x_i < x_{t2} \quad \text{assign} \quad M_i \\ \text{if} \quad x_i > x_{t2} \quad \text{assign} \quad M_b \end{aligned}$$

where, M_0, M_i, and M_b are the void, intermediate, and base material respectively. For instance, if the base material is steel then the intermediate material could be an appropriate material which is lighter than steel (Ex. Aluminum). The relative densities x_{t1} and x_{t2} are the threshold densities, which are used to assign appropriate material to the element based on the element density x_i. The multi-material approach may limit the manufacturing of these complex topology designs. However, the advanced additive manufacturing techniques can be utilized to produce design prototypes for the experimental testing.

REFERENCES

REFERENCES

[1] T. Xu, Y. Li, Q. Li, L. Hao, and W. Song, "Crashworthiness design of frontal rail using strain-energy-density and topology optimization approach," in *Computational Science and Optimization (CSO), 2010 Third International Joint Conference on*, vol. 1. IEEE, 2010, pp. 24–28.

[2] S. Huang and J. Dong, "Optimization study of vehicle crashworthiness based on two types of frontal impacts," in *Transportation Information and Safety (ICTIS), 2015 International Conference on*. IEEE, 2015, pp. 409–413.

[3] D. Wang, G. Dong, J. Zhang, and S. Huang, "Car side structure crashworthiness in pole and moving deformable barrier side impacts," *Tsinghua Science & Technology*, vol. 11, no. 6, pp. 725–730, 2006.

[4] C. A. Soto and T.-Y. Pan, "Optimum topology of structural foam for crashworthiness applications," SAE Technical Paper, Tech. Rep., 2004.

[5] Z. Yang, Q. Peng, and J. Yang, "Lightweight design of b-pillar with trb concept considering crashworthiness," in *Digital Manufacturing and Automation (ICDMA), 2012 Third International Conference on*. IEEE, 2012, pp. 510–513.

[6] H. H. Jang, H.-A. Lee, S.-I. Yi, D. S. Kim, H. W. Yang, and G.-J. Park, "Cross-section design of the crash box to maximize energy absorption," SAE Technical Paper, Tech. Rep., 2011.

[7] K. Liu, Z. Xu, D. Detwiler, and A. Tovar, "Optimal design of cellular material systems for crashworthiness," SAE Technical Paper, Tech. Rep., 2016.

[8] M. Mirzaei, M. Shakeri, M. Seddighi, and S. Seyedi, "Using of neural networks and genetic algorithm in multi objective optimization of collapsible energy absorbers," in *Proc. 2nd Int. Conf. on Eng. Optimization, Lisbon*, 2010, pp. 6–9.

[9] N. M. Patel, B.-S. Kang, J. E. Renaud, and A. Tovar, "Crashworthiness design using topology optimization," *Journal of Mechanical Design*, vol. 131, no. 6, p. 061013, 2009.

[10] Q. Wang, Z. Fan, L. Gui, Z. Chen, and H. Song, "Crashworthiness analysis of a minibus body in white through reverse engineering," *Tsinghua Science and Technology*, vol. 9, no. 3, pp. 338–344, 2004.

[11] L. Tian and Y. Gao, "Crashworthiness design of automotive body in white using topology optimization," SAE Technical Paper, Tech. Rep., 2016.

[12] L. Shi, R.-J. Yang, and P. Zhu, "An adaptive response surface method for crashworthiness optimization," *Engineering Optimization*, vol. 45, no. 11, pp. 1365–1377, 2013.

[13] L. D. K. U. Manual and I. Volume, "Material models," *Volume*, vol. 2, pp. 187–192, 2013.

[14] J. Hallquist, "Ls-prepost manual, version 1.0," *Livermore Software Technology Corporation*, 2002.

[15] P. W. Christensen and A. Klarbring, *An introduction to structural optimization*. Springer Science & Business Media, 2008, vol. 153.

[16] A. Tovar, N. M. Patel, G. L. Niebur, M. Sen, and J. E. Renaud, "Topology optimization using a hybrid cellular automaton method with local control rules," *Journal of Mechanical Design*, vol. 128, no. 6, pp. 1205–1216, 2006.

[17] A. Tovar, "Bone remodelling as a hybrid cellular automaton optimization process," Ph.D. dissertation, University of Notre Dame, 2004.

[18] H. Müllerschön, N. Lazarov, and K. Witowski, "Application of topology optimization for crash with lsopt®/topology," in *11th International LS-DYNA Users Conference*, 2010.

[19] P. Bandi, J. P. Schmiedeler, and A. Tovar, "Design of crashworthy structures with controlled energy absorption in the hybrid cellular automaton framework," *Journal of Mechanical Design*, vol. 135, no. 9, p. 091002, 2013.

[20] C. Mozumder, P. Bandi, N. Patel, and J. Renaud, "Thickness based topology optimization for crashworthiness design using hybrid cellular automata," in *12th AIAA/ISSMO multidiscipinary analysis and optimization conference, AIAA*, vol. 6046, 2008.

[21] C. Mozumder, J. E. Renaud, and A. Tovar, "Topometry optimisation for crashworthiness design using hybrid cellular automata," *International journal of vehicle design*, vol. 60, no. 1/2, pp. 100–120, 2012.

[22] S. Shinde, P. Bandi, D. Detwiler, and A. Tovar, "Structural optimization of thin-walled tubular structures for progressive buckling using compliant mechanism approach," *SAE International Journal of Passenger Cars-Mechanical Systems*, vol. 6, no. 2013-01-0658, pp. 109–120, 2013.

[23] F. Duddeck, S. Hunkeler, P. Lozano, E. Wehrle, and D. Zeng, "Topology optimization for crashworthiness of thin-walled structures under axial impact using hybrid cellular automata," *Structural and Multidisciplinary Optimization*, vol. 54, no. 3, pp. 415–428, 2016.

[24] D. Zeng and F. Duddeck, "Improved hybrid cellular automata for crashworthiness optimization of thin-walled structures," *Structural and Multidisciplinary Optimization*, vol. 56, no. 1, pp. 101–115, 2017.

[25] B. Kang, W. Choi, and G. Park, "Structural optimization under equivalent static loads transformed from dynamic loads based on displacement," *Computers & Structures*, vol. 79, no. 2, pp. 145–154, 2001.

[26] A. Kaushik and A. Ramani, "Topology optimization for nonlinear dynamic problems: Considerations for automotive crashworthiness," *Engineering Optimization*, vol. 46, no. 4, pp. 487–502, 2014.

[27] Z. Ahmad, T. Sultan, M. Zoppi, M. Abid, and G. Jin Park, "Nonlinear response topology optimization using equivalent static loadscase studies," *Engineering Optimization*, vol. 49, no. 2, pp. 252–268, 2017.

[28] H. Wang, Z.-D. Ma, N. Kikuchi, C. Pierre, and B. Raju, "Multi-domain multi-step topology optimization for vehicle structure crashworthiness design," SAE Technical Paper, Tech. Rep., 2004.

[29] X. Luo, W. Du, H. Li, L. Peiyu, C. Ma, S. Xu, and J. Zhang, "Occupant injury response prediction prior to crash based on pre-crash systems," SAE Technical Paper, Tech. Rep., 2017.

[30] Y. Zhang, P. Zhu, G. Chen, and Z. Lin, "Study on structural lightweight design of automotive front side rail based on response surface method," *Journal of Mechanical Design*, vol. 129, no. 5, pp. 553–557, 2007.

[31] W. Roux *et al.*, "Ls-tasc topology and shape computations for ls-dyna user's manual," *Livermore Software Technology Corporation*, 2010.

[32] N. Patel, "Crashwothiness design using topology optimization," Ph.D. dissertation, University of Notre Dame, 2007.

[33] W. Roux, "Topology design using ls-tasc version 2 and ls-dyna®," *Livermore Software Technology Corporation*, 2011.

[34] H. Kurtaran, A. Eskandarian, D. Marzougui, and N. Bedewi, "Crashworthiness design optimization using successive response surface approximations," *Computational mechanics*, vol. 29, no. 4, pp. 409–421, 2002.

[35] H. B. Nielsen, S. N. Lophaven, and J. Søndergaard, "Dace, a matlab kriging toolbox," *Informatics and mathematical modelling. Lyngby–Denmark: Technical University of Denmark, DTU*, 2002.

[36] G. G. Wang and S. Shan, "Review of metamodeling techniques in support of engineering design optimization," *Journal of Mechanical design*, vol. 129, no. 4, pp. 370–380, 2007.

[37] D. R. Jones, M. Schonlau, and W. J. Welch, "Efficient global optimization of expensive black-box functions," *Journal of Global optimization*, vol. 13, no. 4, pp. 455–492, 1998.

[38] N. Cressie, *Statistics for spatial data*. John Wiley & Sons, 2015.

[39] K. Liu, D. Detwiler, and A. Tovar, "Optimal design of nonlinear multimaterial structures for crashworthiness using cluster analysis," *Journal of Mechanical Design*, vol. 139, no. 10, p. 101401, 2017.

[40] L.-D. K. U. Manual and I. Volume, "Version 971," *Livermore Software Technology Corporation*, vol. 7374, p. 354, 2007.